X-RAY DIFFRACTION STUDIES OF

RECONSTITUTED MEMBRANES

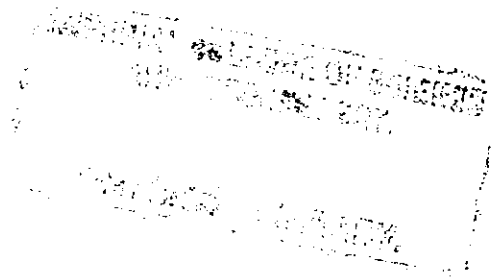

A thesis submitted for the

Diploma of Membership

of Imperial College

by

Kathryn Ann Snook

Biophysics Section

Blackett Laboratory

Imperial College

University of London

June 1983

ABSTRACT

Reconstituted membranes of a chosen composition have been prepared from purified membrane components by the Langmuir-Blodgett multilayer technique of repeatedly dipping a substrate through a lipid monolayer above a protein-containing aqueous subphase. The apparatus and method of making the samples are described. This technique produces multimembrane stacks which are ideally suited for study using low-angle X-ray diffraction. Diffraction patterns have been recorded from reconstituted membranes containing either myelin basic protein or cytochrome c as the protein component. These patterns have been analysed to give one-dimensional electron density profiles which have been interpreted in terms of the conformation and disposition of the protein molecules. The results are discussed in relation to the lipid-protein interaction and it is concluded that there is no significant hydrophobic interaction between the cerebroside sulphate-cholesterol bilayer and either myelin basic protein or cytochrome c in our multilamellar systems. Techniques have also been developed for measuring the proportions of the various components present in the multilayer samples, which are generally only 60 membranes thick.

ACKNOWLEDGMENTS

First and foremost, I should like to thank Dr Nick Franks, whose student I have been, for continual advice and encouragement. I should also like to thank the members of the biophysics group for many useful discussions and, in particular, Ian Coole for his help and encouragement while I was building the surface balance control system. Most of the apparatus of this thesis was made in the physics main workshop under the supervison of Ron Hobbs. I should like to thank Derek Dollard, Ray Swain, Jim Blewitt, Fred Lockyer and Ken Green for their excellent work and the many improvements which they made to the original designs. Derek deserves a special mention for all the thought and effort that he put into making the barrier mechanism. I should also like to thank Dan Kirschner for his collaboration in the initial stages of this project, Otto Albrecht for his suggestions on the design of the surface balance control system, Jenny Fordham for her advice regarding the total nitrogen determination of our samples, Nick Jackson for his skillful photographic work and the Medical Research Council for support as a graduate student. Finally I should like to thank my parents and friends for all the interest that they have shown and for their help in preparing this thesis.

CONTENTS

CONTENTS (contd.)

CONTENTS (contd.)

LIST OF FIGURES

LIST OF FIGURES (contd.)

LIST OF FIGURES (contd.)

LIST OF FIGURES (contd.)

LIST OF FIGURES (contd.)

LIST OF FIGURES (contd.)

LIST OF TABLES

CHAPTER I

INTRODUCTION

The main subject of this thesis is the structure of biological membranes and in particular the conformation and disposition of certain membrane-associated proteins. The basic structure of the biological membrane is a lipid bilayer, generally fluid, in which the lipid molecules are arranged tail to tail so as to produce a hydrocarbon core in the centre of the membrane. The main functional constituents of the membrane, the protein molecules, are embedded in or attached to this lipid bilayer.

There are hundreds of different membrane proteins and they have been classified into two classes depending on their ease of removal from the membrane. Extrinsic proteins can be removed from the membrane by non-destructive techniques, such as high ionic strength, and these proteins are considered to reside on the surface of the bilayer and to interact, for the most part, electrostatically with the lipid headgroups. Intrinsic or integral membrane proteins, on the other hand, can only be removed from the membrane by destructive techniques such as by the use of detergents which disrupt the membrane. These proteins are considered to be embedded within the membrane and usually span the bilayer.

Natural biological membranes are very complex and any particular membrane will contain a wide variety of both lipids and proteins. It is therefore advantageous to

study membrane samples reconstituted from purified membrane components. The proportions of the various membrane constituents present in the sample is then defined and can also be manipulated.

There are various methods used to manufacture reconstituted membrane samples. Firstly the membrane components can be associated into some type of liposome (see Bangham 1982 for a review of the various methods). The easiest type to prepare is the multilamellar vesicle which is made by co-evaporating lipids from an organic solvent, adding an aqueous solution and then mixing. However, for permeability studies single-walled vesicles of uniform size are preferable. Large unilamellar vesicles (LUV) have diameters of around Ø.2 to Ø.8µm and can be prepared by the reverse phase evaporation method. Small unilamellar vesicles (SUV) are about 250Å in diameter and are usually prepared either by sonication or by detergent dialysis. They have the great advantage over the larger vesicles of being homogeneous in size.

Another type of reconstituted membrane is the "black lipid membrane" (Mueller et al. 1962, Huang et al. 1964). This membrane is formed across a small hole in a septum separating two aqueous compartments by spreading lipid in alkane solution across the hole with a brush and allowing it to thin. Thinning is observed using reflected white light. When the lipid layer is only a bilayer thick, light is no longer reflected and so the layer appears black, so giving this technique its name. This type of reconstituted membrane is generally used in electrical

studies such as the measurement of trans-membrane potentials. However, there is a major problem with this method in that solvent is often retained in the lipid bilayer and this can affect its properties.

A "bimolecular" membrane has also been produced from two lipid monolayers at an air-water interface, by lowering a Teflon partition which separates two aqueous phases and in which there is a small aperature through the interface, so causing the two monolayers to come together into a bilayer (Montal & Mueller 1972). This method does not suffer from the problem of solvent retention and has the added advantage of allowing asymmetric membranes to be prepared. As with the solvent-containing films, these membranes are mainly studied electrically.

The type of sample required will depend on the technique used to study it. The technique used in this thesis to study the membrane specimens is low-angle X-ray diffraction. When a membrane specimen is placed in a beam of X-rays, the electrons in the sample scatter some of the incident radiation. The intensity of the scattered radiation is recorded on film and suitable analysis of this "diffraction pattern" will give the distribution of electron density throughout the structure. It is therefore one of the more direct methods of studying membrane structure.

In this thesis, X-ray diffraction results are reported for both lipid and lipid-protein specimens. The results are compared in order to determine the siting of the protein with respect to the lipid bilayer.

Various types of specimen can be studied by X-ray diffraction. Natural membranes such as the purple membrane and the red cell membrane are simply dispersed in buffer. For technical reasons, however (see chapter V), there are important advantages in using membrane stacks. Certain biological membranes, such as myelin and the disc membranes in the rod outer segment, occur naturally in stacks and so can be X-rayed intact. Attempts have been made to stack membranes artifically by centrifugation and/or controlled dehydration, but with limited success.

As already discussed, it is often informative to study reconstituted membranes. Both single-walled and, particularly, multi-walled vesicles are suitable diffraction samples and the latter have been used in this thesis for lipid specimens. Improved resolution has been obtained from oriented lipid multilayers prepared from a solution in organic solvent by evaporation. The two techniques, dispersion and evaporation, used for preparing the lipid samples of this thesis are described in more detail in chapter V.

Our protein-containing samples were made using the Langmuir-Blodgett technique in which a multilayer stack is built up by repeatedly dipping a substrate through a monolayer of purified membrane components spread at an air-water interface. The history, theory and applications of the technique are described in chapter II. This method has been used to build up phospholipid multilayers (Levine et al. 1968, Green et al. 1973, Nakahara et al. 1978, Hasmonay et al. 1979, Johnston et al. 198Ø) which have

been studied by a variety of techniques including X-ray diffraction, electron diffraction and infra-red spectroscopy. McIntosh et al. (1977) have succeeded in building up both asymmetric and polypeptide-containing multilayers of fatty acids, and Hwang et al. (1977) have prepared stacks of natural membrane fragments by dipping through a mixed film of membrane fragments and lecithin. We have developed this technique to produce reconstituted membrane stacks, containing both lipid and protein, which are suitable for low-angle X-ray diffraction studies.

An automated surface balance and dipping mechanism was used to produce the protein-containing multilayers. The apparatus was specifically designed and built for this project, and details are given in chapter III.

There are various advantages in using this technique to build up reconstituted membrane samples. The specimens so prepared are both ordered and oriented and so can produce higher resolution diffraction patterns than other types of specimen. Also the excellent orientation of the specimens means that diffraction in the plane of the membrane, such as from hydrocarbon chain separation or from regularities in the in-plane protein packing, is separated from the diffraction perpendicular to the bilayer plane. Another advantage is that multilayers of asymmetric bilayers can be produced by dipping alternately through two different monolayers. The asymmetry so produced may be either lipid asymmetry or protein asymmetry, both of which occur in natural membranes (Rothman & Lenard 1977).

Detailed analysis of the X-ray diffraction results from these reconstituted membranes requires information on the chemical composition of the samples. In the case of a protein-containing sample this means that the ratios of protein to lipid to water must be known as well as the proportions of the various lipid types used. Techniques have been developed to determine the chemical composition of the sample and these are described in chapter VI. Particular difficulties were caused by the small amount of material in the sample, only about 50µg for a 50 membrane sample, especially as this had to be dissolved off the substrate before analysis, so producing a very dilute solution.

The thickness of sample required for the X-ray diffraction experiments was found to be about 50 membranes. Thinner samples produced weaker diffraction patterns, therefore requiring longer exposure times and hence having smaller signal-to-noise ratios, although diffraction patterns have been recorded from as few as 20 bilayers. The thickness of the sample was limited by the time taken to build it and the size of the spread monolayer.

The techniques developed during the work of this thesis have been applied to the study of myelin structure. Myelin is formed from the membranes of glial or Schwann cells in the central and peripheral nervous systems respectively. These membranes wrap spirally around nerve axons and compact to form the myelin sheath. The effect of myelination is to increase the velocity of conduction

for a particular axon diameter compared with unmyelinated nerve and to reduce the rate of energy expenditure. For example, "in frog, a myelinated nerve fibre 12μ in diameter conducts signals at a velocity of 25 metres per second. So does the unmyelinated giant axon of squid, but it is 500μ in diameter and uses 5000 times as much energy" (Morell & Norton 1980). The importance of myelin is apparent in the critical results of demyelinating diseases such as multiple sclerosis.

The chemical composition of myelin is unusual as it contains only 20-30% protein by dry weight, a much lower fraction than is usually present in other biological membranes. Central nervous system myelin (CNS) contains two major proteins, the proteolipid protein, an intrinsic protein of molecular weight 30,000 (50% by weight of the total protein) and the myelin basic protein, an extrinsic protein of molecular weight 18,500 (30% of total protein). The remaining protein is almost exclusively high molecular weight (about 60,000) intrinsic proteins (Rumsby 1978).

Myelin basic protein (MBP) is a highly basic protein with an isoelectric point of pH12. The amino acid sequence of the basic protein from a variety of sources has been determined (Eylar et al. 1971, Boggs & Moscarello 1978a) and it contains 170 amino acid residues with a total molecular weight of 18,500. 50% of the MBP present in myelin can be extracted by 0.5M ammonium acetate alone, but the remaining myelin basic protein requires a non-ionic detergent for removal. Alternatively almost all the MBP can be extracted by HCl at pH2.0 (Martenson 1980).

Various methods have been applied to aqueous solutions of myelin basic protein which show that the protein takes up a prolate ellipsoid shape in water, with axial dimensions of about 15 × 15 × 150Å (Epand et al. 1974). The structure in aqueous solution appears to be open and flexible at the ends, but with considerable secondary structure near the centre (Chapman & Moore 1976, 1978). No change in this secondary structure is observed at intermediate pH values, pH 5.6-9.2 (Boggs & Moscarello 1982). However, it is evidently the structure taken by the protein when in its natural environment, i.e. associated with the membrane, that is of most interest. A theory exists that there is partial penetration of the protein into the hydrocarbon region of the bilayer and the evidence is discussed in chapter VIII.

This thesis is concerned with studying the siting of myelin basic protein with respect to the lipid bilayer using low-angle X-ray diffraction. Myelin, being a regularly stacked system, can be X-rayed directly and figure 1.1 (see overleaf) shows the high resolution (10Å) electron density profile across the membrane according to Caspar and Kirschner (1971). It should be noted that the membrane is asymmetric. Unfortunately, although the overall bilayer structure is unambiguous, the complex chemical composition of the natural myelin has prevented determination of the exact disposition of the protein molecules.

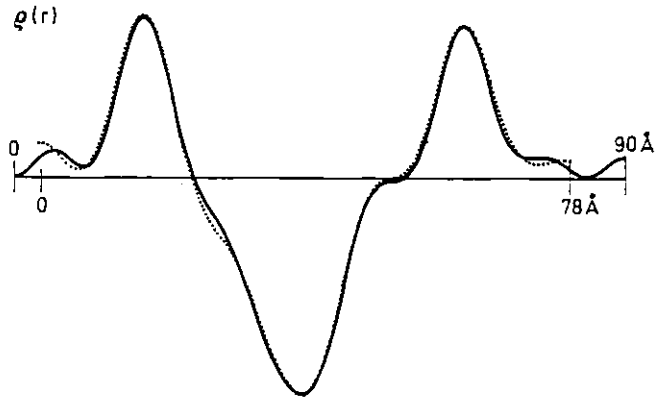

Figure 1.1 High resolution (10Å) electron density profile for rabbit sciatic-nerve (solid curve) and rabbit optic-nerve myelin (dotted curve) according to Caspar and Kirschner (1971).

The Langmuir-Blodgett method is particularly suitable for producing the MBP-lipid reconstituted samples because, unlike multi-walled vesicle studies where the protein interacts with the preformed multilayers, with our method the protein interacts first with the monolayer before being built up into multilayers. This latter method is more akin to that found in nature where the myelin is produced from preformed membranes which wrap around the nerve axon and then compact. It must be realised, though, that our samples contain a higher proportion of MBP (20-30% by dry weight) than is found in native myelin (5-10%).

In order to simplify the analysis of the electron density profiles, once obtained, cerebroside sulphate plus cholesterol were used as the monolayer lipids instead of using total myelin lipids. Cerebroside sulphate (CES) was chosen because of work by Demel et al. (1973) which reported that, from a variety of lipids, myelin basic

protein shows the strongest interaction with cerebroside sulphate. Figure 1.2 gives the strucural formula of cerebroside sulphate. It is present in native myelin but only constitutes about 3-4% by dry weight of the total myelin lipids (Rumsby 1978). Cholesterol was added to the CES at 40mol % as this is the proportion of cholesterol found in native myelin (O'Brien & Sampson 1965) and bilayers without cholesterol behave very differently than those with cholesterol (e.g. Ladbrooke et al. 1968)

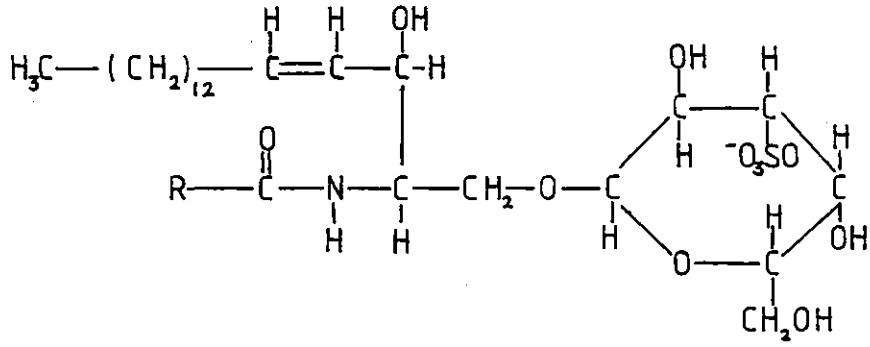

Figure 1.2 The structural formula of cerebroside sulphate. R is a hydrocarbon chain of variable length, often hydroxylated at the primary carbon position.

Previous X-ray diffraction work on myelin basic protein-lipid complexes is very limited. Mateu et al. (1973) studied mixtures of MBP with various fractions of myelin lipids and found that only the acidic lipid fraction gave well-organised phases when myelin basic protein was added. The only phase studied in detail had an unusually large repeat period (154Å) and gave a sharp reflection at 4.2Å as well as a broad reflection at 4.6Å, indicating both frozen and fluid hydrocarbon chains. Analysis of the diffraction data resulted in the proposed

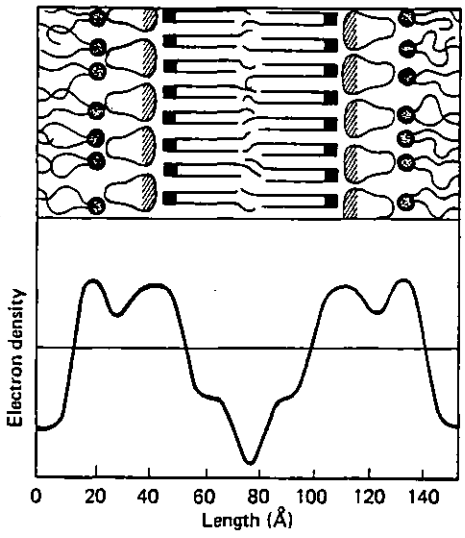

Figure 1.3 Proposed structures and electron density profiles for phase composed of myelin basic protein and the acidic fraction of myelin lipids (Mateu et al. 1973).

structure and electron density profile shown in figure 1.3. It appears that the lipids segregated into two bilayers, one of mainly sulphatides with predominantly frozen chains and the other of mainly phospholipids with fluid chains. The asymmetry in the headgroup peak widths indicates a preferential affinity of the protein for the sulphatides. It is important to realise, however, that this system does not contain cholesterol and, if cholesterol is added, then the repeat period halves and the hydrocarbon chains all become fluid.

Brady et al. (1981) have studied mixtures of MBP and egg phosphatidyl glycerol by X-ray scattering and have found that the addition of the protein results in multilayer formation, as determined by the presence of sharp diffraction peaks superimposed on the diffuse X-ray scatter. They reported that these results "strongly suggest that one of the primary roles of the basic protein in the myelin membrane is to produce and maintain the

highly ordered spiral pattern found in the natural system". Although this may well be true, cytochrome c, another basic protein, has the same effect on lipid vesicles (Blaurock 1973), as does the addition of calcium ions, and I feel their evidence does not fully justify such a strongly worded conclusion.

For comparative purposes, we have also studied the structure of cerebroside sulphate-cholesterol-cytochrome c multilayers by the same techniques. Cytochrome c is an electron-transfer protein, a catalyst in the terminal oxidation chain. It is a very well documented protein with a molecular weight of 12,384 and 104 amino acid residues (these values refer to cytochrome c from horse heart) and is a highly basic protein with an isoelectric point of pH10.65 (Margoliash & Schejter 1966). It is a prolate spheroid in shape with axial dimensions of 30Å × 34Å × 34Å including side chains (Dickerson et al. 1971), and is extremely stable. Margoliash and Schejter (1966) reported that cytochrome c is stable at 20°C between pH values of 1.6 and 12.3 for over 30 hours as judged by its activity in the succinate oxidase system.

Gulik-Krzywicki et al. (1969) have studied the structure of the cytochrome c-phosphatidyl inositol-water system using X-ray diffraction. From knowledge of the lamellar repeat distance D and the relative weight concentrations and mass densities of the constituents, they calculated the partial thicknesses of the components. When the protein was added, the partial thickness of the lipid did not change, indicating that the protein-lipid

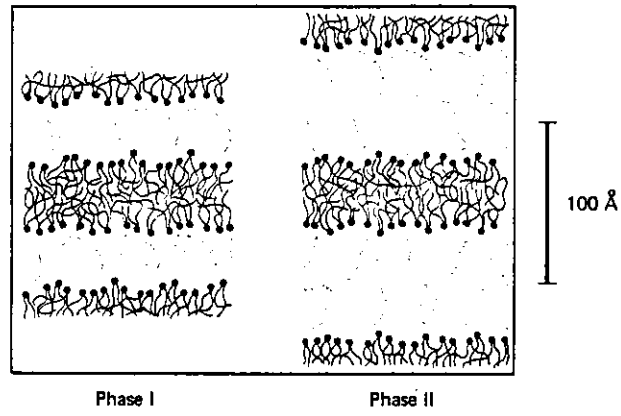

Figure 1.4 Proposed structures for the two lamellar phases formed by mixtures of cytochrome c-phosphatidyl inositol-water (Gulik-Krzywicki et al. 1969).

interaction is purely electrostatic. Two lamellar phases of the cytochrome c-lipid-water system were observed with repeat distances of 78.5 and 112Å. It was proposed that the structure consisted of layers of cytochrome c, one or two molecules thick, sandwiched between lipid bilayers as demonstrated in figure 1.4. Shipley et al. (1969), on the basis of X-ray diffraction studies, proposed similar structures for mixtures of cytochrome c and phospholipid.

Blaurock (1973) added cytochrome c to small single-walled lipid vesicles and found that the resulting diffraction pattern consisted of sharp reflections on top of a broad diffraction band, indicating that the sample contained both vesicles and a multilayered structure. Two electron density profiles were derived, one using the sharp intensities alone and the other including the broad non-multilamellar diffraction. These were compared with the profile of the lipids alone. The resulting profiles are reproduced in figure 1.5 (see overleaf) and were

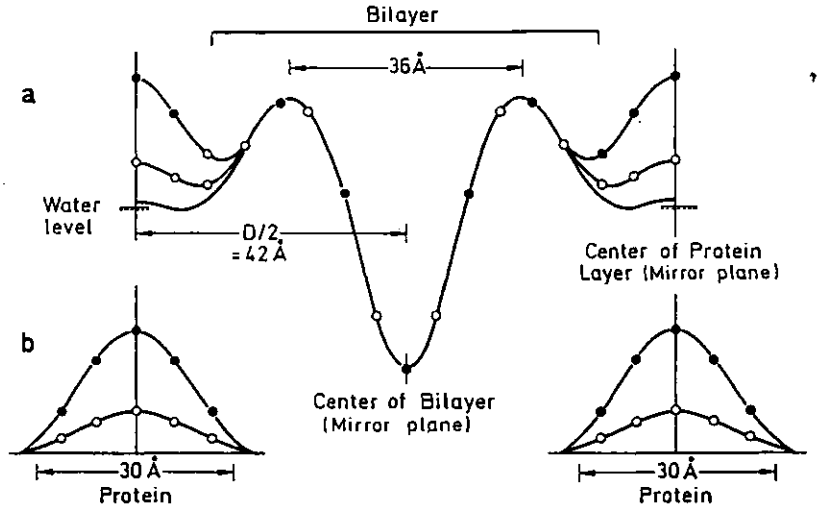

Figure 1.5 Electron density profiles across a lipid bilayer (lower curve) and in the presence of different amounts of cytochrome c (o and ●). The differences between the upper two profiles and the lower one in (a) are shown in (b), (Blaurock 1973).

interpreted as a similar bilayer structure with differing amounts of protein bound to the bilayer surface. It is important to notice that the addition of cytochrome c has not changed the bilayer peak-to-peak separation and also that the structure only contains one protein molecule per unit cell.

In the native system, cytochrome c is associated with the inner mitochondrial membrane and probably interacts specifically with other membrane proteins such as cytochrome oxidase (Franks & Levine 1981). Therefore the study of the cytochrome c-lipid complex is not necessarily relevant to in vivo membrane structure. However, cytochrome c is a well documented protein which, according to Gulik-Krzywicki et al. (1969), interacts electrostatically with the lipid bilayer and in this study was used as a control, the subject of main interest

being the interaction between myelin basic protein and lipid bilayers.

CHAPTER II

THE HISTORY AND THEORY OF THE LANGMUIR-BLODGETT TECHNIQUE

The history of the Langmuir-Blodgett technique began in 1774 with Benjamin Franklin's famous experiment on Clapham Common Pond. He poured a teaspoonful of oil onto the surface of the pond and found that it "produced an instant calm over a space of several yards square, which spread amazingly and extended itself gradually till it reached the lee side making all that quarter of the pond, perhaps half an acre, as smooth as glass" (Franklin 1774). The calming of the pond is due to the presence of an oil film on the surface. Simple arithmetic shows this oil film to be only about 25Å thick and it is now known to be a monolayer, i.e. a layer only one molecule thick.

The first person to control and monitor such monolayers was Agnes Pockels, an amateur physicist whose letter to Lord Rayleigh was published in Nature in 1891 (Pockels 1891). Her experimental apparatus consisted of a trough filled to the brim with water and a strip of tin laid across the trough in contact with the water which divided the surface into two parts. She measured the surface tension by the weight required to remove a small flat disc from the surface of the trough. In 1893 she published the first π-A isotherm (Pockels 1893), a plot of the surface pressure of an oil film at various areas per molecule.

Lord Rayleigh repeated and extended her observations

(Rayleigh 1899) and proposed that the spread films were in fact monomolecular. His experimental method differed only in the measurement of surface tension in that he used the Wilhelmy Plate technique.

The Wilhelmy Plate

The Wilhelmy method of measuring surface tension is as follows. A thin plate, usually of carefully cleaned glass, quartz, mica, or platinum is suspended in the liquid surface from a balance, as shown below (figure 2.1).

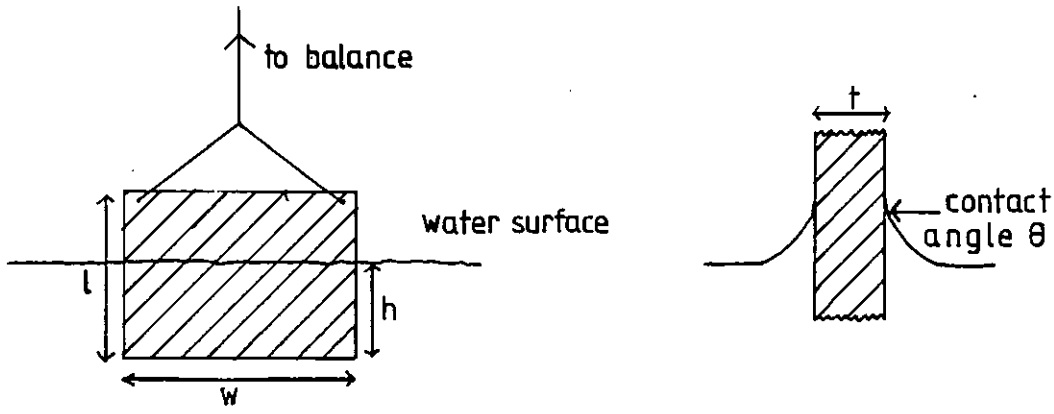

Figure 2.1 Diagram of a Wilhelmy plate partially immersed in a water surface (front and side views).

For a plate of length l, width w, thickness t, and density ρ_p immersed in a liquid of density ρ_l to a depth h, the vertical forces downwards are

$$\begin{aligned} \text{Weight of plate} &= \rho_p glwt \\ \text{Bouyancy force} &= -\rho_l gwth \\ \text{Surface tension} &= 2\gamma(t+w)\cos\theta \end{aligned} \qquad (2.1)$$

where g is the gravitational constant, γ is the surface tension and θ is the contact angle of the liquid on the solid plate. When combined the total downward force F is

$$F = \rho_p glwt - \rho_l gwth + 2\gamma(t+w)\cos\theta \qquad (2.2)$$

The weight of the liquid raised in the meniscus and the effect of air as the second phase have both been ignored in the above equation.

The usual procedure is to use an extremely hydrophilic plate so that it becomes completely wetted by the liquid and the contact angle is then zero ($\cos\theta = 1$). The change in force F for a stationary plate or the change in h for a constant applied force are then measured as the surface tension is altered (Gaines 1966).

When working with oil films on water it is customary to talk in terms of the surface pressure (π) of the monolayer, which is the difference in surface tension between the oil film and a clean water surface.

$$\text{i.e.} \qquad \pi = \gamma_o - \gamma_f \qquad (2.3)$$

where π is the surface pressure, γ_o is the surface tension of clean water and γ_f is the surface tension of water covered with the oil film. The surface tension of clean water is 73.Ø5 dynes/cm at 18°C (CRC Handbook of Chemistry and Physics 1974). The presence of an oil film at the air-water interface or of any surface contamination will

result in a decrease of the surface tension.

The main disadvantage of the Wilhelmy balance is the problem of the contact angle. Although complete wetting is possible at the beginning of an experiment with a freshly cleaned plate and a clean water surface the presence of a monolayer tends to alter the wetting properties of the plate and introduce a non-zero contact angle.

The Work of Irving Langmuir

The major contributer to the field of monolayer studies is certainly Irving Langmuir who in 1932 received the Nobel Prize for Chemistry. His paper on "The constitution and fundamental properties of liquids" appeared in 1917 in which he applied his ideas on the shape of molecules and the forces between them to explain the spreading of oil films on water (Langmuir 1917).

Hardy had previously shown that only oils containing a polar functional group spread on water (Hardy 1912). Langmuir proposed that the molecules in an oil film are orientated at the air-water interface with the polar groups immersed in the water and the long hydrocarbon chains packed side by side rising vertically from the surface (see figure 2.2). This theory was supported by experimental measurement of the cross-sectional areas of molecules spread as a monolayer on a talc covered water surface which showed that saturated fatty acids of varying chain lengths occupy the same area per molecule - about $20Å^2$ per molecule.

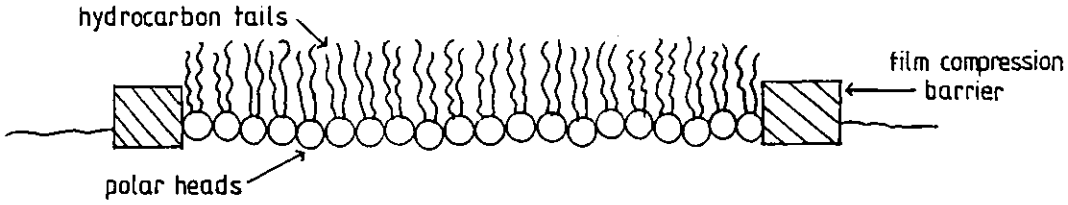

Figure 2.2 Schematic diagram of a lipid monolayer showing the orientation of the aliphatic molecules at the air-water interface.

In order to carry out these experiments, Langmuir developed a new type of horizontal film balance. A diagram of this balance as published in his original 1917 paper is shown below (figure 2.3).

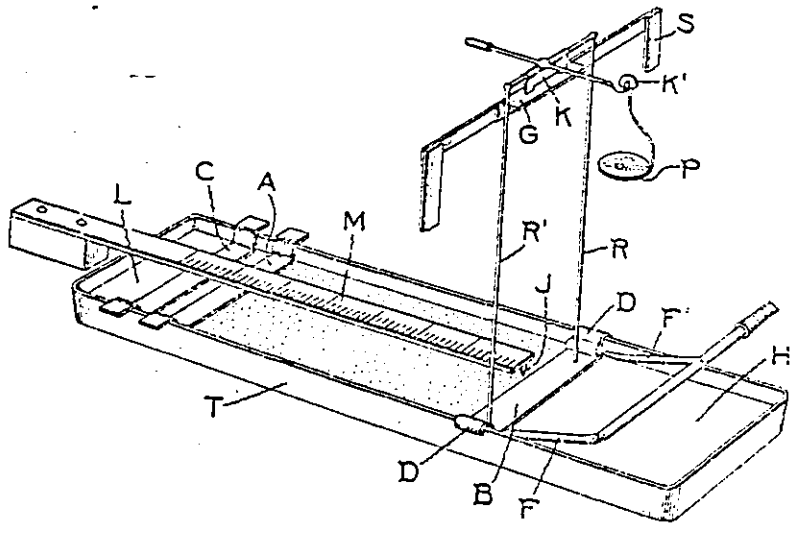

Figure 2.3 Langmuir's original film balance (reproduced from Langmuir 1917).

A and B are strips of waxed paper which float on the water surface and confine the monolayer. However float B, unlike A, is made slightly narrower than the width of the trough so it is free to move under the influence of the monolayer. Float B is attached to a knife edge balance

(K) by rods (R and R′) and the surface pressure of the monolayer can be measured by counteracting the torque on the balance with weights added to the pan P. Leaks around float B are prevented by jets of air from tubes F and F′.

The advantage of this apparatus over the Wilhelmy balance is that the problem of the contact angle no longer exists. However with Langmuir's design it is very difficult to prevent leakage around barrier B especially at high surface pressures.

The Langmuir-Blodgett Method of Building Multilayers

The technique of building multilayers by successive deposition of monolayers on a solid support was developed in the mid 1930's by Katherine Blodgett, a research assistant of Langmuir. Her initial work was on building "stearic acid" multilayers on a glass substrate. However, she soon realised that the substance deposited was in fact calcium or barium stearate depending on which ion was present in the subphase. The samples, once made, were studied both by optical interference methods and by X-ray scattering (Blodgett 1935, Blodgett & Langmuir 1937).

The multilayers were built up by repeatedly raising and lowering a plate through a monolayer-covered water surface. The monolayer had to be maintained at a finite surface pressure during dipping to effect transfer of the film from the water surface to the substrate. In order to keep the film under constant pressure Katherine Blodgett made use of piston oils which were separated from the monolayer by a waxed silk thread. Any surface active oil,

if placed on a water surface in the bulk phase (as a crystal or a drop of liquid) will spread as a monolayer until all the available area is covered. The layer so formed will be in equilibrium with the bulk phase and the final surface pressure of the film is known as its equilibrium spreading pressure. Such an oil, in equilibrium with its bulk phase, can be used to exert a constant surface pressure on a monolayer provided it reaches its equilibrium spreading pressure fairly rapidly and the spreading is reversible. Oils used for this purpose are known as "piston oils".

The Langmuir-Blodgett method of building up multilayers as reported in 1935 (Blodgett 1935), will now be described in more detail. A wax coated trough was filled to the brim with water, usually containing a low concentration of metal ions. The water surface was then cleaned by sweeping with a barrier and a waxed silk thread was placed on the surface. The monolayer material (e.g. stearic acid) dissolved in a suitable spreading solvent (e.g. benzene) was added to the surface on one side of the silk barrier. The solvent spread rapidly dispersing the film-forming molecules at the air-water interface, and then itself evaporated. Piston oil was added on the other side of the silk barrier and the monolayer was seen to contract slightly in area under compression. Layers were then deposited by raising and lowering a glass slide through the film using a hand-operated winch. Each time a layer was deposited the film was depleted by an amount equal to the area of the slide, front and back, and the

thread was pushed forward a corresponding amount by the piston oil. A diagram of the lever and winch system used to raise and lower the glass slide is reproduced below from Blodgett's original paper (figure 2.4).

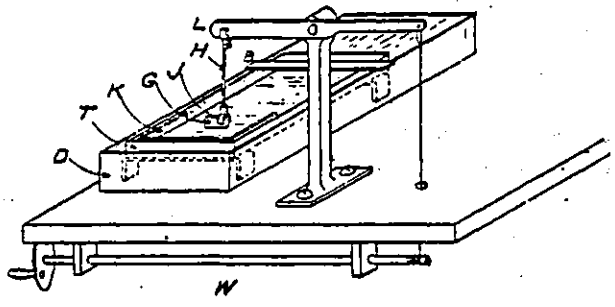

Figure 2.4 Blodgett's original apparatus for depositing multilayers (reproduced from Blodgett 1935).

During the course of her experiments, Dr. Blodgett observed two distinct types of deposition which she called "X-type" and "Y-type". X-type films are built up when deposition occurs only as the slide travels downward from air to water and not on raising the slide while Y-type films are deposited on both upward and downward journeys. The occurence of these two types of deposition was found to depend on the pH and temperature of the subphase as well as on the surface pressure. Z-type deposition, transfer of the film to substrate only on the upward journey, can also occur, particularly when working with more complex molecules than fatty acids.

A diagram of the Y-type deposition process is reproduced below in figure 2.5 demonstrating the successive folding back and forth of the monolayer onto the solid plate as it is dipped in and out of the liquid.

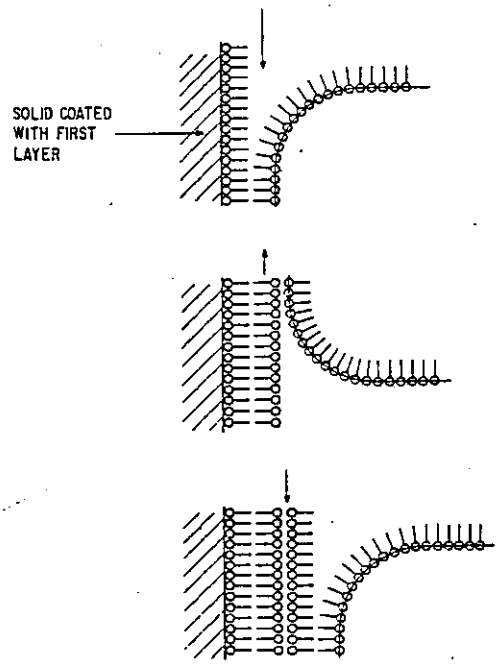

Figure 2.5 Schematic diagram of Y-type deposition (reproduced from Gaines 1966).

The process for X and Z-type deposition has never, in my opinion, been adequately explained. However, as X-ray diffraction measurements show that the spacing between metal ions in calcium and barium stearate multilayers is the same whether they are deposited as X or Y films (Frankuchen 1938, Bernstein 1938), evidently some overturning and rearrangement of the molecules in X and Z-films must occur during or shortly after deposition.

The success of deposition can be quantified in terms of the "deposition ratio" (Langmuir et al. 1937) which is defined as the ratio a_1/a_2 where a_1 is the reduction in area of the monolayer on the water surface when deposited onto a plate of geometric area a_2. As very few solids, even when polished, are smooth on a molecular scale, the actual area of the glass or metal plate is certainly

greater than the geometric area. However Bikerman (1939) showed that stearic acid multilayers deposited on grooved surfaces or even on fine wire gauze still had a deposition ratio of unity. This suggests that at the moment of deposition, the film bridges over the surface roughness of the solid, although drying out of the intervening water layer can result in collapse of the film.

CHAPTER III

THE AUTOMATED SURFACE BALANCE

Our original attempts at building multilayers were carried out in collaboration with Dr Dan Kirshner from the Children's Hospital, Boston, who was at Imperial College for a three month visit. We used a refined version of Blodgett's waxed silk thread and piston oil method which I have described in the previous chapter. In this simple way we succeeded in building multimembrane samples of certain biological molecules from which diffraction patterns were recorded.

However, it was found necessary during these preliminary experiments to monitor deposition of the multilayers. This was especially important when trying to determine the conditions under which multilayers could be built up, as without measurement of monolayer area it was difficult to know whether we were picking up successfully or not. Initially, the only method available to us was to take Polaroid photographs of the position of the thread and then to measure the area enclosed using a planimeter. This method was very rough, especially as we used substrates of small (2 cm^2) geometric area so that we could build up many layers without having to renew the monolayer. Other disadvantages included the high cost of Polaroid film and the time delay between photograph and result while the area was calculated.

It was therefore decided to build an automated

surface balance. A schematic diagram of the system is shown overleaf in figure 3.1. The monolayer is confined by a movable barrier lying across the trough, the position of the barrier hence determining the area of the monolayer. The surface tension is measured using a Wilhelmy plate and transducer assembly, the output from which is fed into a control box. The electronic circuitry in the box is designed to maintain constant surface pressure by moving the barrier in response to changes in Wilhelmy plate output. The system also produces a continuous readout of the monolayer area on a digital display and on a chart recorder and of the surface pressure on the chart recorder alone.

This automated design has other advantages over the piston oil method besides the continuous measurement of monolayer area. Especially at the high surface pressures (about 40 dynes/cm) that we found necessary for deposition of our particular monolayers, there were very few piston oils available which spread sufficiently rapidly to maintain the film's pressure throughout deposition. Also, before setting up the Wilhelmy plate, I had to rely on other peoples values of the equilibrium spreading pressures of the piston oils used, and my experimental conditions often differed from those quoted. The automated design gives complete freedom of choice of the film compression pressure. It also has the added flexibility of allowing π-A isotherms to be measured quickly and directly by stepping the barrier along the trough at a fixed rate, so decreasing the area per

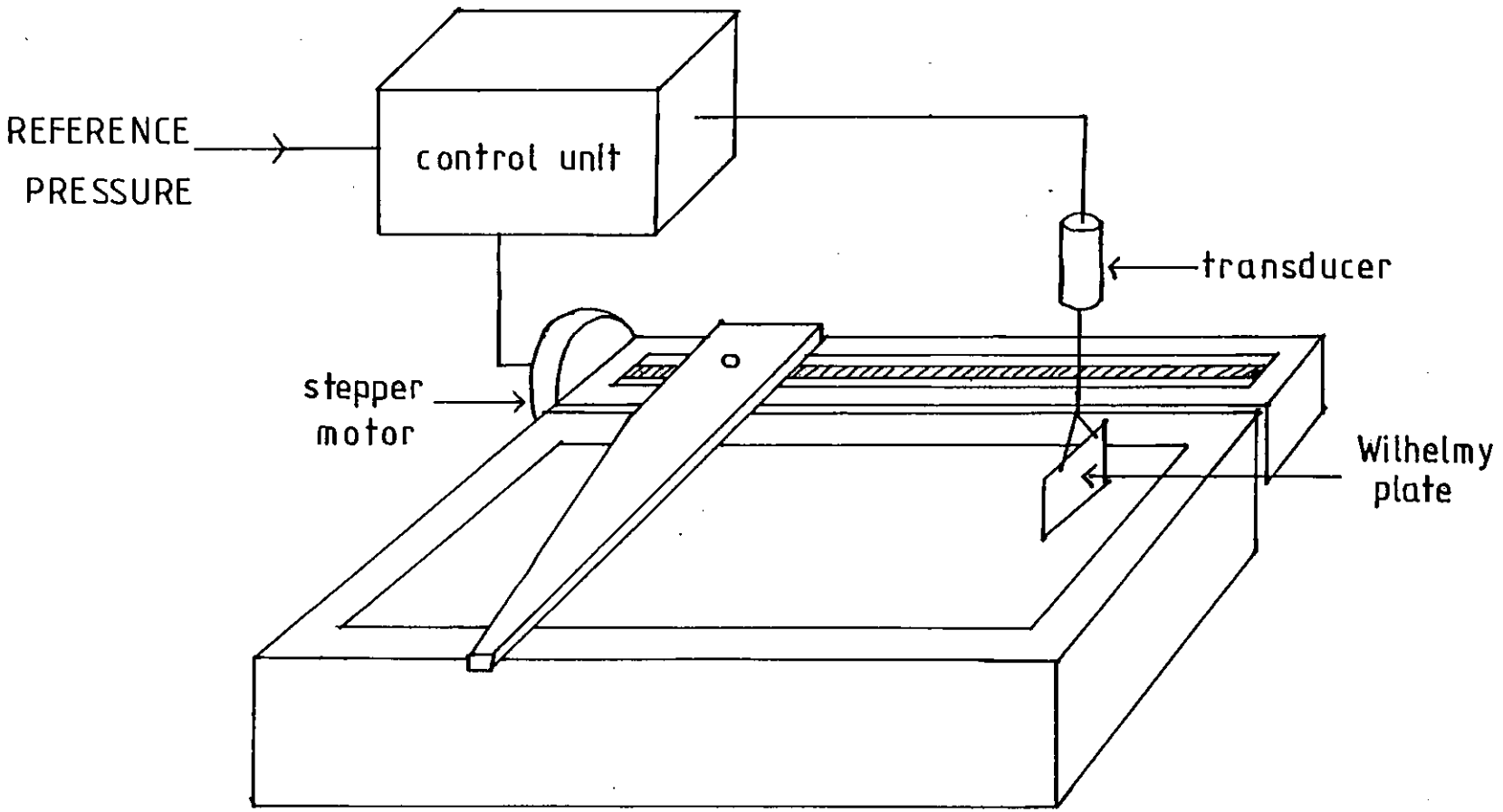

Figure 3.1 Schematic diagram of the automated surface balance.

molecule linearly, and recording the continuous variation in surface pressure (π). The final advantage of the new system is that it avoids the possibility of the film becoming contaminated by the piston oil, either by leakage around the thread or by solution in the subphase.

Design Criteria

The main requirements of the automated system are as follows.

1. Constant π during deposition - The surface pressure of the monolayer has to remain constant during deposition and so the barrier, controlled automatically, has to move quickly to counteract any changes in π as measured by the Wilhelmy plate. The reponse time of the control electronics is therefore critical.

2. Reproducible and accurate area measurement - The area of the monolayer has to be continuously monitored so that the deposition of the film onto the substrate can be quantified. For good X-ray diffraction patterns about 50 membranes are required for one sample. To minimise the time required to make a sample and to prevent variations between first and last layers, I believe it preferable to use only one monolayer for a sample. The trough area therefore has to be large in relation to the sample area and this makes the accurate measurement of the area deposited more difficult. Of course, the area of the film as determined from the barrier position is only meaningful if there is no loss of material from the monolayer either

by leakage around the barrier or by evaporation or solution in the subphase.

Besides the above two requirements, various general criteria had to be taken into account when designing the system.

1. Contamination - This was the most important factor affecting the detailed design of the system. In 1937, Blodgett and Langmuir reported that in the deposition of barium stearate films, copper ions in the subphase at concentrations of 10^{-5}M prevented film deposition completely, yet copper at 2×10^{-6}M had a beneficial effect in building up thick layers (Blodgett & Langmuir 1937). Contamination by surface active substances is even more serious as it is energetically favourable for these molecules to migrate to the air-water interface and so contaminate the monolayer itself. As an example of the scale of the problem, if the whole monolayer could be dissolved in the aqueous subphase, the ensuing solution would only be 10^{-9}M (using a trough of similar dimensions to the one used in this thesis). Dust particles settling on the surface of the monolayer are also to be avoided as these will upset the regular stacking of the layers and so result in poor diffraction patterns. A dust particle is about 500,000 Å in size compared with about 60-120 Å for the thickness of a membrane.

The possibility of contamination was therefore considered very carefully when choosing the materials for the apparatus, especially in the materials to be used for

the trough and barrier which are in contact with the monolayer and subphase. Contamination by lubricants was minimised by using teflon bearings and the whole system was housed in a clean bench to prevent airborne contaminations.

2. Vibration - In order to affect smooth deposition of the monolayer onto the substrate, vibration should be minimised. This factor was taken into consideration both in vibration isolating the trough from its surroundings and in the design of the barrier mechanism.

3. Humidity - The high humidity and the probability of water spillage restricted the choice of materials used.

Detailed description of the system.

Photographs of the apparatus are shown overleaf in figures 3.2 & 3.3. Figure 3.2 is an overall view of the apparatus showing the whole trough assembly sited in a clean bench (the front panel of the clean bench has been removed for this photograph). Figure 3.3 is a closer view showing the monolayer surface, which is enclosed by the barrier and is monitored using a Wilhelmy plate system. An aluminium substrate can be seen on the end of the dipping arm partially immersed in the subphase.

Temperature control

The temperature of the system is maintained at 18^{o}C by siting the whole apparatus in a temperature controlled room. A cooling/heating system was also designed so that

Figure 3.2 Photograph of the system - an overall view showing the whole trough assembly and dipping mechanism situated inside a clean bench. The control boxes for the automated surface balance and the dipping mechanism can be seen beside the clean bench.

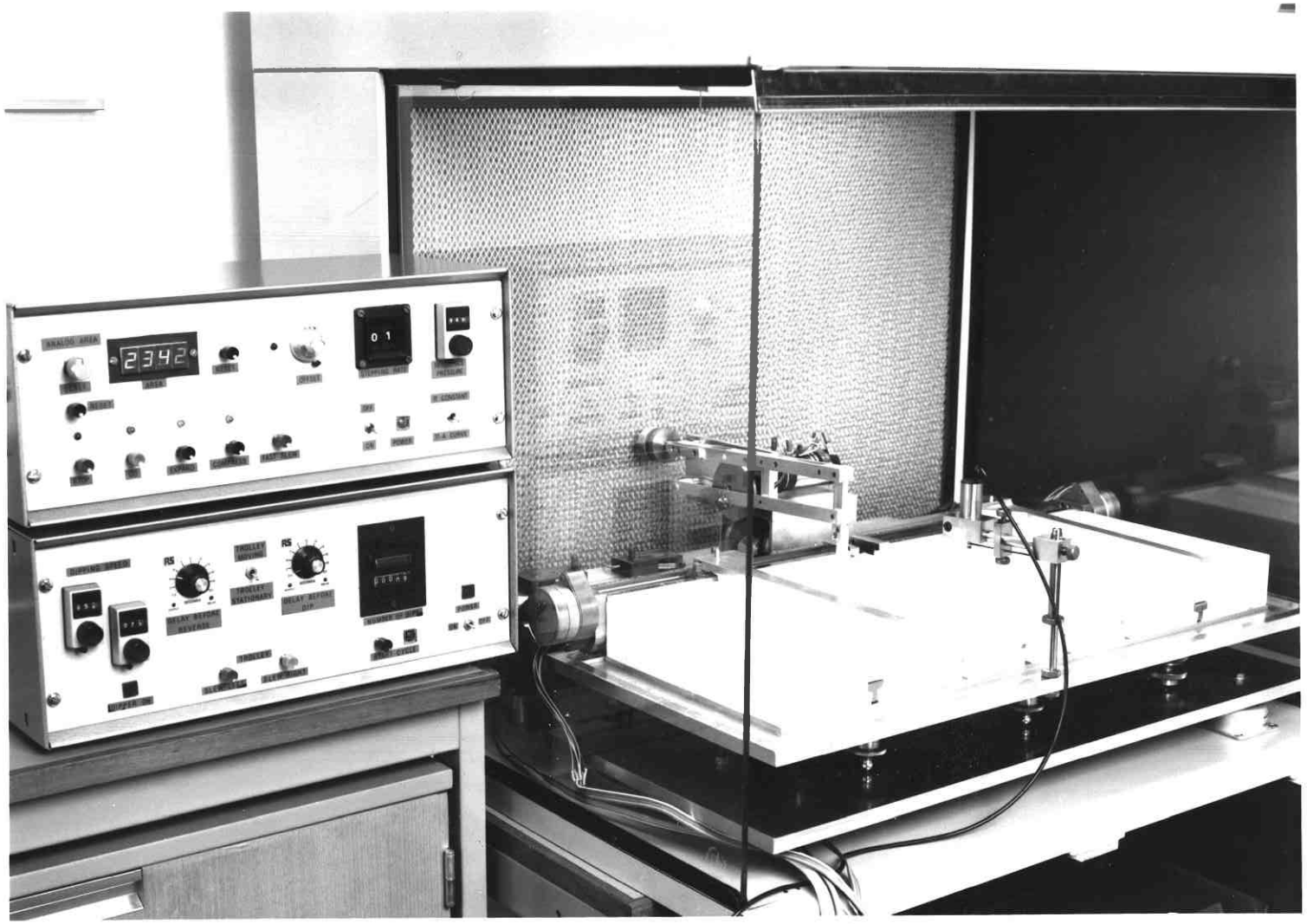
2342
01

Figure 3.3 Photograph of the automated surface balance showing the monolayer surface enclosed by the barrier. The Wilhelmy plate system, which is used to monitor the surface pressure of the monolayer, and the dipping system, with a substrate partially immersed in the subphase, are both visible in this photograph.

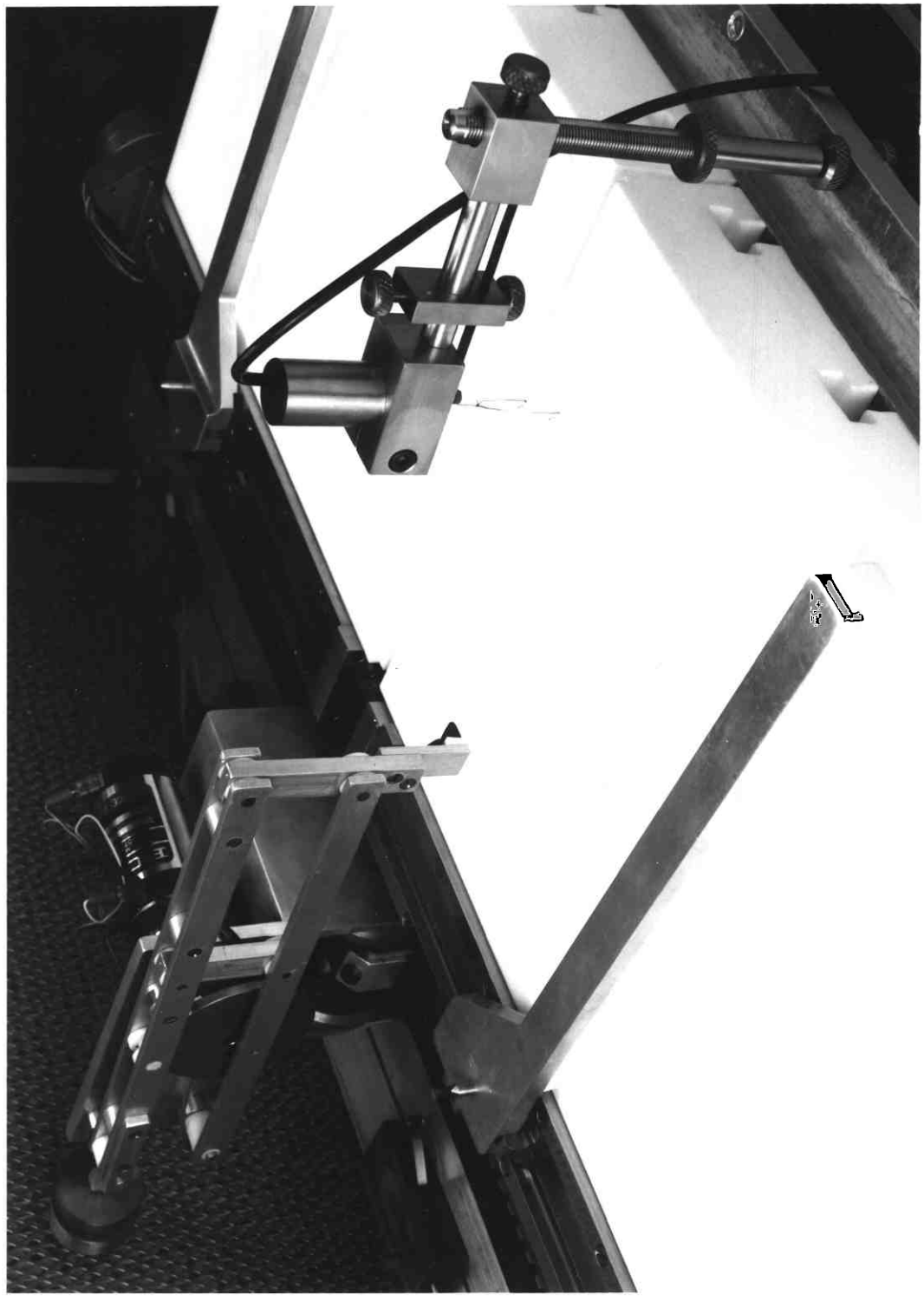

experiments can be carried out at other temperatures. This consists of a glass coil placed in the bottom of the trough through which cooled or heated liquid is passed.

Clean bench

As previously discussed, the trough is housed in a clean bench (internal dimensions - width Ø.73m, height Ø.6m, and depth Ø.5m) to prevent airborne contamination. This naturally restricted the size of the apparatus which could be accomodated. A laminar air flow of filtered air is passed through the clean bench throughout an experiment and the air input has been adapted so that, if required, the clean bench can be filled with oxygen-free nitrogen or an inert gas, such as argon, to reduce oxidation of labile monolayers.

Trough

As can be seen from the photograph (figure 3.2) two identical troughs have been made. This is so that asymmetric bilayers can be built up by dipping alternately through two different monolayers. However, so far this has not been attempted.

The requirements of a monolayer trough are that it does not contaminate the monolayer or the subphase and that it is hydrophobic so that the aqueous subphase can stand proud and so be swept by the barrier. The two troughs described here were made from a solid block of teflon. Other possibilities, such as a glass or metal trough coated with wax or teflon were rejected as more

likely to cause contamination. Teflon does however have its own problems as it cannot be joined by adhesives and it has a tendency to deform with time.

The internal dimensions of a trough are 27.6cm long, 20.7cm wide and 1.9cm deep. Teflon infills were made which can be placed in the base of the trough when using expensive protein in the subphase, so decreasing the volume of the trough from 1.25 l to 0.5 l. The thickness of the teflon block itself is 5cm. This aids stability and allows the possibility of milling out a deeper well if larger substrates are required such as for neutron diffraction work. The edges of the trough are 1cm wide and are milled flat for good contact with the barrier.

The teflon block is bolted to a base plate which stands on levelling feet. The whole assembly stands on a second metal plate which is supported by three vibration isolators.

Barrier Mechanism

The barrier itself is a solid teflon bar, milled flat to make good contact with the edges of the trough and so contain the monolayer without leakage. It is mounted on Dural, an aluminium alloy, the weight of which holds the barrier in contact with the trough sides. The barrier is driven along the trough by a stepper-motor (M^{C}Lennan ID31, 7.5 degrees per step) attached to a precision screw with a thread of 1mm per turn. The change in area of the monolayer is calculated from the number of steps moved by the stepper-motor.

For an accurate measurement of monolayer area, the requirements on the barrier mechanism are stringent. The nut which supports the barrier amd moves it along the trough as the screw turns, must fit tightly onto the screw without backlash. Also the barrier must always lie across the trough perpendicular to the screw without twisting. These factors were both taken into account in the design. Backlash was overcome by using a split nut made of hardened plastic which fitted tightly onto the screw and yet moved smoothly along it without added lubrication. The split nut can be tightened further by a small screw if required, and this can be used to overcome the problem of wear. The nut itself is firmly fixed to a small wheeled carriage which runs smoothly within a V-block. The barrier, which must be removable for cleaning between experiments, push fits onto the carriage by a step and groove mechanism with a locating pin. A photograph of this, with the barrier removed, is shown in figure 3.4. This is designed to keep the barrier fixed perpendicular to the length of the trough. However, the push fixing does allow a little freedom in the vertical direction so that slight differences in the levels of the two milled edges of the trough can be accomodated.

Wilhelmy Plate

The surface tension of the monolayer is measured using the Wilhelmy plate technique. The possibility of using the Langmuir film balance method was rejected because of the problem of leakage around the barrier. The

Figure 3.4 Photograph of the barrier mechanism (barrier removed) showing the carriage on which the barrier fits. This carriage runs in a V-block and is driven via a screw by a stepper motor (the motor can be seen on the far right of the photograph).

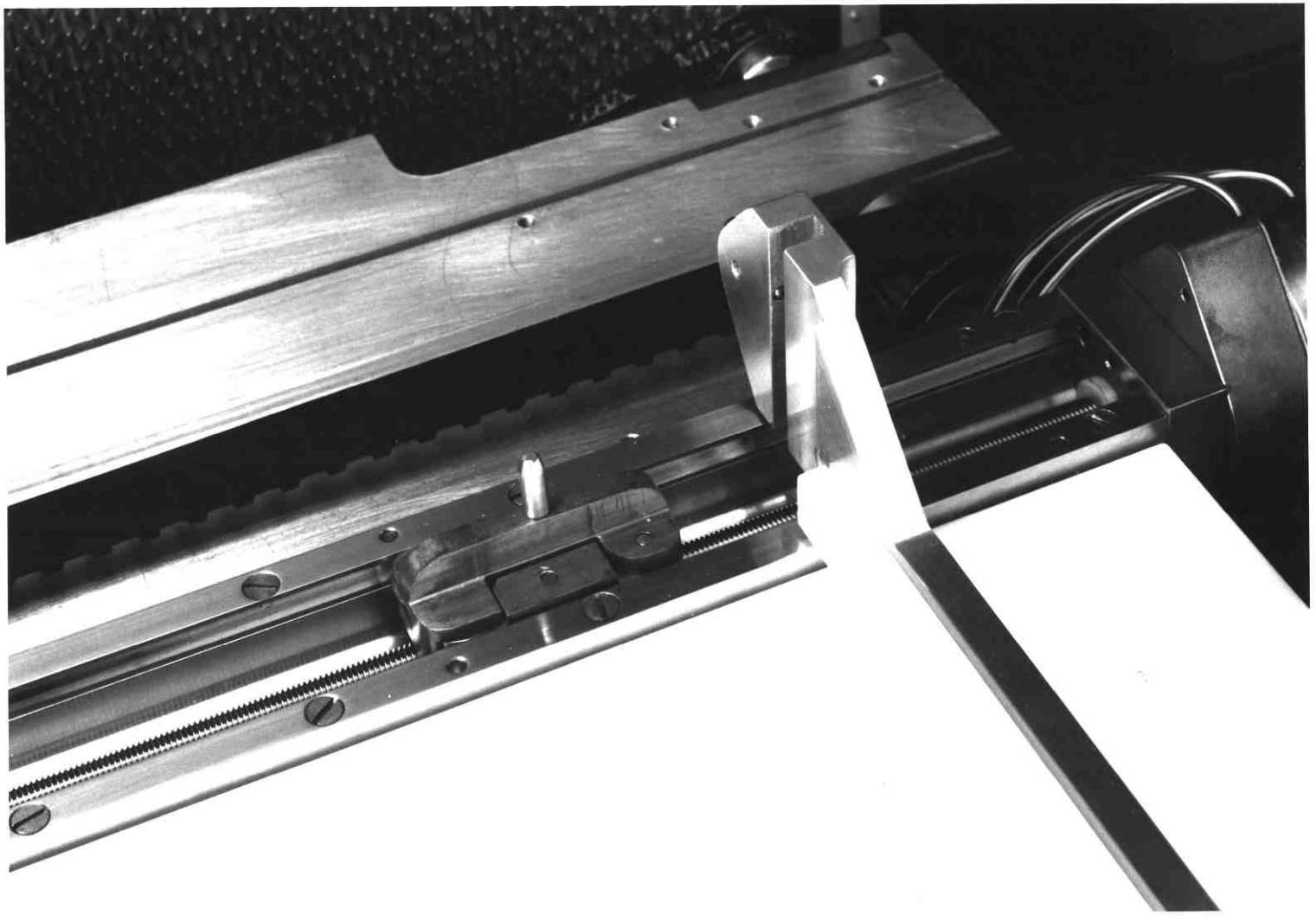

difficulties of non-zero contact angle with the Wilhelmy method are overcome by using filter paper (Whatmans No.1) for the plate material (Gaines 1977). A fresh filter is used for each new monolayer. The plates are all of standard size (3.Ø2cm wide and 2.ØØcm high) with identically positioned support holes and they are cut in a batch from a large sheet of filter paper using a metal template. Care is taken never to touch or otherwise contaminate the filters. The exact dimensions of the template itself are a matter of choice. However, it should be realised that the larger the perimeter of the plate, the larger the downward force on the spring for a given surface tension (see equation 2.2). With the design of filter plates described above, the force on the plate due to surface tension when suspended in a clean water surface at 18^{o}C is equivalent to a weight of 453mg compared with 15Ømg for the weight of the wet filter itself.

The plate is suspended beneath a length of Ø.25mm thick beryllium-copper, clamped at one end, which acts as a spring (see figure 3.5). The length of the spring, and hence its deflection per unit force, can be altered by moving the clamp along the beryllium-copper strip. The apparatus is arranged so that the vertical deflection of the spring is linearly proportional to the force on the filter; (verification is given in chapter IV). The core of a linear dc/dc transducer (SE Labs SE37Ø, ∓2.5mm calibrated stroke) is also attached to the end of the spring, variations in surface tension hence resulting in

Figure 3.5 Photograph of the Wilhelmy plate system showing the rectangular filter plate partially immersed in the surface and suspended beneath a spring, to which the core of the transducer is also attached. The main body of the transducer (cylindrical in shape) can be seen clamped in place above the filter.

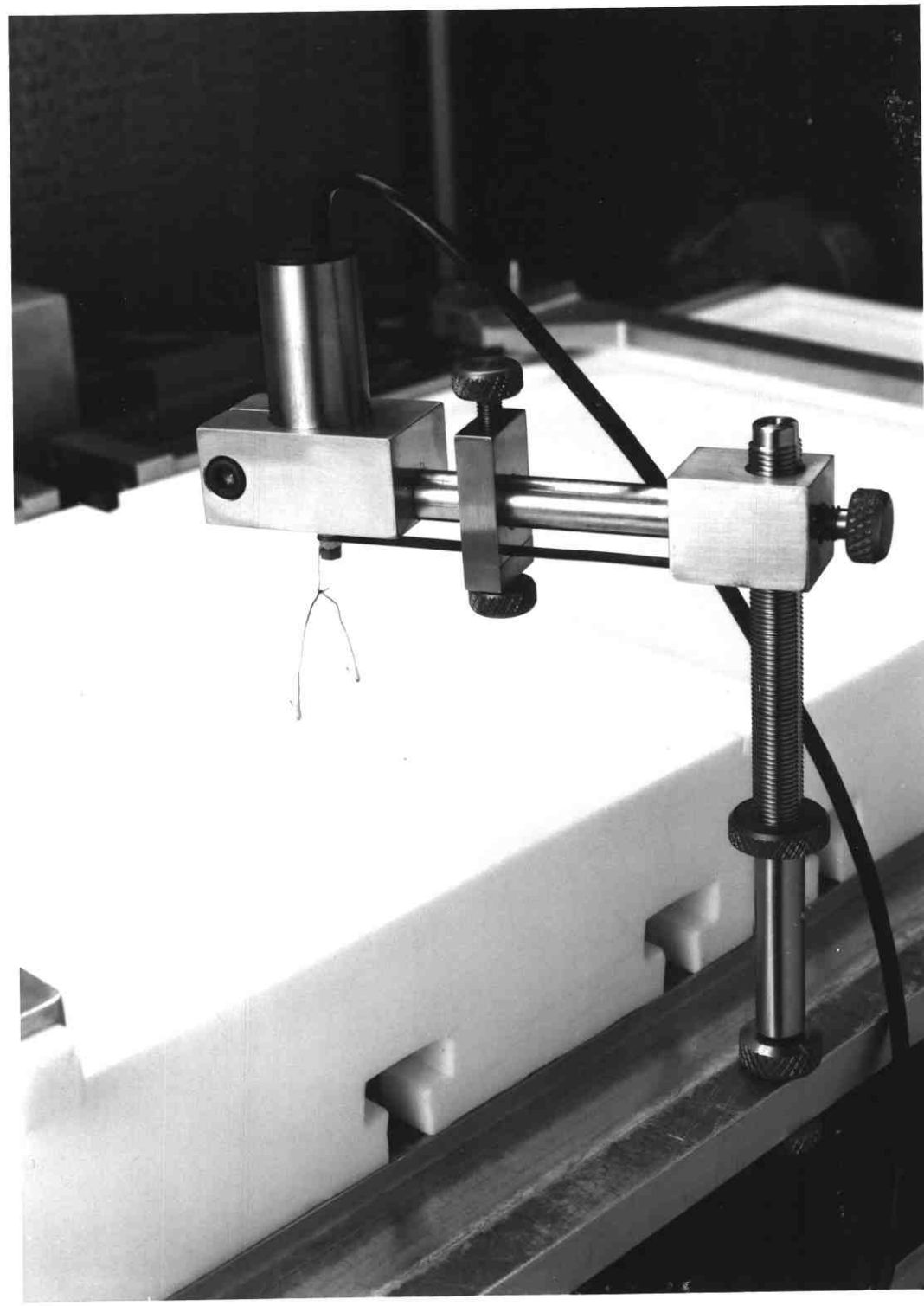

changes in the position of the core within the transducer, and therefore in changes in the transducer voltage output.

The whole assembly can be raised and lowered with respect to the trough by moving the supporting nut up a 1mm per turn screw thread. This method of smoothly moving the filter a known distance in or out of the surface was particularly important when measuring the change in bouyancy force with filter height in order to determine the apparent thickness of the plate (see chapter IV).

Dipper and Trolley

The substrate on which the multilayers are built up is "dipped" in and out of the trough by a lever and cam system designed to effect a constant vertical velocity of the substrate through the monolayer. The heart-shaped cam is turned by a multispeed servomotor, the speed of which is determined by the setting of two potentiometers on the control unit, one for the downward travel of the substrate and the other for the upward. The range of vertical speeds of the sample is from Ø.Ø6 to 15 mm/sec.

The bearings on the lever are all made of teflon to allow smooth motion without the possibility of contamination by lubricants. The dipper is mounted on a trolley which is pulled along the side of the troughs by a motor and timing belt. An electronic control unit has been built which causes the trolley to oscillate between the two troughs, dipping alternately in each and so building up asymmetric membranes. However, this experiment has not yet been attempted.

Control Unit for Surface Balance

The basic principles of the control electronics were developed by Dr Otto Albrecht and I am particularly grateful to him for his advice and his gift of preliminary sketches of the electronic circuits. A block diagram of the control system for the automated surface balance is shown overleaf in figure 3.6. This is followed by a photograph of the front panel of the control unit (figure 3.7).

The system can work in two modes, effectively a manual and an automatic mode. The switch controlling this is the toggle switch labelled "π constant/π-A curve". When switched to "π-A curve" the system is in the manual mode and the motion of the barrier is controlled by the four push buttons (stop, go, compress and expand). This is the mode used to measure pressure-area (π-A) isotherms. Switching to "π constant" mode causes the balance to automatically keep the monolayer at a pre-determined surface pressure and the push button switches are then overridden.

The surface pressure to be maintained is set using the reference pressure control. This fixes a reference voltage which is compared with the amplified transducer output.

The comparative circuit (see block diagram) produces three logical outputs (α, β and γ), the level of which depends on whether the pressure of the monolayer as measured by the Wilhelmy plate is below, above or the same as the reference pressure. These levels are described in

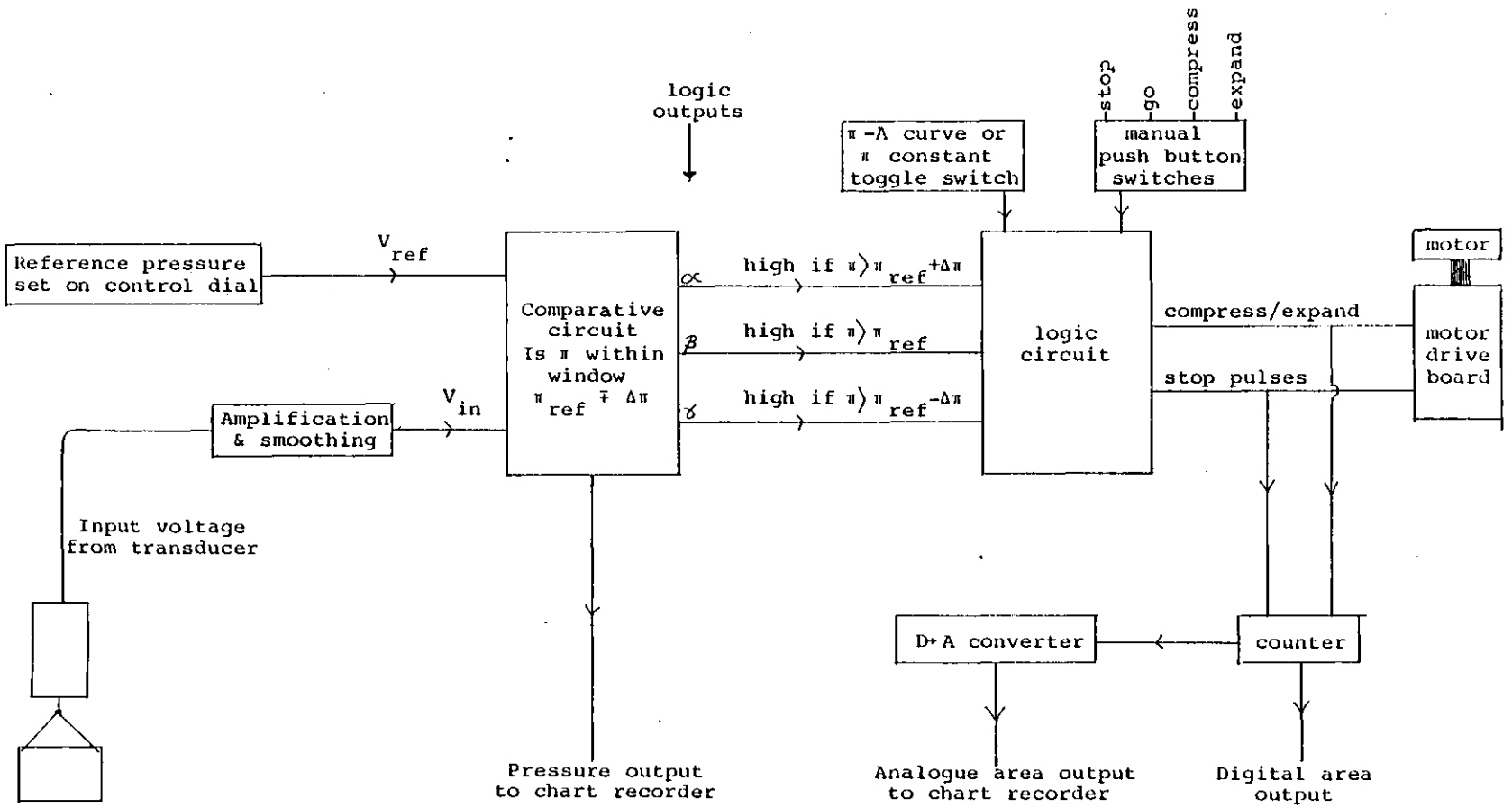

Figure 3.6 Block diagram of the electronic control system for the automated surface balance.

Figure 3.7 Photograph of the front panel of the control system for the automated surface balance.

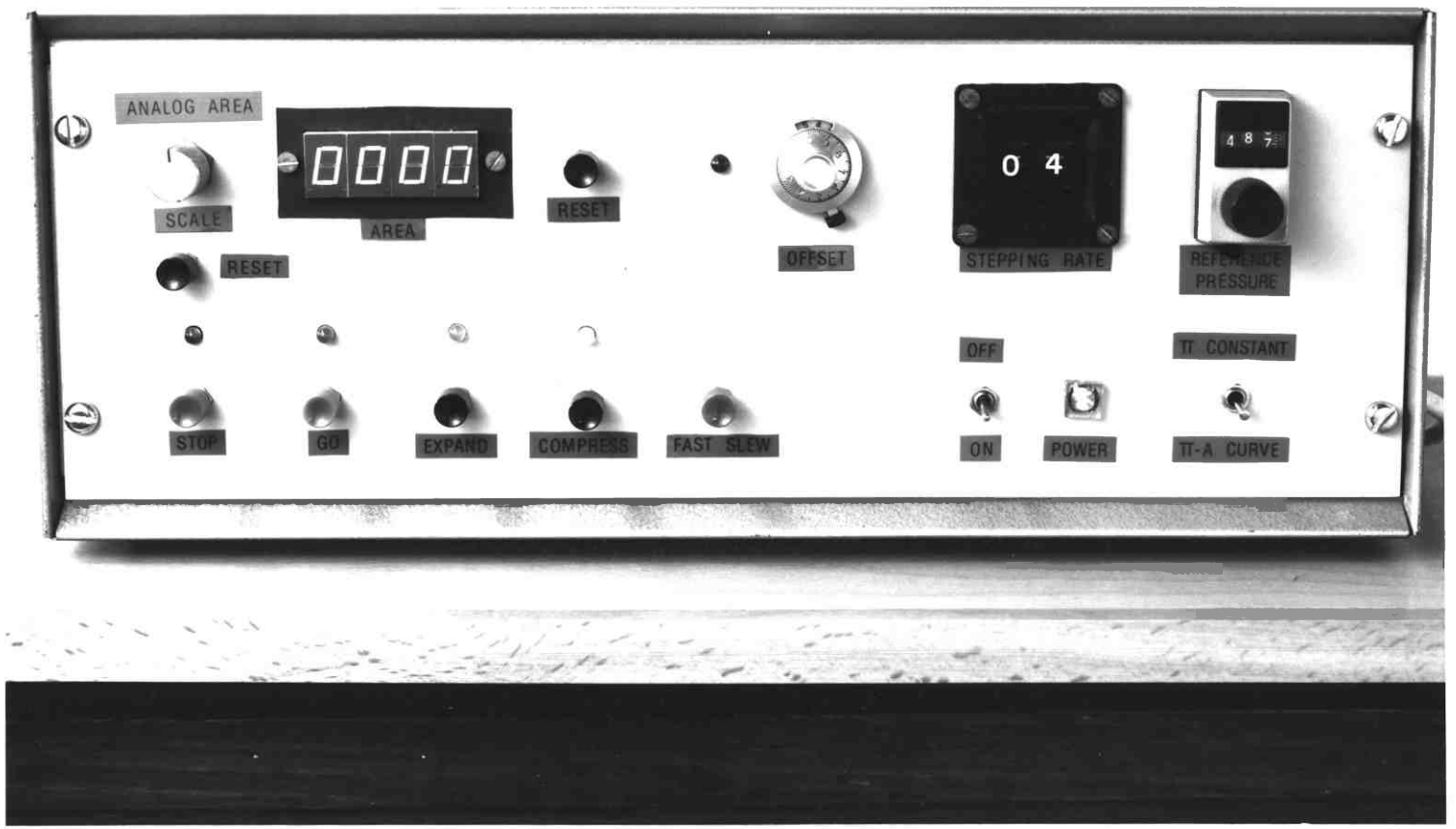
ANALOG AREA
SCALE
RESET
AREA
RESET
OFFSET
0 4
STEPPING RATE
REFERENCE PRESSURE
OFF
TT CONSTANT
STOP
GO
EXPAND
COMPRESS
FAST SLEW
ON
POWER
TT-A CURVE

table 3.1 below.

Output	Condition for switch in signal level	Action within logic circuit
α	$\pi_{in} = \pi_{ref} + \Delta\pi$	causes barrier expansion
β	$\pi_{in} = \pi_{ref}$	stops barrier
γ	$\pi_{in} = \pi_{ref} - \Delta\pi$	causes barrier compression

Table 3.1 The mode of action of the 3 logical outputs (α, β and γ) from the comparative circuit.

It should be realised that without the small pressure window ($\pi_{ref} \mp \Delta\pi$), within which π_{in} is considered equal to π_{ref}, the barrier would be in continuous oscillation and stability could never be achieved. The size of this pressure window is $\mp$Ø.2 dyne/cm.

The motor works by turning 7.5 degrees for every step pulse received, the direction of rotation depending on the logic level of the compress/expand control line. The frequency of the steps is determined by setting the thumbwheel switches on the front panel (labelled stepping rate in the photograph, figure 3.7). The action of the logic circuit is to control the output of signals to the motor drive board depending on the monolayer surface pressure as indicated by the three input levels.

The number of steps taken by the motor determines the change in area of the monolayer. The steps taken are therefore counted and output both digitally by the four 7-segment LED's on the front panel and as an analogue signal to the chart recorder.

CHAPTER IV

PERFORMANCE OF THE SYSTEM AND MAKING OF SPECIMENS

Once the automated system had been built, various tests were carried out on it to check its performance. These tests are reported at the beginning of this chapter. The rest of the chapter is concerned with the method for successful deposition of the multilayer samples.

The Wilhelmy Plate

As described in the previous chapter, the length of the spring and hence its stiffness can be varied by moving a clamp along the beryllium-copper strip. Too long a spring will result in a non-linear relationship between the force applied and the vertical displacement of the end of the spring. Too short a spring will result in the accuracy of the Wilhelmy plate being limited by the accuracy with which the transducer can measure very small displacements. In practice however, there was no difficulty in setting a satisfactory spring length.

The first test which was carried out once the Wilhelmy plate mechanism had been set up, was to check the linearity of the displacement of the spring with respect to the applied force. A light pan was suspended beneath the spring in place of the Wilhelmy plate. Calibration weights were added to the pan and the vertical displacement was measured using a travelling microscope. The results are reproduced overleaf in figure 4.1 and it

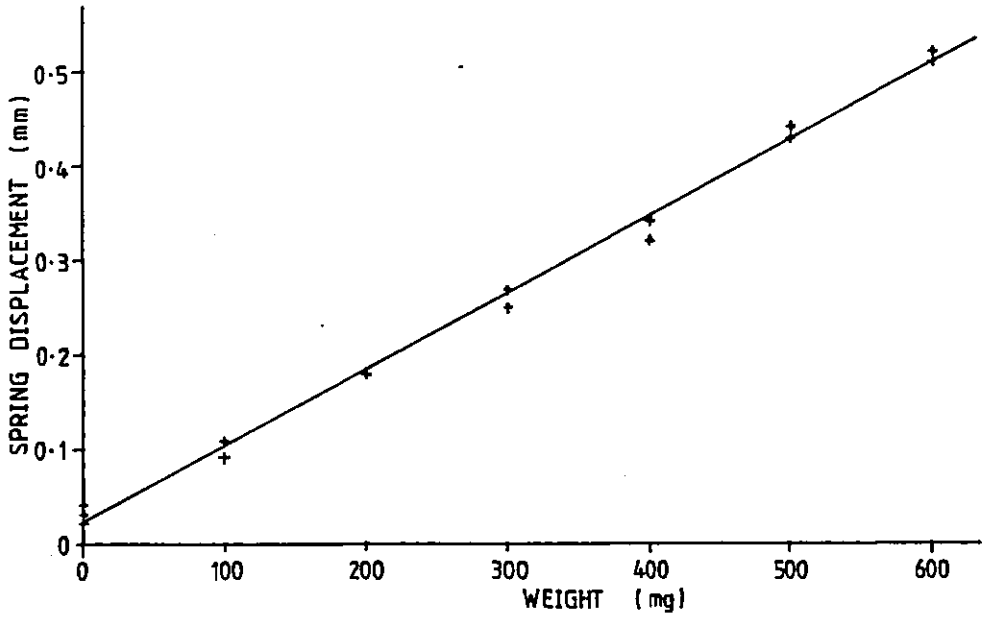

Figure 4.1 Graph of the displacement of the Wilhelmy plate spring as a function of the applied weight.

can be seen that, within the limits of experimental error (limited by the accuracy of the travelling microscope), the vertical displacement of the spring is linearly proportional to the weight added.

It should be noted that the calibration range is from Ø to 6ØØmg. As mentioned in chapter III, the width of the filter is 3.Ø2cm and the downward force on the plate when placed in a clean water surface at 2Ø°C is equivalent to a suspended mass of 453mg. A monolayer covered water surface has a lower surface tension and would hence exert less force on the plate. The weight of the aluminium pan (about 12Ømg) is comparable with that of the wet filter (15Ømg) and therefore Ø to 6ØØmg is a suitable range for calibration.

The next experiment was to check that the amplified transducer output is linearly proportional to the force on the spring. The method used was similar to the previous

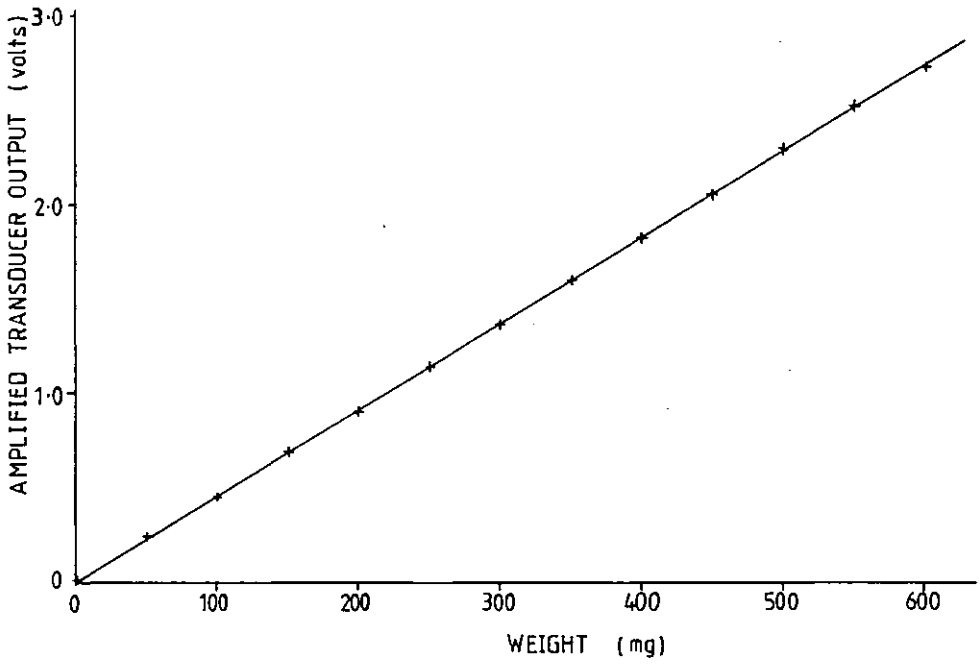

Figure 4.2 Graph of the amplified transducer voltage output (arbitrary origin) as a function of the weight applied to the Wilhelmy spring.

test in that calibration weights were added to the pan and the corresponding amplified voltage output was measured on a digital voltmeter. Figure 4.2 is a graph of the results and shows that, as expected, the transducer voltage output is linearly proportional to the applied force.

A measurement of the effective thickness of the filter Wilhelmy plate was also carried out. Equation 2.1 which describes the total downward force on the spring is reproduced below (the symbols were explained in chapter II).

$$F = \rho_p glwt - \rho_l gwth + 2\gamma(t+w)\cos\theta \qquad (2.1)$$

It can be seen that if the surface tension, the contact angle and the weight and dimensions of the plate all remain constant, the equation simplifies to

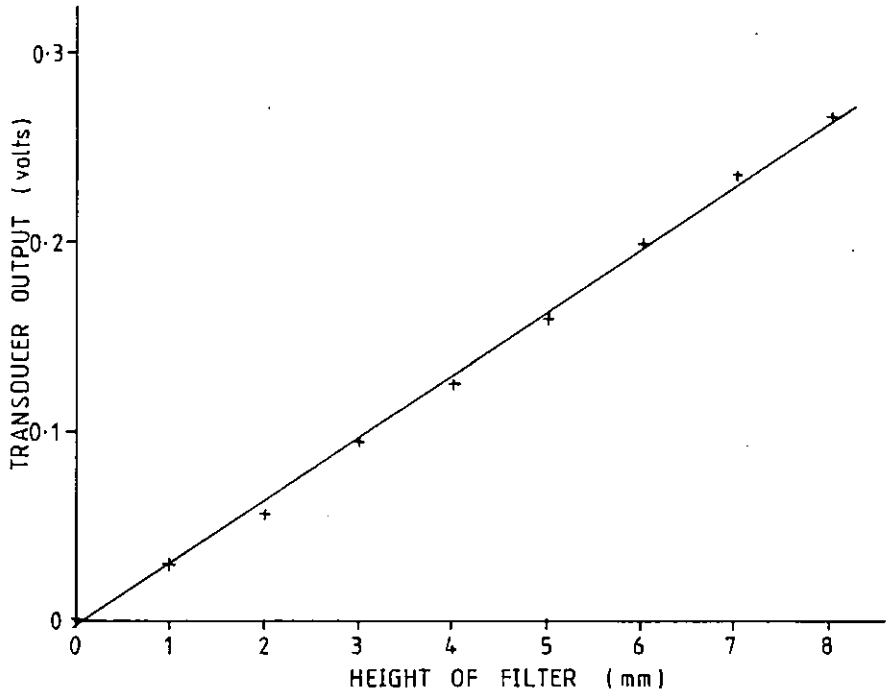

Figure 4.3 Bouyancy experiment - graph of the amplified transducer voltage output as a function of the height of the Wilhelmy plate with respect to the subphase surface.

$$F = -\rho_1 gwth + \text{constant} \qquad (4.1)$$

By measuring the change in the bouyancy force as the filter is raised and lowered through the water surface (so changing h), the effective thickness t can be calculated. The filter was raised and lowered in steps of 1mm by moving the whole transducer and spring assembly on the supporting screw up the 1mm per turn screw thread. A plot of the results is shown in figure 4.3. The calibration of voltage against force was achieved by placing a known weight on the filter support and measuring the change in voltage. Using the gradient of the graph and the calibration factor in equation 4.1 results in a value for the effective thickness of the filter paper of Ø.25mm.

The next experiment was to measure the surface tension of a clean water surface. The voltage was recorded as the plate just left the water surface (so h=Ø) and also when suspended freely above the surface. From the difference in voltage and knowing the dimensions of the filter, the surface tension was calculated. The results were found to be reproducibly high (76.5 ∓Ø.5 dynes/cm) compared with the expected value of 73.Ø5 dynes/cm at 18°C. This can be explained as drainage from the filter as it leaves the water surface and the effect of the weight of water in the meniscus, although no tests have been carried out to prove this theory. However this is not a problem when using the Wilhelmy plate to measure the surface pressure of a monolayer as the filter remains in the water surface throughout the experiment, being initially calibrated against the clean water surface before the monolayer is laid. This will be described in more detail later in this chapter under "Methods".

Barrier Mechanism and Control Electronics

The precision of the barrier mechanism was checked along the whole length of the 1mm per turn driving screw by stepping the motor 2ØØ steps at a time and measuring the distance travelled by the barrier using a travelling microscope. The results, which exhibit excellent linearity between the number of motor steps and the distance travelled by the barrier, are shown overleaf in Figure 4.4.

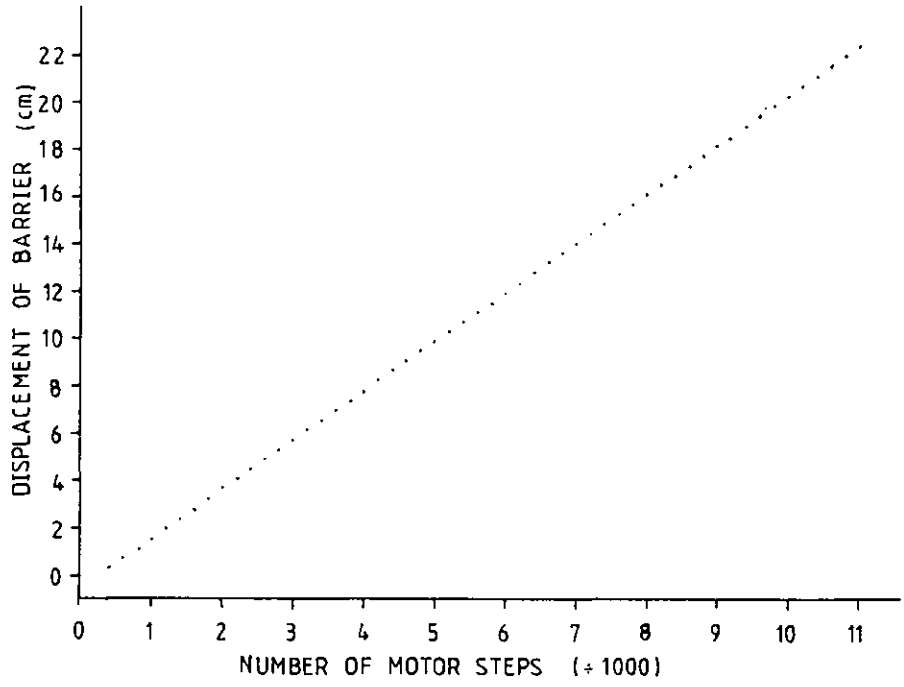

Figure 4:4 The linearity of the barrier driving screw - a plot of the displacement of the barrier as a function of the number of pulses received by the stepper motor (arbitrary origin).

The reproducibility of the area output was investigated by oscillating the motor back and forth and verifying that when the barrier returned to its original position, as determined by the travelling microscope, the digital area readout was unchanged. Before finally cleaning the trough assembly and siting it in the clean bench, the overall operation of the control electronics was tested by using a length of elastic fastened between the Wilhelmy balance and the stepper motor which acted as a pseudo monolayer. These two quick experiments brought to light a timing fault within the control unit which was corrected.

Once the trough had been carefully cleaned and finally assembled, I tested for leakage around the barrier itself by laying a monolayer, compressing it and then

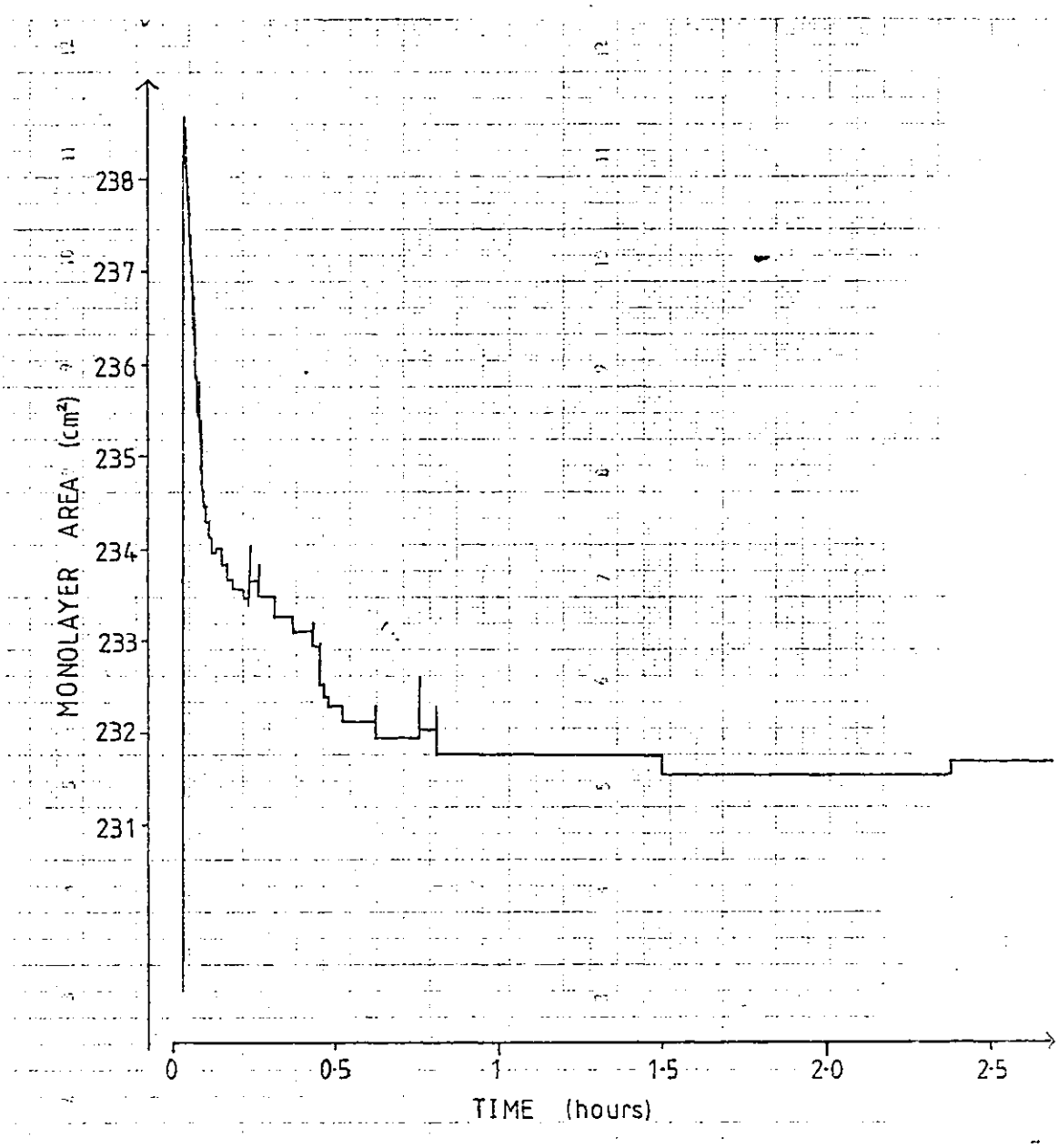

Figure 4:5 Chart recorder trace of monolayer area as a function of time for a cerebroside sulphate-cholesterol monolayer at a surface pressure of 40 dynes/cm above a 10μM $CaCl_2$ subphase. The initial decrease in monolayer area is due to stabilizing of the monolayer and evaporation of the spreading solvent.

observing the change in monolayer area with time at a constant surface pressure. Figure 4.5 shows the chart recorder trace of the area of a sulphatide-cholesterol monolayer at a surface pressure of 40 dynes/cm above a 10μM $CaCl_2$ subphase. As can be seen, after the initial stabilising of the laid monolayer, the area remained constant for over 1½ hours so the monolayer was evidently not leaking around the barrier. This test also shows that there was negligible evaporation or solution of the monolayer.

Constancy of Pressure during Deposition

As explained in chapter III, there is a pressure window of about 0.2 dynes/cm within which the pressure of the monolayer is assumed to be equal to the reference pressure and the barrier remains stationary. If the monolayer pressure drifts outside this window, the barrier expands or compresses accordingly. Figure 4.6 shows the two pen chart recorder output (pressure and analogue area) during one dipping cycle. The monolayer in this case is sulphatide-cholesterol at π=40 dynes/cm over a cytochrome c subphase and the dipper speeds are fast into the subphase (9.1 mm/sec) and then a slow withdrawal of the sample (0.08 mm/sec). The barrier stepping rate is 10 steps per second. It can be seen that the pressure is kept constant to within 0.2 dyne/cm throughout the cycle except during the fast deposition as the slide travels down into the subphase. This fast driving in of the slide is necessary for good deposition of these particular

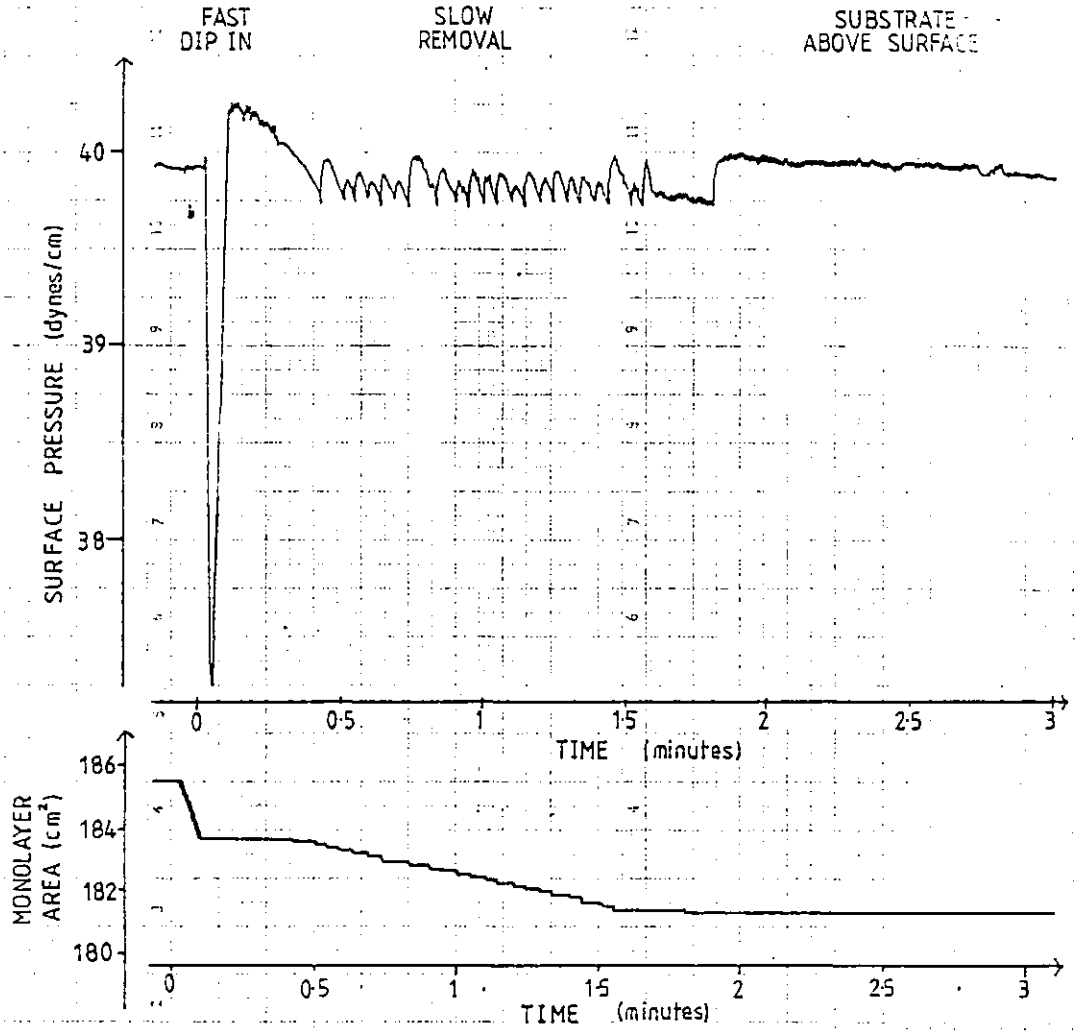

Figure 4.6 Chart recorder trace showing both pressure and analogue area outputs during one dipping cycle. The time scales of the two traces are slightly displaced from each other due to the staggered positioning of the pens on the chart recorder.

multilayers. When using the substrates of 2 cm^2 geometric area, the drop in monolayer pressure is initially about 2 dynes/cm as the sample travels down into the subphase. As the monolayer decreases in total area due to deposition, the drop in pressure rises to a maximum of 5 dynes/cm (see also figure 4.8).

I tried to overcome this drop in pressure by using a faster barrier stepping speed of 25 steps per second, but this had little effect except in causing oscillations around the reference pressure. The problem could probably be reduced by redesigning the control unit circuits to limit time delays. However, as the multilayers were being deposited successfully and diffraction patterns were being recorded, I did not feel it necessary at that time to try and improve the electronics.

Contamination

Before the surface balance was placed in the clean bench, it was disassembled and each piece thoroughly cleaned in Decon 90 solution, a laboratory cleaner, before rinsing with distilled water. The trough itself was cleaned in Decon 90 solution using a soft brush, care being taken not to damage the milled edges. It was then rinsed in copious quantities of distilled water and finally in deionised water. Once assembled, the trough itself has always been kept filled with deionised water to protect the surfaces from airborne surface active contaminants.

My method of checking for surface active

contamination is to place the barrier at the far end of the trough and monitor the surface tension of the subphase surface as the barrier is swept towards the Wilhelmy plate. If contamination is present, the surface tension will fall as the area available to the contaminant is decreased. If no measurable change in the surface tension occurs (i.e. γ is constant to within Ø.2 dyne/cm) when the barrier is swept as far as is allowed without touching the Wilhelmy plate, then I assume the water surface is free from contamination. When the clean bench fan is operating, a clean deionised water surface will stay uncontaminated for over half an hour.

Protein Denaturation

The technique described above is also used to investigate the extent of denaturation of proteins (in this thesis cytochrome c and basic protein) when dissolved in the subphase. A dilute aqueous solution of protein (2ØØnM, the same concentration as is used for multilayer deposition) is placed in the trough and the extent of contamination with time is observed. Cytochrome c is known to be a very stable molecule (Margoliash & Schejter 1966) and only begins to show surface contamination after one hour. Myelin basic protein evidently denatures more rapidly than cytochrome c at an air-water interface as it shows equivalent contamination after 1Ø to 15 minutes. I believe however that this rate of contamination is perfectly acceptable as a monolayer can be laid in a few minutes and the myelin basic protein is then protected

from the air-water interface, interacting instead with the monolayer itself. Of course, the protein can be injected underneath the surface once the monolayer has been laid to prevent denaturation at the air-water interface but this produces problems of how to stir the subphase effectively. I concluded that the method of quickly spreading the monolayer above a subphase already containing the protein was acceptable.

Method of Making Specimens

Materials

Deionised water obtained from a Milli-Q water purification system with a filter arrangement of a carbon filter, two ion-exchange filters, an Organex-Q filter and finally a Gelman Versacap Ø.2μ end filter was used throughout this experiment. This system was fed from a single stage super-four Fisons water still.

The cerebroside sulphate, (listed in the catalogue as sulphatides [bovine]), was purchased from Supelco Incorporated, Bellefonte, and the cholesterol and the cytochrome c (horse heart, type VI) were purchased from Sigma Chemical Company, Poole. The myelin basic protein (rabbit brain) was purchased from Calbiochem, La Jolla, USA.

Substrate

Both glass and aluminium can be used successfully as substrates for deposition of multilayers, but aluminium is

preferred as glass substrates produce strong diffuse X-ray scattering at around 4Å. The aluminium used for the substrates is Ø.1mm thick 99% pure aluminium foil purchased from Goodfellow Metals, Cambridge.

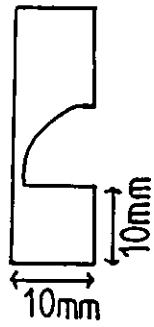

Figure 4:7 The design of the template used for the aluminium substrates.

The substrates are cut from the metal sheet using a template (see figure 4.7). The design of the substrate is a 1cm by 1cm square area on which the sample is built, joined to the supporting part by a narrow neck. There are two reasons for this style of substrate. The first is that the geometric area of the substrate available for deposition (a figure required for evaluation of the deposition ratio) depends on the depth to which the sample is dipped. Inaccuracies in the height of the sample with respect to the surface of the trough have proportionally less effect on the total deposition area with this narrow-necked design. Also, our preliminary experiments suggested that allowing the monolayer to reseal above the sample before the outward dip aids in the successful building up of multilayers.

Once the aluminium substrate has been cut to size, it is bent around a 6.8mm diameter glass rod. This curvature of the substrate is required so that when the sample is placed in the X-ray beam the Bragg diffraction conditions

for all the resolvable orders can be simultaneously satisfied; (see chapter V for further explanation).

The substrate is always cleaned before use by sonication in chloroform. It is then placed in the spring holder of the dipper arm with the outward curve of the sample towards the barrier. Before laying the monolayer, the clean substrate is inserted beneath the surface so that the initial layer is deposited on an upward dip. The reason for this is that aluminium is hydrophilic so it seems sensible to deposit the first layer in such a manner that the polar heads of the lipid molecules are in contact with the aluminium surface (see figure 2.5). However experiment has shown that multilayers can be deposited on aluminium equally successfully if the initial dip is downwards from air to water.

Method

The trough is always left clean and filled with deionised water after an experiment. This water is removed from the trough using an aspirator and is replaced by fresh deionised water which may contain quantities of protein, salt or buffer, if required. A fresh filter is hung on the Wilhelmy balance and the height of the plate assembly is then adjusted so that the filter is immersed in the subphase to a depth of about 5mm. The barrier is cleaned in deionised water and is carefully placed on the carriage ensuring that there is no gap between the barrier and the trough edges. The barrier is initially positioned at the Wilhelmy plate end of the trough so that the

subphase surface is swept clean as the barrier moves to the far end of the trough. This is only a precaution and additional sweeping of the surface was found to be unnecessary.

The Wilhelmy plate output, which is fed to a chart recorder, is then calibrated using the clean water surface to set the zero pressure point (π=Ø dynes/cm) and using a calibration weight of Ø.124Øg, which is equivalent to a surface pressure of 2Ø.Ø dynes/cm for our size filters, to set the scale. Once the pressure output has been calibrated and the required reference pressure has been set on the control unit, the monolayer is laid. The monolayer material is dissolved in a suitable spreading solvent, usually chloroform or chloroform-methanol in these experiments, and the solution is added to the trough surface drop by drop from a chloroform cleaned Agla all-glass micrometer syringe. The requirements of a good spreading solvent are that it should fully dissolve the monolayer material, be insoluble in the subphase and evaporate totally and rapidly from the trough surface. The concentration of the spreading solution (about 3mg/ml) is chosen so that about 5-1Ø drops will result in a monolayer with an initial surface pressure of 5-15 dynes/cm. The monolayer is then left for a few minutes to allow the solvent to evaporate before switching the control electronics to automatic mode and compressing to the reference pressure (4Ø dynes/cm throughout these experiments). If too little monolayer material is added and the surface pressure has not risen above 5 dynes/cm

before compression, the resulting compressed monolayer will be too small for deposition of many layers. If too much material is added to the surface, the monolayer may collapse or, conceivably, the high pressure may prevent evaporation of the spreading solvent.

Before dipping can begin, the monolayer must have stabilised. Throughout an experiment, the area of the monolayer is monitored on the chart recorder and when the area of the monolayer remains constant (within a few steps) for five minutes or so, dipping can begin. Stability usually takes of the order of 2Ø mins to achieve but this varies considerably depending on the composition of the monolayer and subphase.

The speeds at which the sample travels into and out of the subphase are set on two potentiometers on the dipper control unit. The speeds used are whichever result in successful deposition of multilayers and they are determined empirically for each material studied. A fast downward velocity of 9.1mm/sec and a slow removal of Ø.Ø8mm/sec were the speeds usually employed throughout these experiments. Once started, the dipper arm moves continuously up and down, changing speed at the top and bottom of its movement. However, as the total range of movement of the dipper arm is 25.4mm and the height of the sample is only 1Ømm, for 3/5 of the time (about 3mins per cycle) the sample is free of the surface. This few minutes wait before the next dip was found benefical to the building of multilayers. It is also important that, on switching from slow velocity to fast, the sample does

not begin to enter the subphase until the motor has accelerated to the correct speed.

Dipping continues until the required number of multilayers have been built up, usually 50-60 membranes for X-ray samples. The total dipping time for such a sample is about 5 hours.

Conditions for Successful Deposition

Throughout deposition both the surface pressure and the monolayer area are monitored on a two pen chart recorder. A complete trace of one experiment is shown overleaf (figure 4.8), annotated to point out the calibration of the pressure output, laying of the monolayer, compression, the wait for stability and, finally, the dipping. It must be noted that the pressure and the area trace are slightly displaced with respect to each other due to the staggered positioning of the pens on the chart recorder. The sample being deposited is CES-cholesterol-cytochrome c.

A plot of the deposition ratio for this substrate is shown in figure 4.9. As can be seen, more of the monolayer is picked up during the slow outward removal of the substrate than on the fast downward dip. It seems possible that the fast dip results in slightly patchy deposition, and the gaps are filled during the outward transfer, but this is only speculation.

Other multilayers besides CES-cholesterol-protein have been deposited, but not usually as successfully. In preliminary experiments using the waxed silk thread

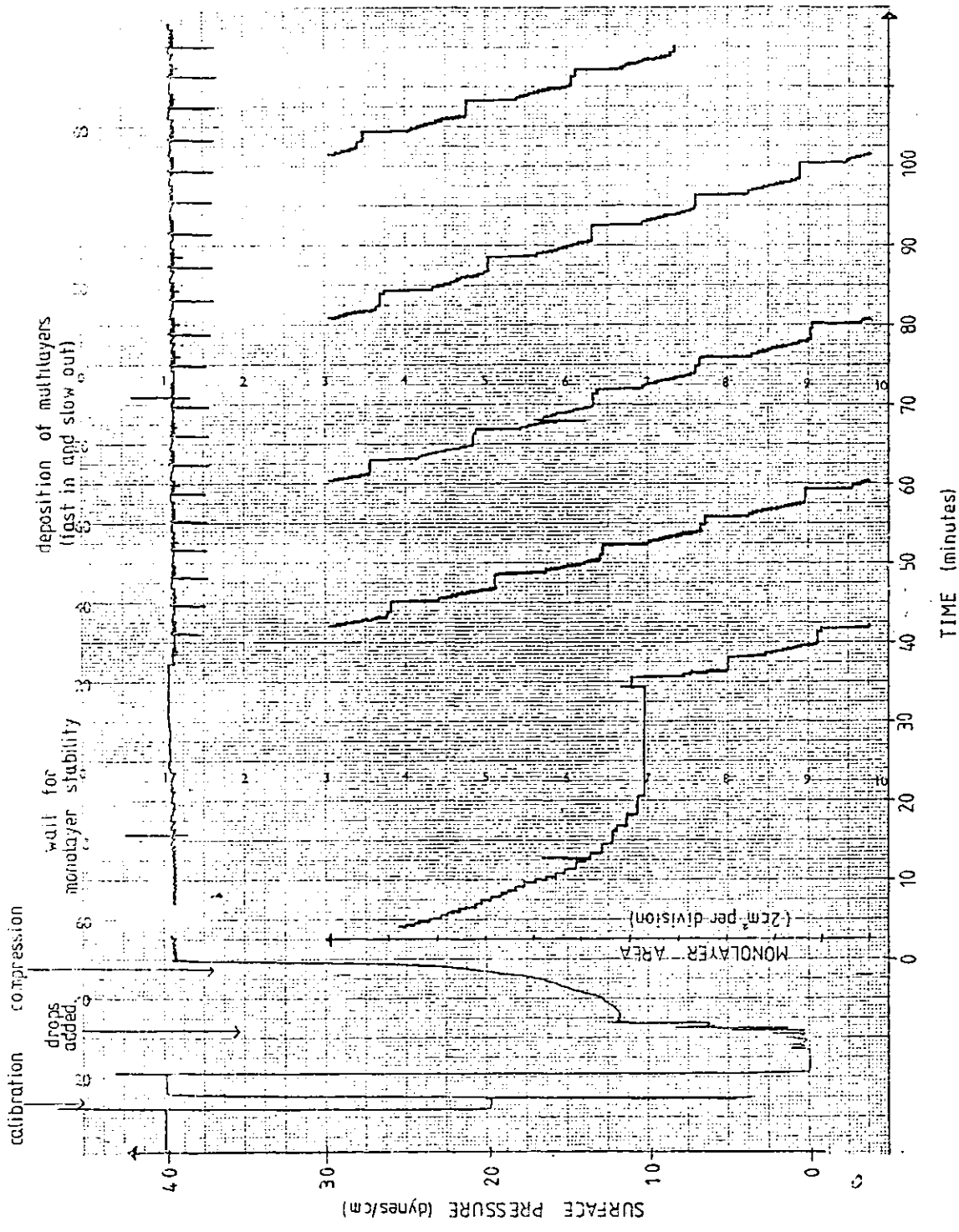

Figure 4.8 Annotated chart recorder trace from the production of one sample (only 21 bilayers). The time scales of the two profiles (area and pressure) are slightly displaced with respect to each other due to the staggered poisitioning of the pens on the chart recorder. Note that the monolayer area output resets every 11.Ø3cm^2.

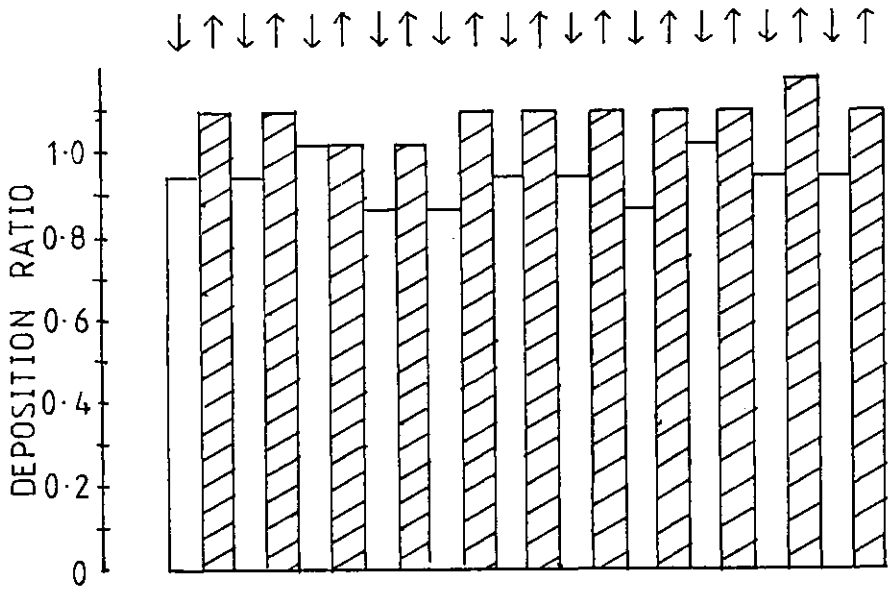

Figure 4.9 Plot of the deposition ratio for eleven cycles of the cerebroside sulphate-cholesterol-cytochrome c sample of figure 4.8. The downward or upward motion of the substrate through the monolayer is indicated by arrows.

method, multilayers of dipalmitoyl lecithin and of cerebroside sulphate were both deposited by dropping the substrate into the trough and then withdrawing slowly, using tetradecanol as the piston oil, which exerts a surface pressure of 43 dynes/cm. CES-cholesterol multilayers were also deposited by the same technique but deposition was uneven and the specimen so produced was very patchy. These samples had a tendancy for Z-type deposition particularly for the first few layers, in comparison with the protein-containing samples which were always deposited as Y-layers. Attempts were also made to build up dimyristoyl lecithin-cholesterol multilayers, but these proved unsuccessful.

The conditions for deposition of these multilayers were found empirically in each case and a few general points on these experiments are reported below. Firstly,

as previously noted in Katherine Blodgett's work with fatty acid multilayers (Blodgett & Langmuir 1937), additions of ions and, in our case, of proteins to the subphase, even in low concentrations greatly affects both the stability of the monolayer and the formation of multilayers. Both the CES and the CES-cholesterol multilayers were deposited using a 1μM calcium chloride subphase and, as previously seen, the inclusion of protein in the subphase results in a great improvement in the regularity and quality of deposition. The protein is evidently neutralising the charge on the monolayer and cross-linking it. An attempt was made to produce this same effect by placing 1Øμ M spermidine in the subphase beneath a CES-cholesterol monolayer. Spermidine, the structural formula of which appears in figure 4.1Ø, is a hydrocarbon chain with basic amino groups at each end and in the middle. However, instead of anchoring the monolayer, it causes collapse, even at the low surface pressure of 2Ø dynes/cm.

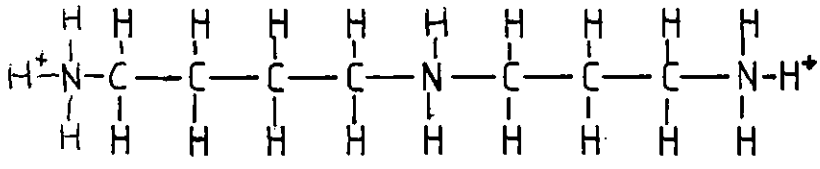

Figure 4.1Ø The structural formula of spermidine (N-[3-Aminopropyl]-1,4-butanediamine).

When determining the conditions for building up the multilayers, it is instructive to watch the meniscus as the sample enters and leaves the subphase. Figure 4.11, shown overleaf, explains the various terms used to describe the types of meniscus observed. In my

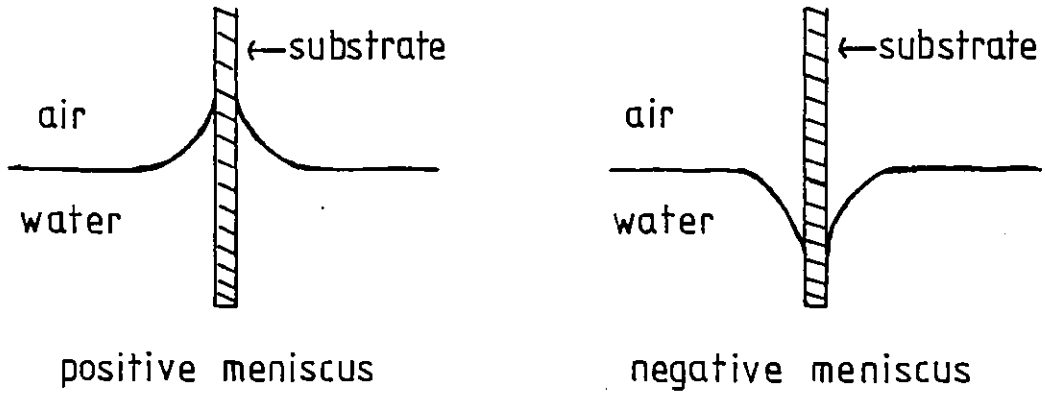

Figure 4.11 Diagram to demonstrate the definition of a positive and a negative meniscus.

experience, a good layer is only picked up on the downward dip if the sample is driven in fast enough to cause a negative meniscus, so causing the monolayer to fold back on itself (as shown schematically in figure 2.5). If the speed is too slow the meniscus becomes slightly positive and often seems to "crawl" or jump irregularly up the sample as the substrate is driven into the subphase. When this occurs the deposition is poor and often a layer actually peels off the substrate back onto the trough surface. For good deposition as the substrate travels out of the surface, the speed must be slow enough to allow the water to drain back from the sample. If the speed is too fast the sample will be wet on removal.

A further point noted in my experiments is that using a lower monolayer surface pressure, 30 dynes/cm instead of the usual 40 dynes/cm, results in poorer deposition. It must be realised that all the above observations are based on my experience with a limited number of monolayer materials and these generalisations may not apply to other systems.

Interaction of the Protein with the Monolayer

During the course of these experiments I have observed interaction of the protein with the uncompressed monolayer both for cytochrome c and for myelin basic protein. Figure 4.12 shows the change in surface pressure with time for a monolayer of sulphatide-cholesterol initially at 5.5 dynes/cm laid above a subphase of 200nM cytochrome c. It can be seen that an increase in surface pressure to 20 dynes/cm occurs over a time scale of about 5 minutes. This time scale is possibly determined by the rate of diffusion of the protein molecules to the interface.

During the preliminary experiments all protein interaction was allowed to occur before compressing to the final surface pressure. However, for the samples and results described in this thesis the monolayer was compressed almost immediately after spreading allowing only sufficient time (about a minute) for the solvent to evaporate. With this latter method any protein interaction which occurs will take place at 40 dynes/cm, the final pressure, as interaction at a lower surface pressure may not be reversible. It would be interesting to compare electron density profiles of membranes where protein interaction has occured at a low surface pressure before compression with those where interaction has only occured with the compressed monolayer.

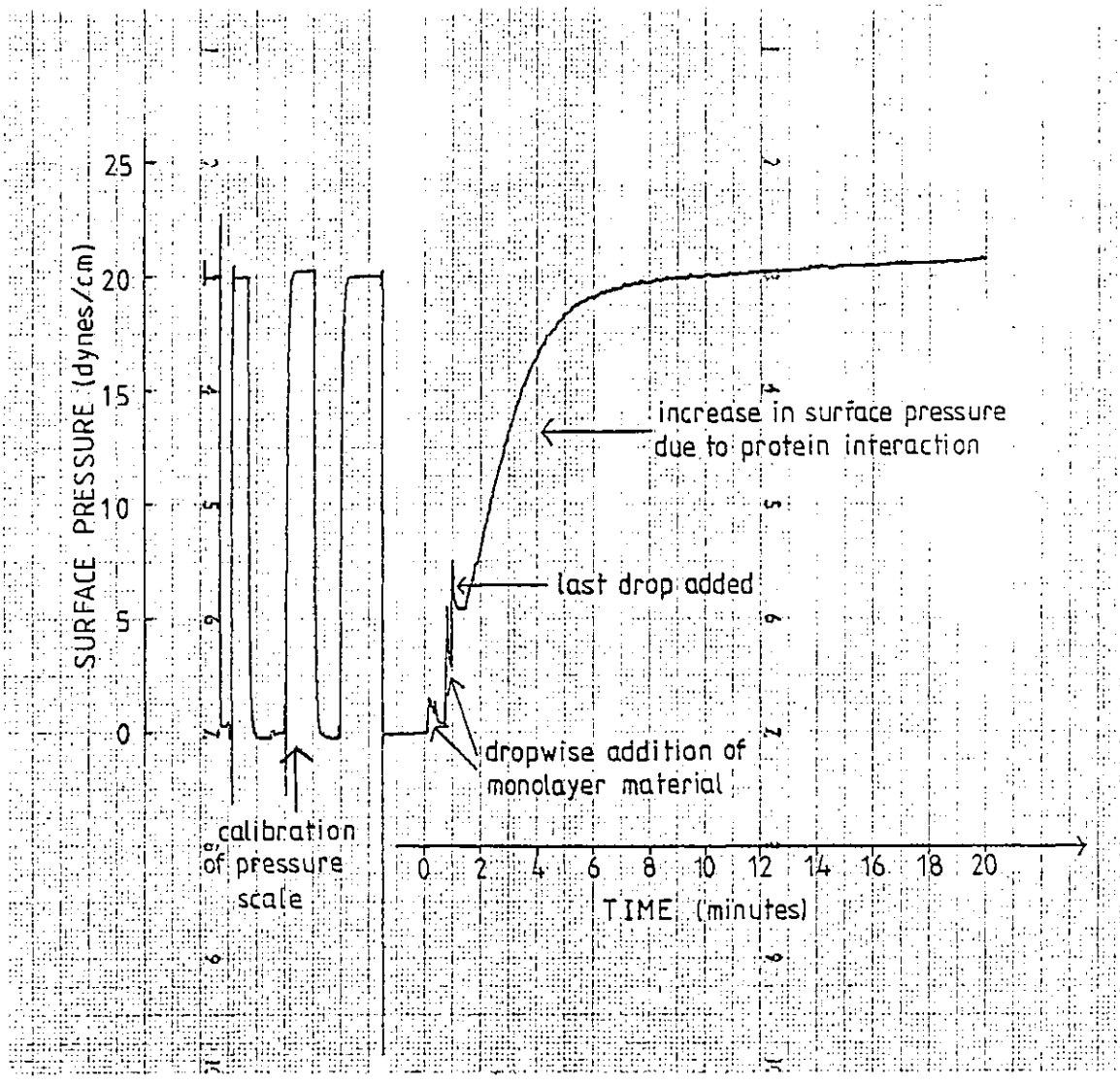

Figure 4.12 Chart recorder trace of monolayer surface pressure as a function of time showing the increase in pressure due to interaction of cytochrome c (at a subphase concentration of 200nM) with the CES-cholesterol monolayer.

CHAPTER V

LOW-ANGLE X-RAY DIFFRACTION EXPERIMENTS

Theory

The theory of low-angle X-ray diffraction will only be described here in sufficient detail to allow explanation of the diffraction method and results. For further information the interested reader is referred to Franks and Levine (1981) and Franks and Lieb (1981).

X-rays interact with the electrons in a structure and the amplitude of the scattered radiation from each region of the structure is directly proportional to the local electron density. The diffraction pattern results from interference between the waves scattered from the various regions of the structure and hence reflects the time averaged electron density distribution.

The relationship between the scattering structure and the scattered radiation is described in one dimension by the following equation.

$$F(R) = \int_x \rho(x) \exp(2\pi iRx)\, dx \qquad (5.1)$$

$\rho(x)$ is the electron density of the structure at a distance x from some arbitrary origin. R is the reciprocal space vector and is the coordinate used to describe the positions of reflections is the diffraction pattern. It is related to the scattering angle ϕ (the angle between the incident beam and scattered beam) by the relationship

$|R| = 2 \sin(\phi/2)/\lambda$. $F(R)$ is called the structure factor and defines both the amplitude and phase of the scattered radiation.

Equation 5.1 is a Fourier integral and therefore defines a unique and reciprocal relationship between the electron density $\rho(x)$ and the structure factor $F(R)$. The inverse relationship, also known as the inverse Fourier transform, is given below in equation 5.2.

$$\rho(x) = \int_R F(R) \exp(-2\pi iRx) \, dR \qquad (5.2)$$

Hence if $F(R)$ is known at every value of R then the electron density $\rho(x)$ can be obtained from the above relationship.

Unfortunately, in diffraction experiments it is not the structure factor $F(R)$ but the diffracted intensity $I(R)$ which is observed. The intensity is related to the structure factor $F(R)$ as follows;

$$I(R) = F^*(R).F(R) = |F(R)|^2 \qquad (5.3)$$

where $F^*(R)$ is the complex conjugate of $F(R)$ and $|F(R)|$ is the modulus of $F(R)$. Therefore by measuring the intensity of the diffraction pattern the amplitude of the scattered radiation is easily calculated, but all the phase information is lost. This is the well known "phase problem" and is the principle difficulty in the analysis of X-ray diffraction patterns. The phase problem is enormously simplified if the structure is centrosymmetric,

i.e. $\rho(x) = \rho(-x)$, since the allowed phases are then restricted to integral multiples of π only (see Franks and Levine 1981). These phase angles correspond to the structure factor having either a positive or negative sign.

Three-dimensional versions of the Fourier transforms (equations 5.1 and 5.2) exist, but for the study of membrane systems the one-dimensional form is usually sufficient. In general, membranes have only random structure in the plane of the membrane and it is only in the one-dimension perpendicular to the membrane plane that the time-averaged electron density profile is of interest.

Diffraction patterns can be taken using dispersions of single walled vesicles. These patterns are circularly symmetric and consist of very broad bands of continuous diffraction. However, throughout the experiments of this thesis, stacked membrane samples have been used, either multi-walled vesicles, evaporation samples or the Langmuir-Blodgett multilayer specimens.

The appearance of the diffraction pattern of stacked samples is very different from that of single walled vesicles, and consists of a series of sharp peaks, approximately equally spaced. These are commonly called Bragg reflections as the positions of these peaks are described by the well-known Bragg's Law.

$$2D \sin\theta = h\lambda \qquad h = \emptyset, \mp 1, \mp 2, \ldots \qquad (5.4)$$

where D is the membrane repeat distance, θ is the Bragg

angle (half the scattering angle between the incident and diffracted beams), h is an integer and λ is the wavelength of the radiation.

It is very important to note the inverse relationship between the Bragg angle θ and the spacing D in the structure. This is a general relationship in that long range structural periodicities of a membrane stack give rise to diffraction at low angles whereas the finer details of the membrane structure itself will give rise to diffraction at higher angles. In order to resolve the fine structural detail, the diffraction pattern must be recorded out to as high an angle as possible. The Bragg spacing corresponding to the highest observable reflection is said to be the resolution of the pattern.

In the context of X-ray diffraction experiments, the main difference between the multi-walled vesicle samples and the Langmuir-Blodgett multilayers is that the latter are oriented samples. There are two important advantages in using oriented rather than disoriented samples. Firstly, the Bragg diffraction rings recorded from disoriented samples will be concentrated into arcs (or even spots for perfect orientation) if the samples are oriented. The concentration of the diffracted radiation onto a smaller area of the film will reduce the recording time for a pattern and will increase the signal to noise ratio of the pattern thereby possibly increasing the resolution of the data. Secondly, diffraction arising from structure perpendicular and parallel to the membrane planes will be separated on the diffraction pattern. An

example of structure parallel to the membrane planes is the side by side packing of the lipid chains which produces diffuse equatorial diffraction at about 4.6Å.

Experimental Methods

Making the Lipid Samples

Dispersion Samples - Multiwalled vesicle samples of sulphatide-cholesterol are prepared in the following manner. The lipids and cholesterol are weighed out in the required proportions and are dissolved in chloroform with a little methanol. The organic solvent is evaporated under a stream of O_2-free N_2 and the sample is dried down overnight under vacuum. The lipid is then dispersed in 25mM calcium chloride solution, this ionic concentration being required to flocculate the lipids. The sample is transferred by syringe to a 1mm diameter thin-walled glass capillary tube and the lipid is spun down into a pellet at 2500 rpm for 2 minutes. The capillary tube is then sealed by flaming, the lipids being protected from oxidation by the aqueous layer.

Evaporation Samples - The lipid and the cholesterol are weighed out in the required ratio and are dissolved in chloroform-methanol as above. The excess organic solvent is then slowly evaporated under a stream of O_2-free N_2 until the solution becomes slightly viscous. A drop of the solution is than placed on a curved glass substrate (6.8mm in diameter) and the remaining solvent allowed to slowly evaporate. The sample is kept in a humidified atmosphere

at all times and is placed in the humidified X-ray specimen chamber as soon as the organic solvent has evaporated.

General Principles and Diffraction Geometry

The method for obtaining a diffraction pattern is conceptually very simple. The sample is placed in a collimated monochromatic X-ray beam and the diffraction pattern is recorded either on film or using a position-sensitive detector.

The X-rays are normally produced by bombarding a metal target with electrons. The radiation produced consists of a few high intensity sharp spectral lines at wavelengths characteristic of the metal target superimposed on a continuous background. This radiation is then collimated by passage through a series of slits. It may be focused using mirrors or passed through a monochromating crystal or through filters. Whatever the methods employed the object is always to produce a collimated X-ray beam at a single wavelength.

The beam then passes through the sample. As mentioned earlier in this chapter, diffraction can only occur when the Bragg condition is satisfied and therefore only when the stacked bilayer planes are oriented at certain angles to the incident beam. In order that the Bragg condition can be satisfied for all the resolvable orders simultaneously, the membrane stacks in the sample must have a range of orientations. For a multiwalled vesicle sample this condition is evidently satisfied since all

angles between bilayer planes and the incident beam are equally likely. For oriented samples it is necessary either to build the sample on a curved support or to rotate a flat sample in the beam in order to obtain the required range of angles. The Langmuir-Blodgett multilayer samples are always built on a curved substrate for this reason, as described in chapter IV. Figure 5.1, which appears below,illustrates the diffraction geometry for a curved substrate.

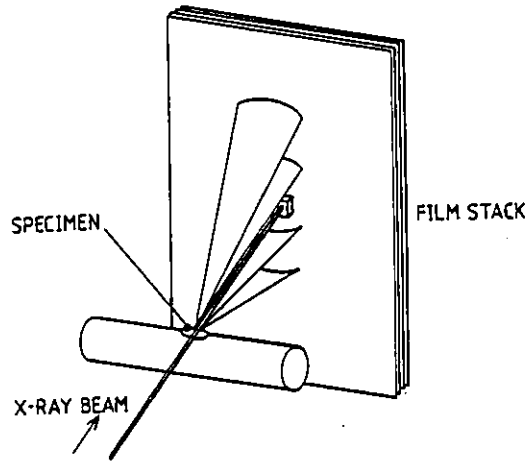

Figure 5.1 The diffraction geometry of an oriented lipid sample (from Franks & Lieb 1981).

The distance between the sample and the film (known as the specimen-to-film distance) can vary, but in our experiments it is about 54mm for the dispersion samples and 74mm for the Langmuir-Blodgett specimens. The main beam is far more intense than the diffracted beams and will overexpose the film and obliterate the diffraction pattern if it is not absorbed by a lead backstop placed in front of the film. The specimen-to-film distance must therefore be large enough so that the first order is clearly separated from the backstop shadow on the

diffraction pattern. A large specimen-to-film distance results in better resolution between reflections from two phases of similar but not equal spacing and also increases the signal to noise ratio of the pattern. However, the distance between specimen and film is limited because the time taken to record a diffraction pattern increases as the square of the distance. The space between the specimen and film must be evacuated or filled with helium because air will strongly scatter the X-rays producing a high background on the film.

The geometry relating the radii of the Bragg reflections (r) to the Bragg angle (θ) is illustrated below in figure 5.2.

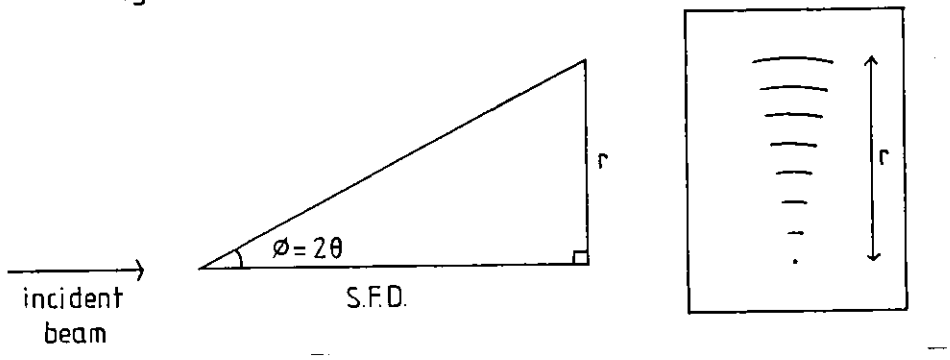

Figure 5.2 Geometry relating the radius of a Bragg reflection (r) to the Bragg angle θ (ϕ is the scattering angle and SFD is the specimen-to-film distance).

It is evidently necessary to know the specimen-to-film distance in order to calculate the Bragg angles corresponding to the reflections recorded on the film. This can be directly measured but it is more accurate to sprinkle onto the sample a standard such as calcite, which diffracts strongly at a known scattering angle.

The Apparatus and Methods used in these Experiments

Generator and camera - The X-rays are produced by an Elliott rotating anode X-ray generator. The filament current used is usually 20mA and the electrons are accelerated by a voltage of 30kV. The anode is copper so about 85% of the characteristic energy is in the Kα spectral line at 1.54Å and most of the rest in the Kβ line at 1.39Å.

The diffraction patterns in this thesis were taken on one of two different focusing cameras. The first is a point-focused "toroid" camera in which the X-rays are focused by a toroidal mirror made of glass. The beam then passes through a series of carefully shaped masks to remove background scattering and so "clean up" the beam. A nickel filter .0125mm thick is placed in the beam as it absorbs most of the Kβ radiation with tolerable reduction in the intensity of the Kα radiation. The focusing mirror and masks are all contained in a helium chamber to prevent scatter and the exit window is made of 6μ aluminium to minimize absorbance.

The second type of focusing camera is the line-focused single-mirror camera. This camera was designed specially for use with the highly oriented Langmuir-Blodgett specimens. A single elliptical mirror is used to focus the beam in the horizontal direction and lead slits are used to absorb background scattering and to define the beam length, resulting in a line-focused beam about 3mm high and 80-100μ wide. The focusing mirror is nickel

coated as this produces a focused beam of greater intensity than a glass mirror and has the added advantage of absorbing most of the Kβ radiation so overcoming the need for a nickel filter. The angle of the camera is set up so that the unfocused beam is incident on the mirror at the critical angle (about $\emptyset.4^{o}$ for nickel) and therefore all the short wavelength background radiation is absorbed.

The Sample - When setting up the sample in the beam it is important to know exactly where the beam is. This is accomplished by placing a fluorescent crystal in the path of the beam, focusing a telescope onto the crystal and then setting the crosswires of the telescope to define the beam position. This is particularly useful when aligning the Langmuir-Blodgett specimens as the sample must be parallel to the line-focused beam. Once the sample has been oriented parallel to the beam it is then moved into the beam until 50% of the incident intensity is absorbed, as measured by a Geiger counter. The lipid evaporation samples are similarly moved into the beam but only until 30% of the beam is absorbed as this was found empirically to give stronger diffraction. The dispersion specimens, which are contained in thin glass capilliary tubes, are aligned using the crosswires of the telescope.

The Langmuir-Blodgett specimens and the evaporated lipid samples are contained in humidified specimen chambers throughout a diffraction experiment. The chamber windows are made of 6μ aluminium foil (Beryllium would be preferable as it does not produce any coherant scatter at

low angles but it is, unfortunately, destroyed by high humidities). The chamber is kept humidified by bubbling helium through water or a saturated salt solution and then passing the moist gas through the chamber. A filter soaked in water or salt solution is also kept in the chamber to help maintain the required humidity throughout the exposure (the time for an exposure is often 15-20 hours). A table of the salt solutions used and their relative humidities is given below in table 5.1. Distilled water was used when the required relative humidity was 100%.

Saturated Salt Solution	Relative Humidity at 25°C
KH_2PO_4	97%
K_2CrO_4	88%
KCl	86%

Table 5.1 The relative humidities above various saturated salt solutions at 25°C (from O'Brien 1948).

Maintaining the humidity of the sample is a crucial and often difficult task. Samples are often destroyed by too dry an atmosphere and some seem to lose their lamellar structure if condensation forms on them (observed with CES-cholesterol evaporation samples). Also any change in the water content of a multilayer sample during an experiment will have the same effect as a disordered sample, the Bragg reflections being broadened and therefore the resolution of the pattern probably being reduced.

The temperature of the room containing the X-ray set is maintained using a temperature control unit within ∓1°C throughout an exposure. The mean ambient temperature is 23°C. I made various attempts to control more accurately the temperature of the specimen by encasing the sample chamber in a temperature controlled copper yoke. However, although by this method the temperature could be maintained within ∓Ø.2°C, it always led to difficulties with the humidity of the sample either by producing humidity variations during the exposure or by causing condensation to form on the specimen or on the chamber windows.

The specimen-to-film distance is determined by sprinkling calcite onto the sample as a standard. I have had some indication, although certainly not conclusive, that the addition of calcite to my protein containing samples may induce disorder and so the calcite is now added to the sample only for a final calibration exposure once all the data sets have been recorded from the specimen.

Backstop Cone - Between the specimen chamber and the film pack there is a cone which is filled with helium to minimise scattering of the X-rays. The cone used with the toroid camera is 50mm long and that used with the single mirror camera is 60mm long. On the window nearest to the film pack is attached the lead backstop which absorbs the main beam. The shape of the backstop is obviously very different for the line focused and the toroid cameras.

The Film Pack - Throughout these experiments film has been used to record the diffraction data. A position-sensitive detector has recently been set up and this has two main advantages. Firstly, the diffraction data can now be recorded far more quickly than before; in a matter of minutes instead of many hours. Secondly, the results are produced immediately and in a form suitable for feeding directly into the computer whereas film requires developing before the results are apparent and then it must be scanned on a densitometer to convert the data into a computer analyzable form. However, I would strongly recommend the continued use of film in conjunction with the detector as film can record far more information than a one- dimensional detector. If a diffraction pattern is recorded on film, poor alignment of the sample (e.g. A Langmuir- Blodgett specimen not being parallel to the line focused beam) is immediately obvious. The degree of disorientation in a specimen, the presence of cholesterol separation and the nature of the lipid chain diffraction are also more easily determined using film.

The diffraction patterns of this thesis have all been recorded on high-speed Reflex 25 film obtained from Ceaverken, Sweden. The exposure times required for collection of one data set varied from 6 hours for some evaporation samples to 15-20 hours for Langmuir-Blodgett specimens. A stack of 7 to 12 films was used for each data set, the exact number depending on the type of specimen. A stack of films is required because some diffraction orders, particularly the first, are much more

intense than others. As the blackening of the film is linearly proportional to the incident intensity only up to a certain level,on a film on which the low intensity orders are visible, the high intensity orders are over exposed. Each film in the stack absorbs a certain fraction of the radiation incident on it and the ratio of the incident intensity to the transmitted intensity for one sheet of film is known as the film factor.

Analysis of the Diffraction Patterns

The first step in the analysis of a diffraction pattern is always a thorough study of the film itself to define the origin of the various structures in the pattern, such as the lamellar diffraction from the specimen, the diffraction from the aluminium substrate or windows and the calcite diffraction, if it exists. If the orders were very broad due to humidity variations or disorder in the sample, or if more than one phase was present, further analysis was not be justified and a new sample was prepared. The radii of the diffraction maxima were then measured using a Mitutoyo PJ-25ØC projecting microscope and, once the specimen-to-film distance was known, the lamellar spacing of the membranes was calculated. If the data set was to be analysed to produce an electron density profile, the intensity of the films was measured on a densitometer. The X-ray films of this thesis were scanned on a Joyce Loebl Scandig 3 micro-densitometer controlled by a Data General Nova 3 computer

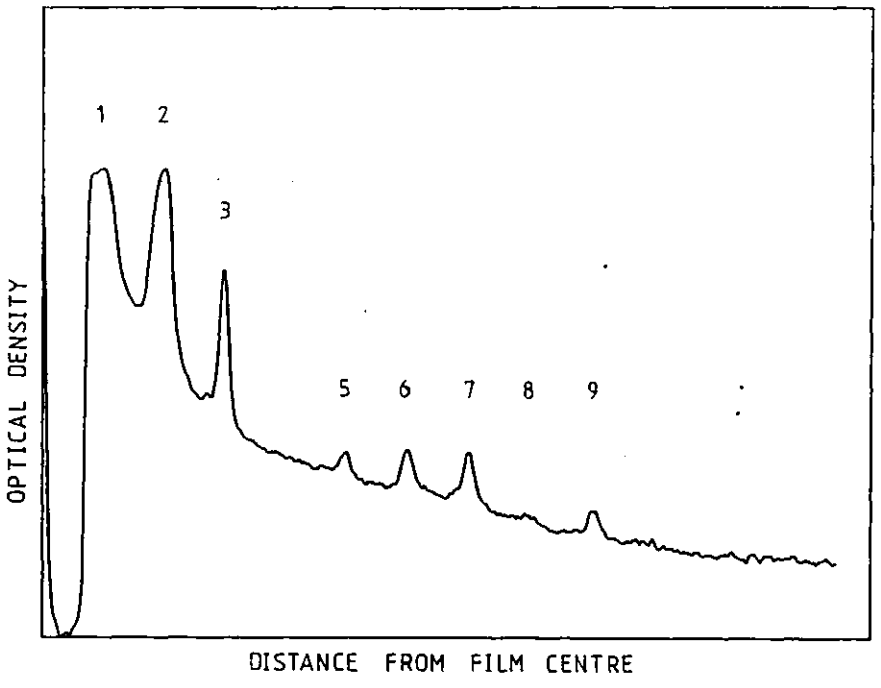

Figure 5.3 An example of a densitometer trace for the second film of a set of films. The peak on the far left of the trace is the centre of the pattern, defined by removing the backstop and allowing the main beam to hit the film for a few seconds. The first three orders were found to be overexposed on this film. [Sample is a Langmuir-Blodgett specimen — CES-cholesterol-cytochrome c].

using a 25μ raster step. Depending on whether the pattern was taken using the toroid or the line-focused camera, the intensity distribution was integrated around an arc or along a line respectively to yield a one-dimensional optical density distribution as a function of radius. An example of such a densitometer trace is reproduced in figure 5.3.

The intensity for each reflection was then obtained by summing the total intensity beneath each peak and subtracting the background. As already explained each data set contains many films, the weak orders being measurable on the top film and the stronger orders on the lower films. Because of the non-linearity of the films

above a certain level, any reflection containing a point with a optical density greater than 1.4 was measured on a lower film.

The measured intensities were next corrected for a variety of factors using the formula given below (equation 5.5),

$$I_c(h) = I_o(h) \frac{h\, A_f^{(n-1)/\cos 2\theta}}{\frac{1}{2}[1 + \cos^2 2\theta]} \qquad (5.5)$$

where $I_c(h)$ is the corrected intensity, $I_o(h)$ is the observed intensity, h is the order number of the Bragg reflection, n is the number of the film, A_f is the film absorbance factor as described earlier in this chapter and θ is the Bragg angle. No specimen absorption correction (Franks & Lieb 1979) was included because the oriented samples used, particularly the Langmuir-Blodgett specimens, were so thin.

The film factor A_f can be measured directly (see Franks & Lieb 1979) or an experimental value can be obtained by comparing the optical density for one reflection on two adjacent films. The value of the film factor of A_f=3.Ø5 (σ=Ø.15) which has been used throughout this thesis is an average of thousands of such experimental values measured in the course of protein crystallography investigations. Of course, the wavelength and the type of film used in the protein crystallography investigations were the same as in our experiments. An average experimental film factor, which had a large error due to the relatively few values in the average, was also

calculated from our own data and it agreed with the crystallography value within error limits. The protein crystallography data used in calculating the film factor was collected and analysed by Dr A. Leslie. The exponent $n-1/\cos 2\theta$ of the film factor in equation 5.5 is due to the increase in path length through the films with increasing film number and diffraction angle.

The factor h in the numerator of equation 5.5 is the Lorentz correction and takes into account the spreading out of the diffraction in reciprocal space due to the disorientation in the specimen. In the case of a point-focused diffraction pattern from a lipid specimen the disorientation perpendicular to the X-ray beam results in spreading out of the diffraction into arcs or circles on the film. This is taken into account during measurement of the film by integrating the total optical density around the arc or circle. Disorientation in the beam direction is accounted for by the correction factor h as the higher orders are spread out over a larger area in reciprocal space than the lower orders. The Langmuir-Blodgett specimens are, effectively, perfectly oriented perpendicular to the X-ray beam and so no correction factor is required even with the line-focused patterns which are integrated along a line. However, in the direction of the beam the specimen has been deliberately "disoriented" by curvature of the substrate in order to satisfy the Bragg condition for the higher orders. The correction factor of h is therefore also required for the Langmuir-Blodgett specimens.

The $\frac{1}{2}[1 + \cos^2 2\theta]$ factor is the polarisation correction. This is a minor correction at low angles but is needed because the electrons in the sample do not scatter the incident radiation isotropically.

The structure factor amplitudes $|F(R)|$ were then calculated from the corrected intensities. The phases of the structure factors were assigned as described in chapter VII. Then, using the inverse Fourier transform, or rather the form of this equation referring to a regular stack of centrosymmetric structural units (equation 5.6), the one-dimensional electron density profile was calculated.

$$\rho(x) = F(\emptyset)/D + 2/D\sum_{h=1}^{h_{max}} F(h/D)\cos(2\Pi hx/D) \qquad (5.6)$$

The variables in this equation have the same meanings as before, $\rho(x)$ is the one-dimensional electron density distribution across a single membrane and h_{max} is the maximum resolvable Bragg order in the diffraction pattern. $F(h/D)$ are the various structure factors, the amplitudes of which are measured from the diffraction pattern and the phases of which (positive or negative) are assigned. The first term, $F(\emptyset)/D$, is the mean scattering density over the repeat distance D. Since $F(\emptyset)$, the zeroth order structure factor is proportional to the amplitude of the radiation scattered in the same direction as the main beam, it cannot be experimentally observed. However this value affects only the mean level of the electron density profile and does not change the profile shape.

CHAPTER VI

CHEMICAL ANALYSIS OF THE SAMPLE

The X-ray diffraction studies on a sample produce electron density profiles of the bilayer. However, this is not, in itself, sufficient to determine the position of the various components within the bilayer. Before attempting to assign the various levels of electron density to the chemical constituents, it is necessary to know both the relative proportions of the components present in the bilayer (i.e. cerebroside sulphate, cholesterol, protein and water) and also their respective electron densities.

The main difficulty of the chemical analysis lies in the small amount of material present in the sample. The X-ray samples are of $2cm^2$ geometric area and consist of about 50 membranes. An average sample contains about 50µg of lipid and 20-40µg of protein, but since all the analyses must be carried out on the same sample, the amount of material available for any particular analysis is only part of the total material present.

The methods used in the chemical analysis of the samples are, briefly, as follows. The CES to cholesterol ratio is determined by weight ratio when the monolayer spreading solution is prepared. The amount of cholesterol present in the sample is ascertained using radioactively labelled cholesterol in the sample. A satisfactory method of measuring the protein content of the sample was

particularly difficult to develop with our small samples and various techniques were tried and rejected. The method now used is a modified micro-Kjeldahl total nitrogen determination. A non-destructive radioactive diffusion technique will hopefully prove successful in determining the water content of the sample, but this is still being developed.

Protein Determination

As already explained, the Langmuir-Blodgett specimens contain about 20-40µg of protein. Before analysis, the sample is removed from the substrate by sonication in a detergent solution (1% Triton X-100). The resulting solution is of low protein concentration (0.03mg/ml) and this was of prime consideration in the search for a suitable protein analysis. Also protein analyses are often interferred with by the presence of other substances such as lipid, salts or detergent, and this was another factor to be considered.

The Dye-binding Technique of Esen

The first method attemped was a dye-binding technique based on the work of McKnight (1977) and Esen (1978). Esen's method was simpler and so was the one we initially followed. However, on developing the technique some of McKnight's ideas were included.

The procedure of Esen is essentialy as follows. Known volumes of the protein solution are spotted onto

filter paper and are stained in a solution of Coomassie brilliant blue R-250. The staining solution also contains isopropyl alcohol and acetic acid to fix the protein onto the filter paper. After rinsing away excess dye, the dye-protein complex is eluted from the filter paper in 1% SDS (sodium dodecyl sulphate) solution and the absorbance of the supernatant is measured at 600nm. This method was adapted in various ways to make it sensitive enough for the low concentrations of protein encountered in our experiments. Modifications included concentrating the protein sample by repeated spotting at a single site on the filter, decreasing the elution volume, increasing the concentration of the staining solution and using an improved destaining technique (see McKnight 1977).

Once the technique had been shown sensitive and accurate enough for the low protein concentrations encountered in our experiments, the effect of lipid on the analysis was investigated. Unfortunately, as shown overleaf in figure 6.1, the presence of lipid had a marked effect, reducing the measured absorbance for a given protein concentration by 50-75%.

There appeared to be two possible explanations. Either the lipid was acting as a detergent and preventing fixing of the protein onto the filter or the lipid was binding to the protein in such a way as to prevent staining. This was investigated further by soaking a cytochrome c spotted filter in a "staining solution" which did not contain any Coomassie blue stain. The isopropanol and acetic acid in the solution denature and fix the

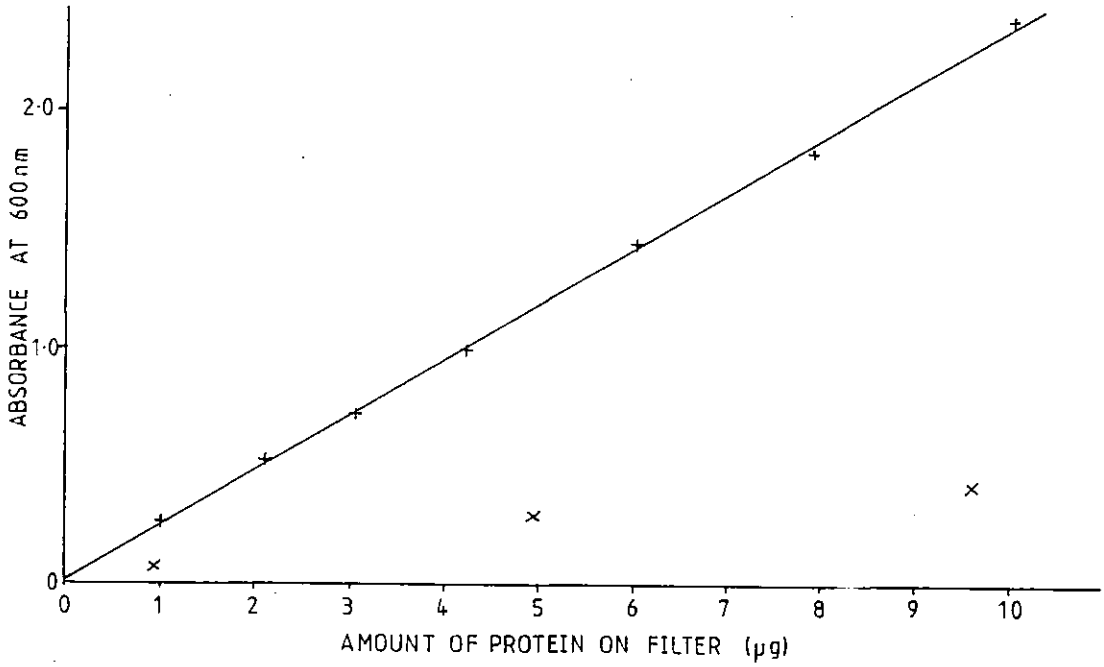

Figure 6:1 The effect of lipid on Esen's dye-binding method - graph of absorbance at 600nm as a function of the amount of cytochrome c on the filter for cytochrome c samples (+) and cytochrome c-CES-cholesterol samples (×), (weight ratio protein to lipid of 1:2).

protein onto the filter and I noted that a cytochrome c spot lost all its red colour by soaking in the solution whereas a cytochrome c-lipid spot maintained some of its colour. Evidently the lipid is protecting the protein from denaturation in the staining solution and so is preventing destaining of the protein. Coomassie blue R-250 is a dye-anion which, in slightly acid media, is electro- statically attracted to the NH_3^+-groups of the protein (Fazekas de St. Groth et al. 1963). It is therefore not suprising that it competes with the cerebroside sulphate for the protein.

Attempts were made to separate the lipid from the protein by partitioning between organic and aqueous phases. The aqueous lipid-protein solution was vortexed

with chloroform-methanol solution. The vial was then centrifuged and the protein content of the aqueous phase determined by the staining method. Unfortunately, the results showed that the presence of lipid was still affecting the protein determination. High salt concentrations were added to try and reduce the interaction between the lipid and protein. This was unsuccessful, the high salt concentrations both resulting in sedimentation of the protein and also affecting the staining technique.

Other Techniques Attemped

It was evidently extremely difficult to separate the protein and the lipid, so a technique was required which was unaffected by the presence of lipid. Radioactive labelling methods were unsuitable because of the difficulty and cost involved in obtaining labelled basic protein.

A few tests were carried out to investigate using the native fluorescence of the tryptophan ring to determine the protein content of the sample. However, the preliminary results were not promising as a very high gain was required and the spectrum was dominated by quenching effects.

A further possibility was the measurement of the ultra-violet absorbance of the sample (Thorne 1978). Due to the low concentration of the protein solutions which are to be analysed, the wavelength used must be short, 190-220nm, as the absorbance is then high. Sadly, at these wavelengths lipid, salts and SDS solution as well as

protein all absorb strongly. Some tests were carried out to compare the absorbance of lipid and protein solutions separately with the absorbance of a mixed lipid and protein solution in the hope that the absorbances were strictly additive. The results were not very encouraging probably reflecting conformational changes and complex formation due to interaction between the lipid and protein.

Total Nitrogen Determination Method

The method which finally proved successful in determining the protein content of our samples was a modified micro-Kjeldahl total nitrogen determination reported by Jaenicke (1974). I would like to thank Jenny Fordham of Kings College Biophysics Department, London, whose experience with this method was of great help during our initial attempts. The procedure as described below is that used routinely to determine the total nitrogen content of our Langmuir-Blodgett specimens and is slightly modified from that of Jaenicke. All reagents are of AnalaR grade, unless unavailable (as is the case for the sodium hypochlorite solution), when the highest possible purity is used.

The method is based upon ashing the samples with perchloric acid at its boiling temperature to fully convert all the nitrogen in the samples to NH_4^+. The quantity of ammonia produced is determined using the indophenol blue method, the chemical reaction between the ammonia and the added reagents producing indophenol blue

dye which is quantified photometrically. It must be remembered that, although the protein is the major source of nitrogen in the sample, the lipid also contains nitrogen. Before the protein content of the sample is calculated, the nitrogen present due to the lipid in the sample must be taken into account.

The procedure for the total nitrogen determination is as follows. 26 pyrex test-tubes (100mm long, 12mm external diameter), 25 glass marbles and 6 glass vials are soaked overnight in concentrated chromic acid to remove any organic contamination. The glassware is then rinsed thoroughly in fresh deionised water and dried. The cleanliness of the glassware is crucial and experiments have been ruined by rinsing the glassware in distilled water which has not been freshly prepared.

The Langmuir-Blodgett specimen is placed in one of the clean test-tubes with 0.7ml of 1% Triton X-100 solution and sonicated for one hour to aid removal. The Langmuir-Blodgett samples are very tenacious and sometimes even after 30 minutes sonication the cytochrome colour can still be seen on patches of the substrate.

10, 20, 30 and 40µl of the sample solution are added in triplicate to the test-tubes (15 tubes in all including a triplicate blank) using micropipettes with disposable tips. 1mM ammonium sulphate solution is used as the nitrogen standard and 10, 20, 30 and 40µl of this solution is added in duplicate to the remaining test-tubes with 10µl of deionised water being used as a blank. 25µl of perchloric acid (a 72% $HClO_4/H_2O$ azeotrope) is added to

each test-tube and each tube is covered with a clean marble. The sample tubes, including the triplicate blanks, are placed in a test-tube heater block which is preheated and thermostated to 210°C ∓2°C. After heating for 40 minutes to ash the samples, the tubes are removed and allowed to cool at room temperature.

The ammonia content of each tube is then determined using the indophenol blue method. Firstly, 0.5ml of deionised water is added to each tube, vortexing after each addition. Then 0.5ml of phenol reagent (2% phenol and 0.01% sodium nitroprusside) is similarly added and vortexed. Finally 0.2ml of hypochlorite reagent (20mM sodium hypochlorite in 2.5M sodium hydroxide) is added to each tube and immediately vortexed, rapid mixing after each addition being vital. After allowing the colour to develop for 30 minutes, the absorbance is measured at 635nm using a Beckman DU-8 Spectrophotometer.

Figure 6.2 shows typical results of such a nitrogen determination. The sample is CES-cholesterol-myelin basic protein, 48 membranes thick, dissolved in 0.7ml of 1% Triton X-100 solution. From these results, it is calculated that this multilayer sample contains 0.473μmoles of nitrogen atoms, assuming all the sample is removed by sonication from the substrate. Once corrected for the nitrogen content due to the lipid, usually about 10-20%, the protein content of the sample can be calculated. The number of nitrogen atoms per protein molecule is derived from the known amino acid sequence of the protein. Myelin basic protein contains 268 nitrogen

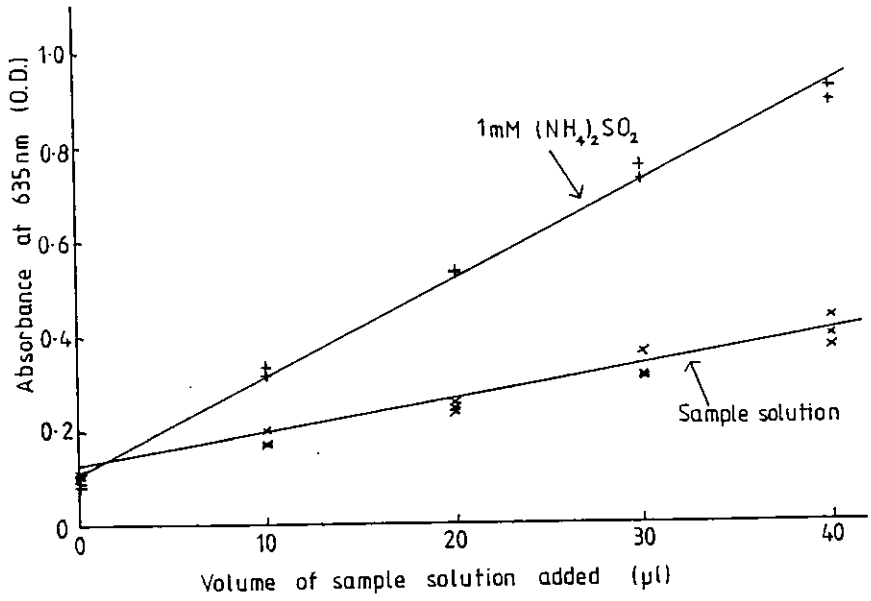

Figure 6.2 Typical results of the total nitrogen determination showing the absorbance at 635nm as a function of the volume of solution tested, for the sample solution (×) and the 1mM ammonium sulphate standard (+).

atoms per protein molecule (Eylar et al. 1971, Boggs & Moscarello 1978) and cytochrome c contains 148 (Dickerson 1972).

During the development of the total nitrogen determination, various tests of the technique were carried out. The first experiment was to check that the interaction between lipid and protein did not interfere with the technique. The nitrogen contents of protein solutions, of lipid solutions and of mixed lipid-protein solutions (all aqueous solutions of known concentration) were determined. It was found that the result for the mixed lipid-protein solutions agreed with those from the lipid and the protein samples to within 1%. Therefore, as required, the protein content of the sample can be determined in the presence of lipid, provided the amount

of lipid present is known.

Experiments were also carried out using known quantities of material to check for complete digestion by the perchloric acid. The expected and measured nitrogen content agreed within 4% for tryptophan, within 5% for cytochrome c and within 6% for cerebroside sulphate. The measured nitrogen content of the samples was lower than expected for the tryptophan and the cytochrome c and higher than expected for the cerebroside sulphate. Therefore, within the limits of the experiment, complete digestion is taking place. The tryptophan, lipid and protein all were dried down under vacuum before use.

The final test was to check the nitrogen content of the 1% Triton X-100 solution used to dissolve the multilayer sample. As expected, the solution was found to be nitrogen-free.

Lipid Analysis

As already explained, the cerebroside sulphate to cholesterol ratio of 60:40 mol % is defined when the monolayer spreading solution is prepared. The lipids must therefore be dried down under vacuum before being carefully weighed out in the required proportions.

The cholesterol content of the multilayer specimen is measured using a radioactive technique. Radioactive cholesterol, labelled with C^{14}, at the end of the tail is included in the monolayer spreading solution at a known proportion (about 4% of the total cholesterol in the

sample is radioactive) and the spreading solution is deposited as normal. The presence of C^{14} cholesterol in the specimen has no effect on the diffraction results. Once all the required diffraction data has been collected, the sample is dissolved in Ø.7ml of Triton solution and sonicated as described for the protein determination. 1ØØµl aliquots of this sample solution are then placed in triplicate in scintillation vials containing 1Øg (1Ø.95ml) of Beckman Ready-Solv HP scintillation fluid. This particular scintillation fluid was chosen because it is a high performance cocktail designed for aqueous solutions. Duplicate blanks are prepared using 1ØØµl of 1% Triton X-1ØØ solution instead of the sample solution. The radioactivity of these vials is then measured using a Searle Isocap/3ØØ scintillation counter with full window for 2Ø minutes per sample.

In order to calculate the amount of cholesterol in the sample, a calibration factor relating scintillation counts to the amount of cholesterol is required. This is determined when the stock monolayer spreading solution is first prepared. The radioactive cholesterol (type 26,(27)-C^{14}), is obtained in 5Øµ Curie aliquots from the Radiochemical Centre, Amersham. The activity of the cholesterol is 53.5mCi/mmole and the total sample, which is supplied in toluene solution, is only .39mg in mass. The radioactive solution is transferred to a clean vial and the toluene is evaporated away under vacuum. About 1Ømg of non-radioactive cholesterol (this can be brominated cholesterol) is added to dilute the sample

activity. Next, the required weight of cerebroside sulphate for a final CES:total cholesterol molar ratio of 6Ø:4Ø is added and the lipid-cholesterol is then dissolved in a known volume of chloroform-methanol (about 2% methanol). The calibration factor for the scintillation counts per unit mass of cholesterol is determined by taking 1Øµl samples of this known concentration lipid-cholesterol solution, inserting them into scintillation vials containing 1Øg of the Ready-Solv HP scintillation fluid and then counting on the scintillation counter.

It should be noted that the samples used in both the lipid and protein analyses are from the same solution (the multilayer specimen dissolved in 1% Triton solution). Therefore, the measured lipid to protein ratio should be unaffected if not all the sample is removed from the aluminium substrate by sonication.

Water Content Experiment

The principle behind this technique is the exchange of the water in the multilayer sample at a known relative humidity with tritiated water. It is assumed that the amount of unexchangable water in the sample is negligible. A rough calculation suggests that about 1Øµg of water vapour can be expected per sample, too small an amount to be accurately measured gravimetrically due to its volatility.

The apparatus for use in this experiment has been

designed and built (see figure 6.3), but, so far, only a few preliminary tests have been carried out using it. Extreme care was taken during the design and manufacture to make the apparatus air-tight and tests have shown that this aim has been achieved.

The intended method is shown schematically in figure 6.4. The multilayer sample is first allowed to equilibrate with a drop of either tritiated water or tritiated salt solution depending on the required relative humidity. The tritiated drop is then removed and replaced by a second drop (about 10mg) of untritiated water or salt solution, again depending on the required relative humidity. The drops are on filter paper and are held on wire supports. The, now tritiated, sample equilibrates with this second drop and, as the drop is in effect an infinite reservoir, essentially all of the sample radioactivity will be transferred. The radioactivity of this second drop is then either measured directly or a further vapour diffusion step takes place between the drop and a reservoir of water or salt solution. The disadvantages of not using this final step are that counts are lost by evaporation on transferring the drop to a scintillation vial and also the filter and wire support must be transferred along with the drop and these cause quenching effects.

In calculating the water content of the sample from the amount of tritiated water vapour transferred to the scintillation vial, the number of exchangable hydrogens on the protein must be taken into account. It must also be

Figure 6.3 Photograph of apparatus for water content determination experiments. There are two equivalent sets of cells and in this photograph the set on the right are in use and the set on the left have stoppers removed to show the O-ring seals.

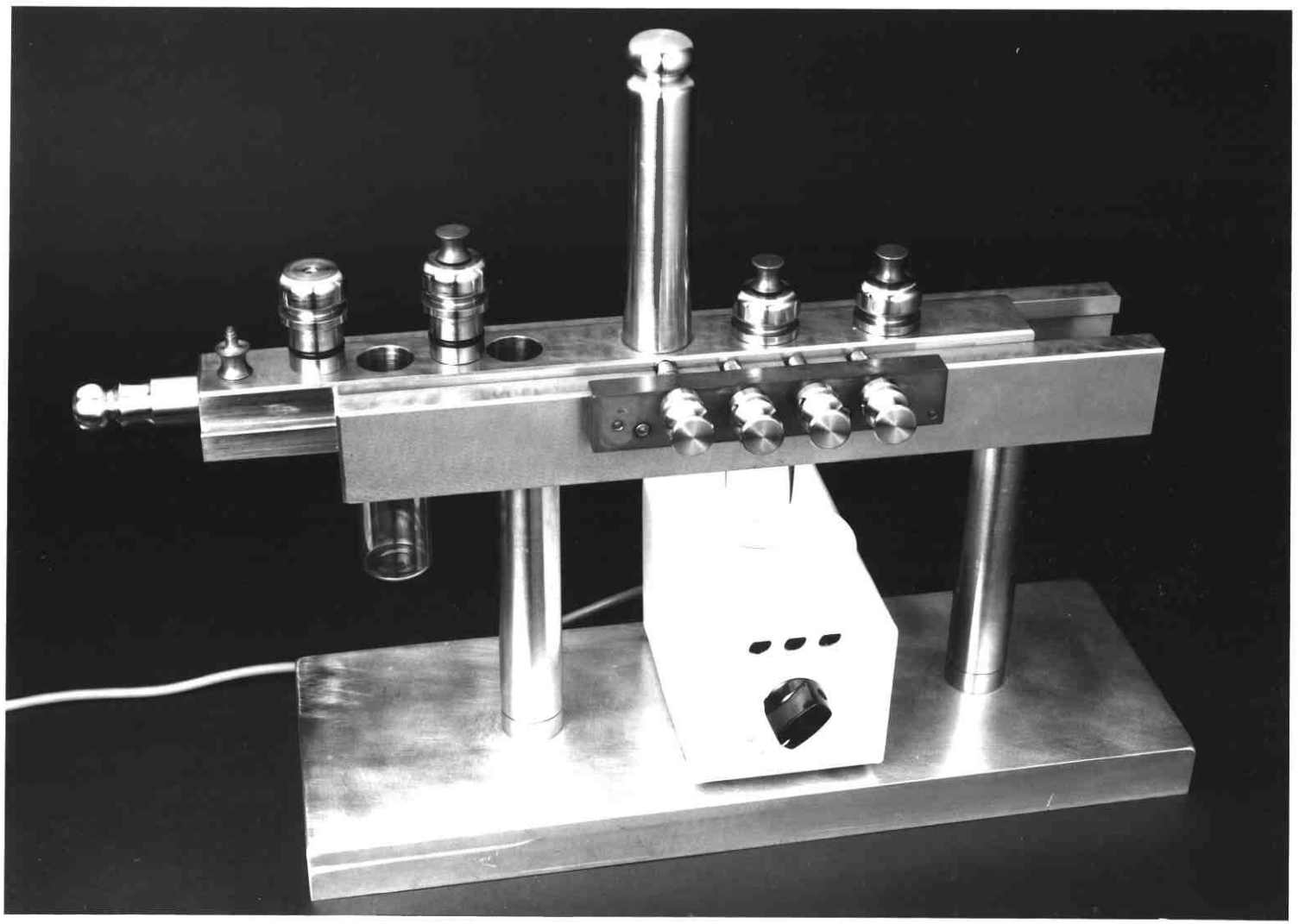

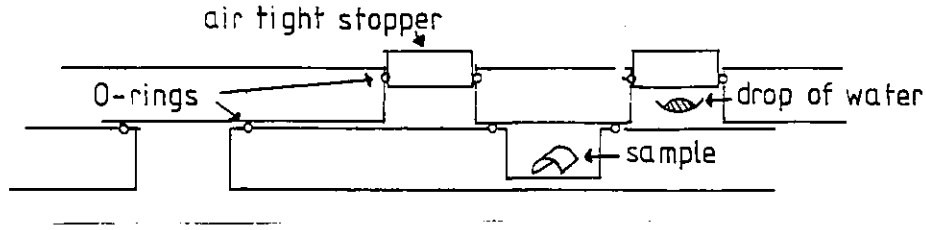

Position 1. - Closed position.

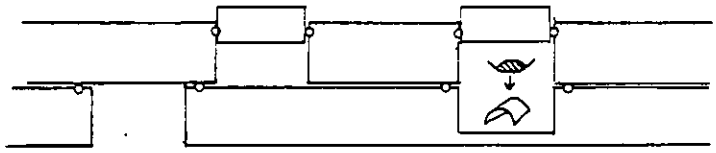

Position 2. - Sample equilibrating with drop of tritiated water or tritiated salt solution.

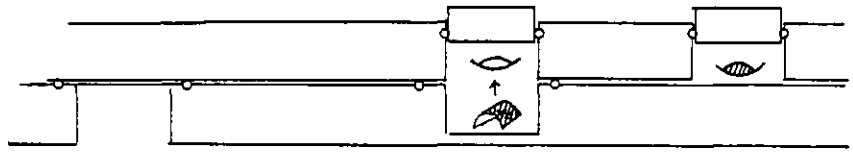

Position 3. - Tritiated sample equilibrating with drop of untritiated water or saturated salt solution.

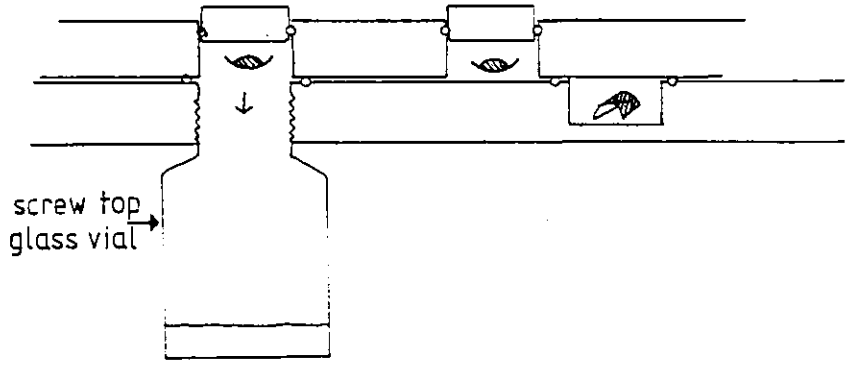

Position 4. - Final vapour diffusion step between drop and water or salt solution reservoir.

Figure 6:4 Schematic diagram of the water content experiment.

realised that a certain volume of water vapour is transferred from one cell to another at each exchange and, although the apparatus has been designed to make this volume as small as possible, at room temperatures this can be a dominating factor in the experiments. For this reason, the experiments will probably be carried out at low temperatures, e.g. $4^{o}C$.

CHAPTER VII

ANALYSIS OF X-RAY DIFFRACTION RESULTS

There are two principle difficulties inherent in the nature of X-ray diffraction experiments, phasing and scaling. It is relatively simple to produce the structure factor amplitudes |F(R)| from the diffraction data, as described in chapter V, but before the one-dimensional electron density profile can be calculated, signs, either positive or negative, must somehow be ascribed to each structure factor amplitude. Once this has been achieved, the resulting electron density profile is still only on a relative electron density scale. When, as in this thesis, profiles are compared with each other, some method of scaling one profile relative to another is imperative, and before attempting to assign the different levels of the profile to particular membrane components, an absolute electron density is required.

Phasing

There are various methods used in determining the signs of the structure factor amplitudes, but, as none of these is definitive (Franks & Levine 1981), in the work of this thesis many methods have been used in conjunction. Whenever possible, a series of data sets at various relative humidities, and therefore at various water contents, was collected for each sample. This is known as a swelling series because, as the relative humidity is

increased, the higher water content results in a larger lamellar spacing (D).

Before the data were plotted, the corrected intensities I(h) from different swelling series were normalised (Franks & Lieb 1979) such that, for a data set at lamellar spacing D,

$$\sum_{h=1}^{h_{max}} I(h) = D/D_{min} \qquad (7.1)$$

where D_{min} is the minimum in the swelling series and h_{max} is the maximum observed order. This normalisation is only an approximation since only a finite number of reflections are recorded and I(Ø) is not observed.

Shannon's theorem (Shannon 1949) states that if the value of the Fourier transform is known at points h/D for h=Ø, ∓1, ∓2 ..... where D is the lamellar spacing, then its value at all points in reciprocal space can be calculated by using the summation

$$F(R) = \sum_{-\infty}^{+\infty} F_h \frac{\sin\{\pi(RD-h)\}}{\pi(RD-h)} \qquad (7.2)$$

where R is the dimension in reciprocal space and F_h is the sampled value of the transform at R=h/D. F(R) is referred to as the reconstructed transform. It must be realised that the above equation is only exact for an infinite summation and because only a finite number of reflections can be measured, truncation effects can occur.

Provided F(Ø) is chosen such that the Fourier transform is defined relative to the swelling fluid, a constant membrane structure separated by various thicknesses of fluid layer would have a constant Fourier transform but be sampled at different points in reciprocal space. Therefore, assuming a constant structure for our membrane during swelling, each set of data should have unique phase assignments such that all give the same reconstructed Fourier transform. However, in reality, the structure does change during swelling, but provided the changes are continuous and small, the same general approach can be used (Franks & Levine 1981).

Phasing the swelling series data is also helped by the minimum wavelength principle (Perutz 1954) which states that for a structure of maximum width W , the Fourier transform will contain a minimum wavelength component of 2/W. Therefore the distance between adjacent loops in the transform is unlikely to be less than 2/W, although for certain combinations of the component wavelengths, this can occur.

In conclusion, the phases were initially assigned by plotting the swelling series data in such a manner that they appear to lie on one continuous transform and the minimum wavelength principle was then used to reject phasings which result in rapid oscillation of the transform.

Once the phasings had been assigned as far as possible using the methods described above, the electron density profiles were calculated for the remaining

possible phasings. Certain phase assignments were rejected on inspection, as described in more detail later, on consideration of the resulting electron density profile and additional information such as the variation in the profile with chances in humidity.

The final technique employed in phasing the structure factor amplitudes made use of the inclusion of brominated cholesterol in the samples. The brominated cholesterol has a bromine atom substituted for a hydrogen on the end carbon of the hydrocarbon tail (Franks et al. 1978). This atom, which is strongly scattering and is assumed to be non-perturbing, was initially included to allow absolute scaling of the electron density profiles, as discussed later, but it was also used in the phasing of the data. Providing the bromine atoms lie close to the centre of the bilayer, which is defined as the origin of the unit cell, they contribute positively to the unit cell transform for all values of R (Franks et al. 1978). The signs of the structure factor amplitude can therefore be simply deduced since all reflections with positive signs will increase in intensity while those with negative signs will decrease. Unfortunately, the effect falls off at the higher orders.

Scaling

Relative scaling

The initial scaling of two profiles relative to each other is a purely empirical process. If profiles are obtained for two samples, identical in structure except that in one case the cholesterol has been bromine

substituted, then the difference between the two profiles, when correctly scaled, is simply the electron density of the bromine atoms. Difference profiles are calculated and plotted for various relative scalings, and the correct relative scaling is chosen on the basis of the best looking difference, the criterion being a smooth, flat profile except for the electron density peak due to the bromine atoms at the centre of the bilayer. Figure 7.1 shows the difference profiles between CES-brominated cholesterol-cytochrome c, scaled at Ø.9, Ø.8 and Ø.7, and CES-cholesterol-cytochrome c. The chosen scaling in this case is Ø.8. The scaling of the profile is achieved by multiplying all the phased structure factor amplitues by Ø.8 which results in a reduction in the profile height by Ø.8 without any change in its shape (see equation 5.6).

The technique of relative scaling has also been used to compare protein-containing samples with lipid-cholesterol samples, the criterion for the best difference now being a smooth, flat region at the centre of the profile. In order to compare the two structures, the width of the lipid profile has to be increased to that of the protein by extending the lipid profile at the electron density of water (see figure 7.2). This extending of the lipid profile can be achieved by resampling the Fourier transform (as determined using Shannon's theorem) at a different D spacing. As mentioned earlier, providing the zero order structure factor has been chosen correctly, the resulting profile will be identical to that of the initial lipid profile except that the thickness of the surrounding

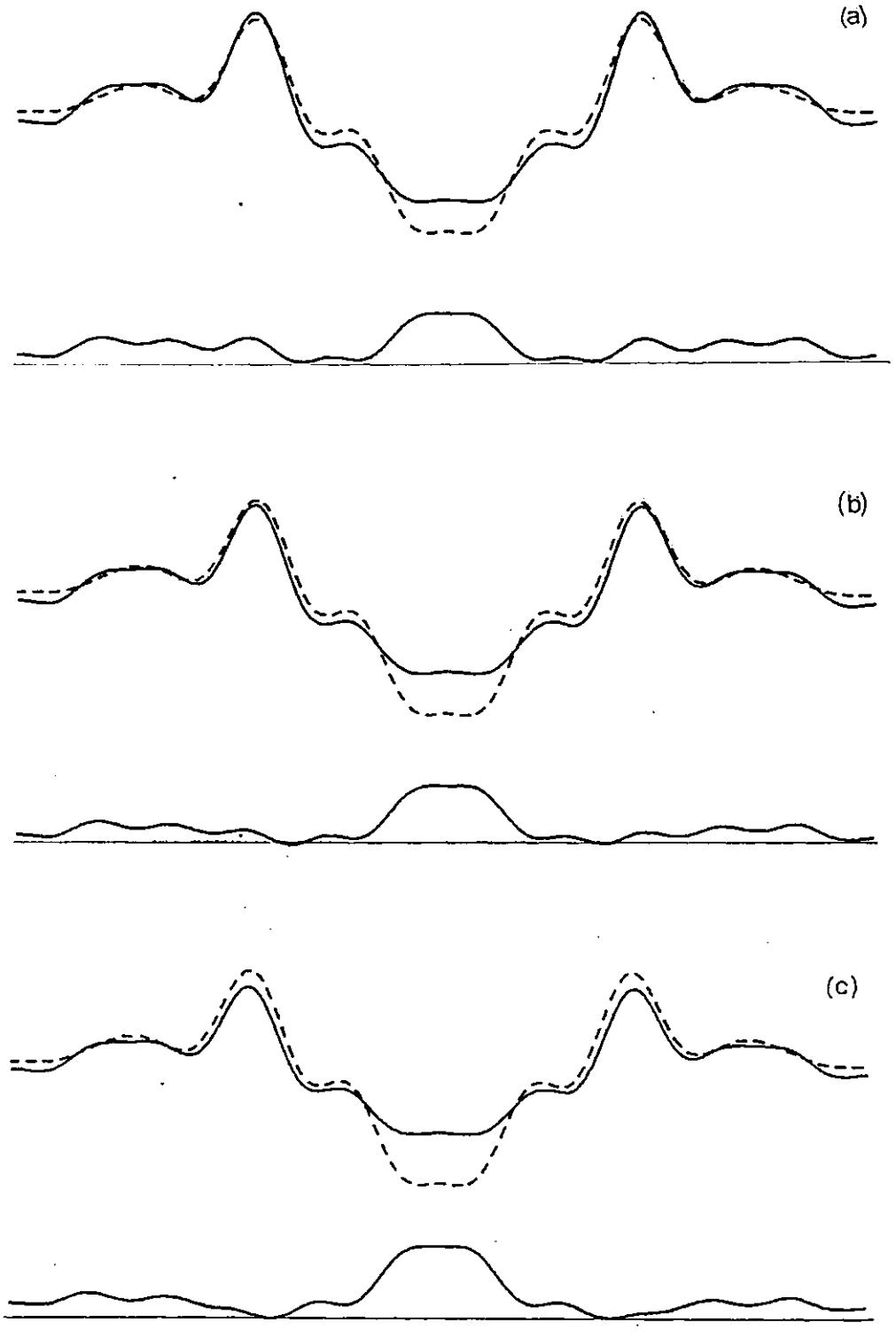

Figure 7.1 The difference profiles between CES-brominated cholesterol-cytochrome c (full line) scaled at Ø.9 (a), Ø.8 (b) and Ø.7 (c), and CES-cholesterol-cytochrome c (dotted line). The straight base line has been added to help with comparison of the profiles. The preferred scaling is (b).

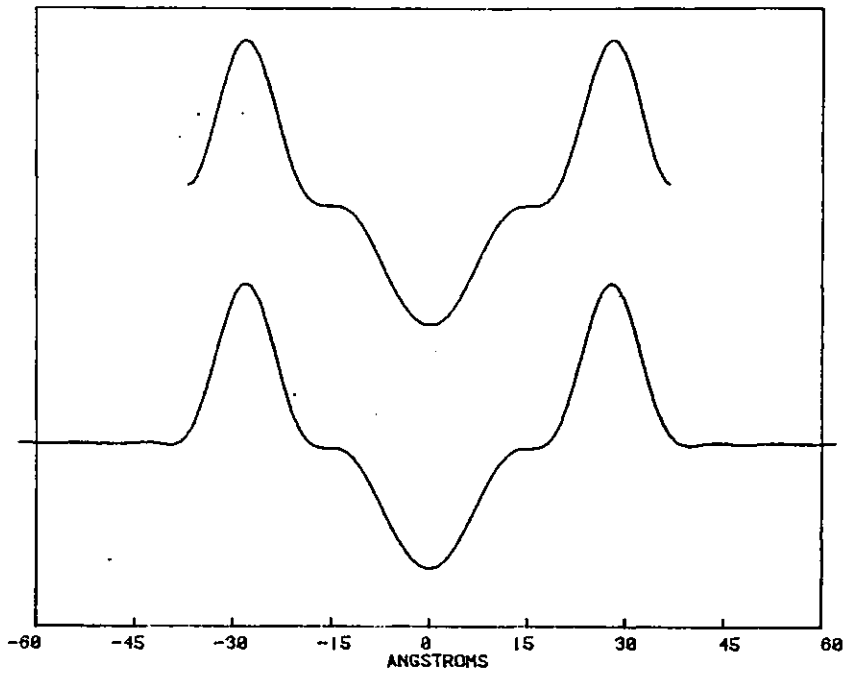

Figure 7:2 Comparison of cerebroside sulphate-cholesterol profile (above) with the extended profile obtained by sampling the Fourier transform at a new spacing of 124.8Å (below). The two profiles are displaced from each other for clarity.

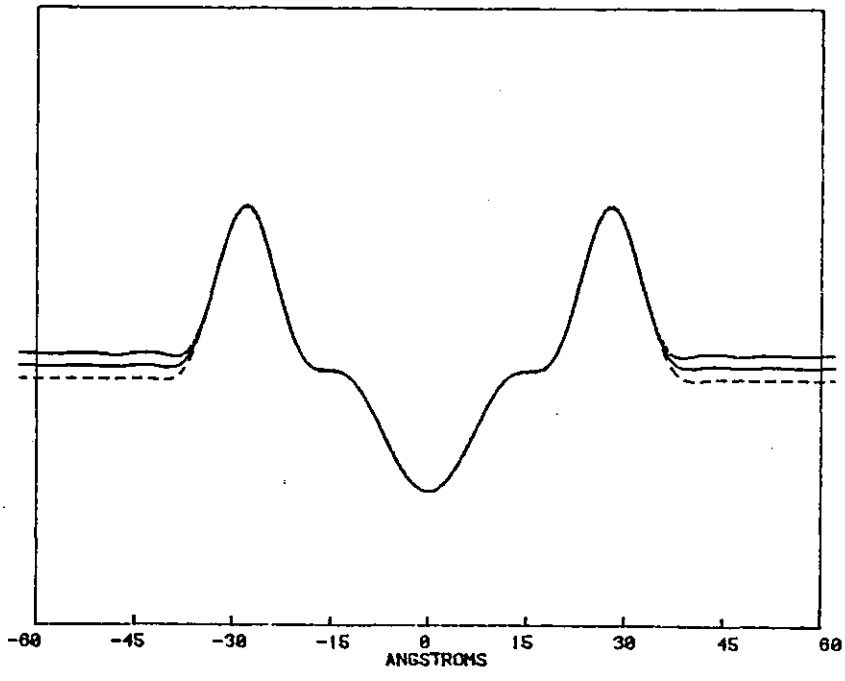

Figure 7:3 Comparison of extended profiles obtained by sampling, at D=124.9Å, the Fourier transforms produced using different values of F(Ø). The dotted profile has F(Ø) set at Ø.25, the full profile has F(Ø) set at Ø.15 (the preferred value) and the dashed profile has F(Ø) set at Ø.Ø5. Notice how the electron density of the extended level, which should be at the electron density of water, varies with respect to the lipid profile.

water layer has been increased. This method has the interesting corollary of allowing the zero order structure factor F(Ø) to be determined empirically, as only the right choice of F(Ø) will result in the electron density of the surrounding water layer being set at the correct level relative to the lipid bilayer (see figure 7.3). The electron density level of water is known to be very close to that of the cholesterol nucleus (Franks et al. 1982), which appears as a shoulder in the profile.

Absolute Scaling

The absolute scaling of the electron density relies on the fact that the difference between the correctly scaled brominated and unbrominated profiles is only due to the bromine atoms. Provided the size of the unit cell, the mean electron density and the number of brominated cholesterol molecules per unit cell are known, then the absolute scale of electron density can be calculated from the area under the difference profile.

An attempt was made to use iodinated cholesterol, as well as brominated, to determine the absolute scaling. However, the difference in electron density due to the iodine atoms was much smaller than expected. This was possibly due to degradation of the iodinated cholesterol with time since the only material available, although stored at -20°C, was five years old.

Preliminary Analysis of the Data

Table 7.1 is a summary of the X-ray diffraction samples studied in this thesis. Before describing the detailed phasing and scaling of each data set, it is worth considering the data in a rough and simple manner.

The first point to note is the different spacings of the various data sets. Comparing the membrane thickness with and without protein, the addition of cytochrome c has increased the membrane thickness by about 52Å (about 26Å per cytochrome c molecule) whereas the myelin basic protein has only increased the membrane thickness by 27Å (about 13½Å per MBP molecule). Assuming that the layer of protein attached to the monolayer is only one molecule thick, and remembering that the cytochrome c (molecular weight 12,384) is about 2/3 the size of the MBP molecule (molecular weight 18,500), it is apparent that the two molecules are very different in shape. This increase in thickness of the membrane due to the addition of protein agrees well with previous values of molecular size, Dickerson et al. (1971) having described cytochrome c, from crystallography results, as an oblate spheroid of axial dimensions 30Å × 34Å × 34Å and Epand et al. (1974) having reported the myelin basic protein molecule as being a prolate ellipsoid of dimensions 15Å × 15Å × 150Å.

Knowing the lipid to protein ratio, and assuming an area per CES + 2/3 cholesterol molecule (all our samples are 40mol % cholesterol) of 75Å^2 (this will be justified in the section on absolute scaling), the surface area of the membrane taken up by one protein molecule can be

	Sample composition	Type of specimen	Sample number	Relative humidity	Lamellar spacing	No. of orders	Resolution	% protein (dry wt.)
lipid samples	cerebroside sulphate-cholesterol	dispersion		excess water	73.8Å	5	14.8Å	Ø
	cerebroside sulphate-brominated cholesterol	dispersion		excess water	73.3Å	5	14.7Å	Ø
	cerebroside sulphate-iodinated cholesterol	dispersion		excess water	74.5Å	5	14.9Å	Ø
	cerebroside sulphate-cholesterol	evaporation		100% 97% 88%	70.4Å 69.0Å 67.1Å	9 9 11	7.8Å 7.7Å 6.1Å	Ø
	cerebroside sulphate-brominated cholesterol	evaporation		100% 97% 88%	72.4Å 69.8Å 66.6Å	12 12 11	6.0Å 5.8Å 6.1Å	Ø
myelin basic protein samples	cerebroside sulphate-cholesterol-myelin basic protein	Langmuir-Blodgett		100% 97% 88%	98.2Å 93.5Å 88.2Å	8 7 7	12.3Å 13.4Å 12.6Å	31%
	cerebroside sulphate-brominated cholesterol-myelin basic protein	LB	1	100%	102.7Å	6	17.1Å	33%
		LB	2	100% 100%	103.4Å 106.3Å	6 6	17.2Å 17.7Å	26%
		LB	3	100% 97% 86%	104.6Å 98.4Å 92.3Å	6 7 5	17.4Å 14.1Å 18.5Å	27%
cytochrome c samples	cerebroside sulphate-cholesterol-cytochrome c	LB		100% 97% 88%	124.9Å 119.9Å 115.3Å	10 9 9	12.5Å 13.3Å 12.8Å	45%
	cerebroside sulphate-brominated cholesterol-cytochrome c	LB		100% 97% 88%	124.8Å 117.5Å 112.7Å	11 9 10	11.3Å 13.1Å 11.3Å	46%

Table 7:1 Summary of the X-ray diffraction samples studied in this thesis.

calculated. From the cytochrome c data, the area occupied by each protein molecule is 1122Å^2 which is equivalent to a square of side 33Å and so agrees well with Dickerson's value. Using similar calculations, the area occupied by each myelin basic protein molecule is approximately 2445Å^2 (from sample 1), which is equivalent to a rectangle of sides 15Å × 16ØÅ and so agrees well with Epand's value. However, it is important to realise that our experiments so far have only been able to produce evidence of the area occupied by the protein molecules in the plane of the membrane and not of its shape within this plane.

The results of these rough calculations are substantiated by an experiment to investigate the absorption at 4Ø9nm of CES-cholesterol-cytochrome c multilayers. 54 membranes (27 on each side) were built up on a glass slide using the Langmuir-Blodgett deposition method. The absorbance at 4Ø9nm (the peak of the absorbance band for cytochrome c in the oxidised state) was measured, corrected for the glass absorbance, and compared with the absorbance of cytochrome c in solution. The absorbance of the multilayers was found to be equivalent to that of Ø.Ø277 mg/ml cytochrome c solution with a path length of 1Ømm. Taking into account the cross-section of the beam and assuming two layers of protein molecules sandwiched between each lipid bilayer, the area per molecule occupied by cytochrome c in the membrane stack is 8ØØÅ^2 which is equivalent to a square of side 28Å. This is in reasonable agreement with a cytochrome c molecule of axial dimensions 3ØÅ × 34Å × 34Å.

Study of the absorbance spectrum of the cytochrome c-containing multilayers also showed that the cytochrome c was still in the oxidised form and, as there was no major change in the spectrum compared with that of cytochrome c in aqueous solution, that the cytochrome c is unlikely to have denatured.

Unfortunately there seems no way of checking that the myelin basic protein has not denatured. Even checking for its encephalogenic action by injection into live animals would not be a definitive test because various fragments of the polypeptide also show encephalogenic activity (Boggs et al. 1982). I would, however, tentatively suggest that the myelin basic protein is less likely to denature when associated with lipids in a multilayer stack than in aqueous solution, the natural state of the protein being associated with the myelin membrane.

Phasing the Structure Factors

Lipid Samples

The initial lipid samples prepared were dispersion samples. They had the advantage of being easy to prepare and produced data of similar resolution to the protein-containing samples. Also, with only five measurable diffraction orders, the structure factors were easily phased. The diffraction patterns produced by the dispersion samples are reproduced in figure 7.4a and b. The iodinated cholesterol sample has not been included as it has not been used in further analysis.

As swelling series data could not be collected for

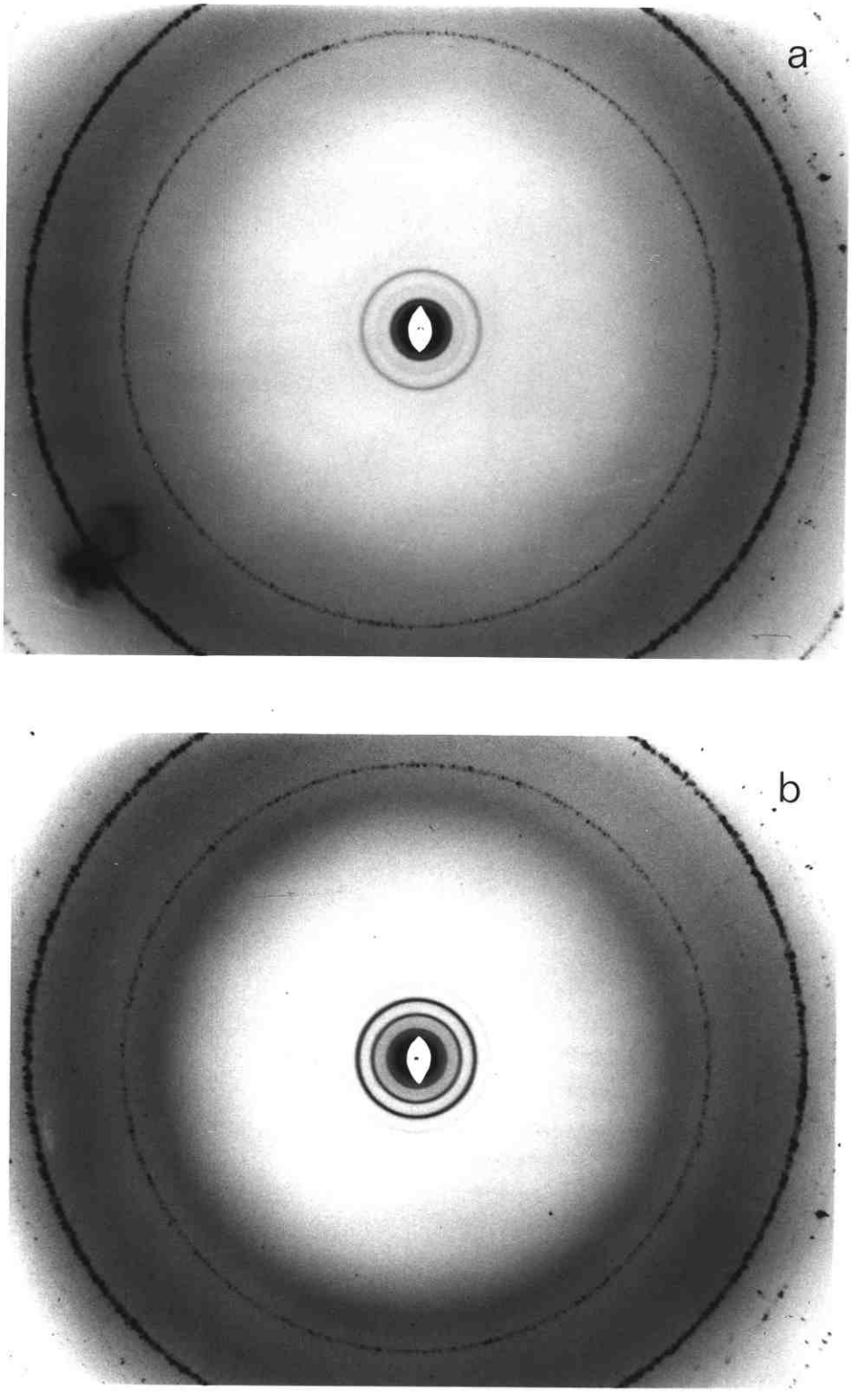

Figure 7.4 X-ray diffraction patterns of the lipid specimens taken using the toroid camera. Pattern (a) was obtained from the CES-cholesterol dispersion specimen, pattern (b) from the CES-brominated cholesterol dispersion specimen, pattern (c) from the CES-cholesterol evaporation specimen at 100% relative humidity and pattern (d) from the CES-brominated cholesterol evaporation specimen at 100% relative humidity. Note the diffuse hydrocarbon chain diffraction which is present in all the films. Patterns 7.4c and 7.4d are shown overleaf.

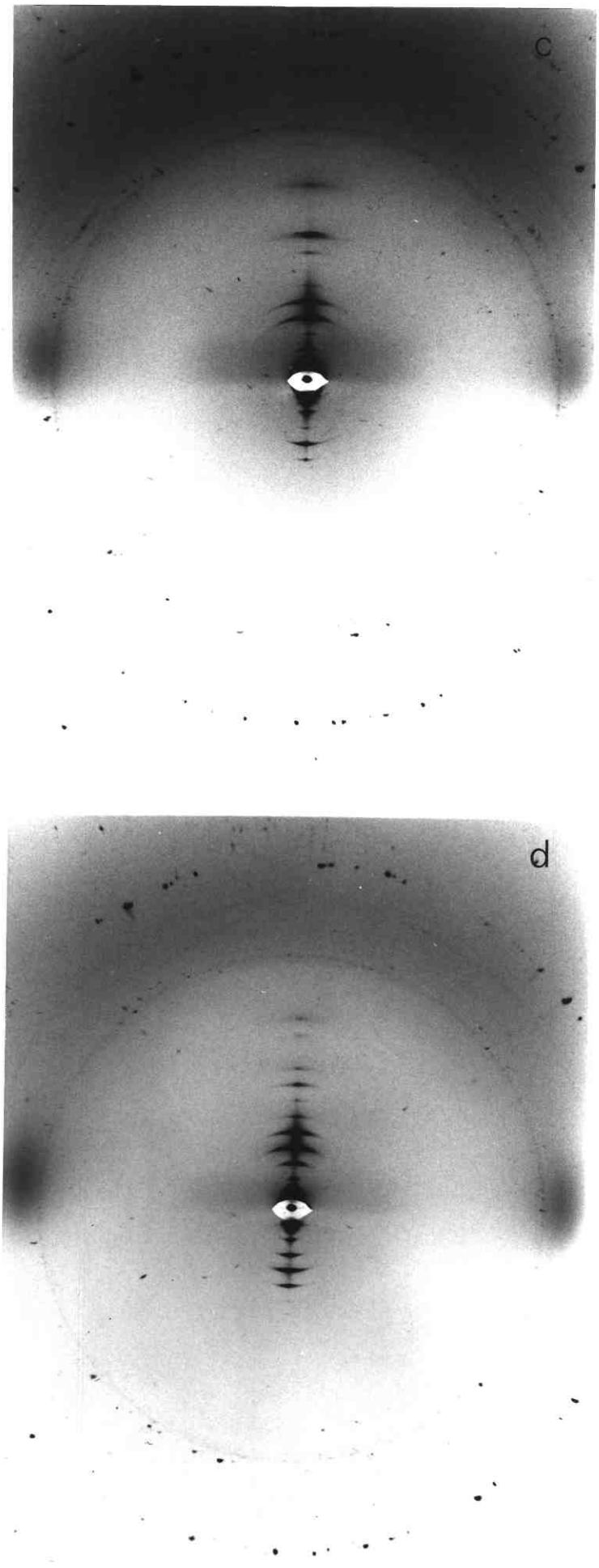

Figures 7:4c & 7:4d See previous page for figure legend.

the dispersion specimens, the methods used in phasing the data were inspection and bromination. The phasing --+-+ was initially decided upon as it gave the only realistic electron density profile for a lipid-cholesterol bilayer (figure 7.5a and 7.5b for the unbrominated and brominated samples respectively). This phasing was subsequently confirmed by comparison of the brominated and unbrominated data and also by comparsion with the lipid evaporation data. The phased structure factors for the unbrominated and brominated samples are compared in figure 7.6 where the brominated amplitudes have been scaled by Ø.8. This scaling of the brominated data relative to the unbrominated was chosen as giving the best looking difference profile (figure 7.7).

The dispersion lipid data is of lower resolution than almost all the data for the protein-containing samples (see table 7.1). Also the difference profile between the brominated and unbrominated data is very broad and I therefore attempted to collect higher resolution lipid data by preparing oriented lipid specimens using the evaporation method. X-ray diffraction patterns from the evaporation samples are reproduced in figures 7.4c and 7.4d. These patterns show diffuse equatorial diffraction at about 4.5Å indicating that the hydrocarbon chains are in the liquid-crystalline state. It would have been preferable if the lipid specimens had, like the protein-containing specimens, been produced by the Langmuir-Blodgett technique, but unfortunately this proved very difficult.

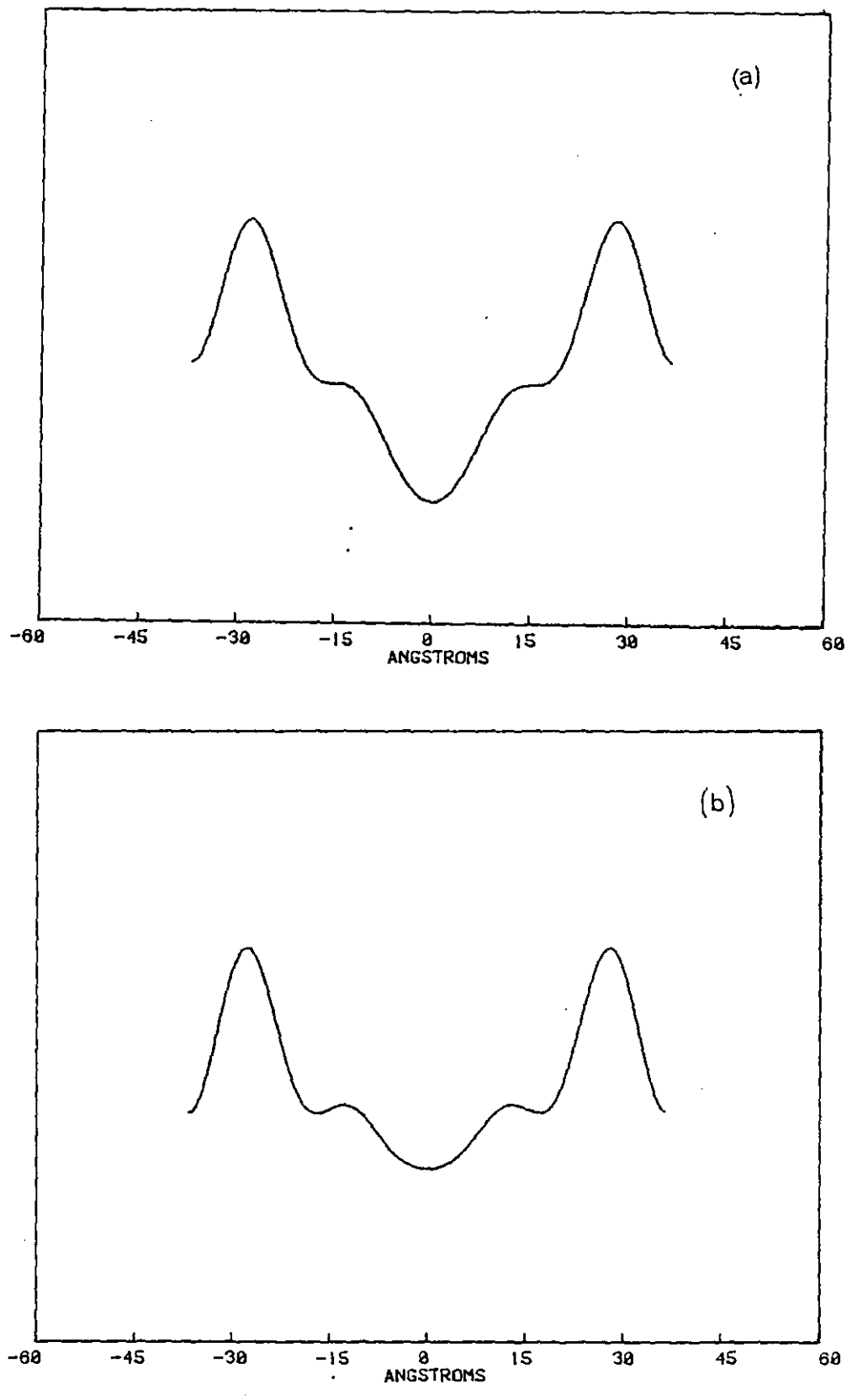

Figure 7.5 Electron density profiles across the bilayer for the lipid dispersion specimens. (a) is of cerebroside sulphate-cholesterol and (b) is of cerebroside sulphate-brominated cholesterol. The origin of the patterns in all cases is the centre of the hydrocarbon region of the bilayer.

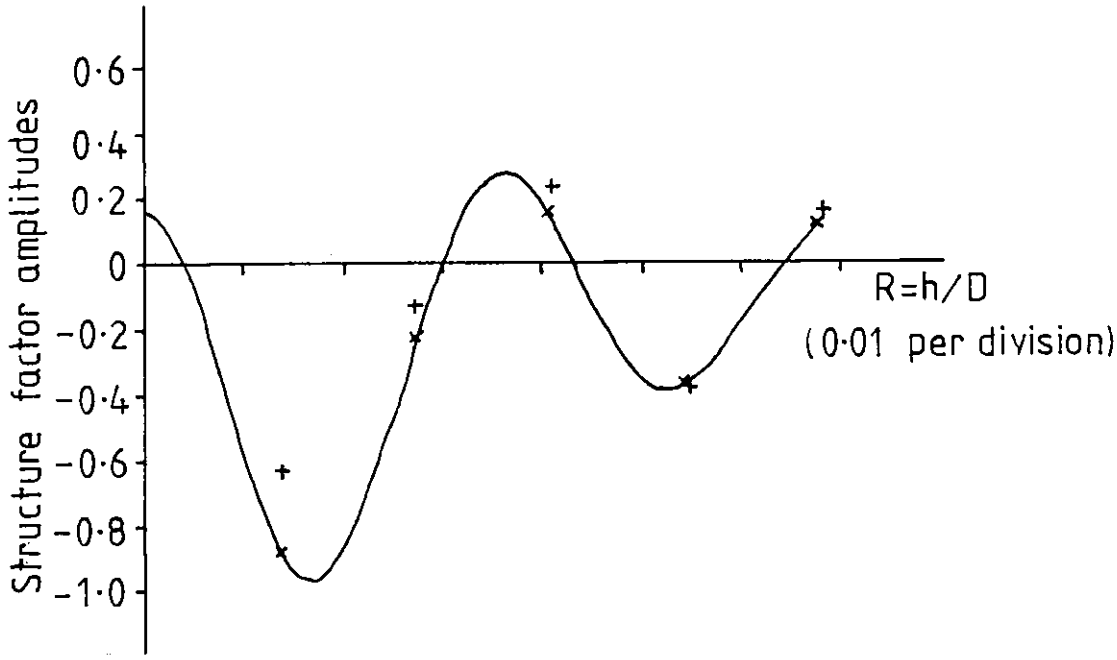

Figure 7.6 Comparison of the phased structure factors of the CES-brominated cholesterol dispersion data scaled at Ø.8 (+) and the CES-cholesterol dispersion data (X) plotted as a function of the reciprocal space vector R=h/D. The full curve through the unbrominated data is the Fourier transform of this data set.

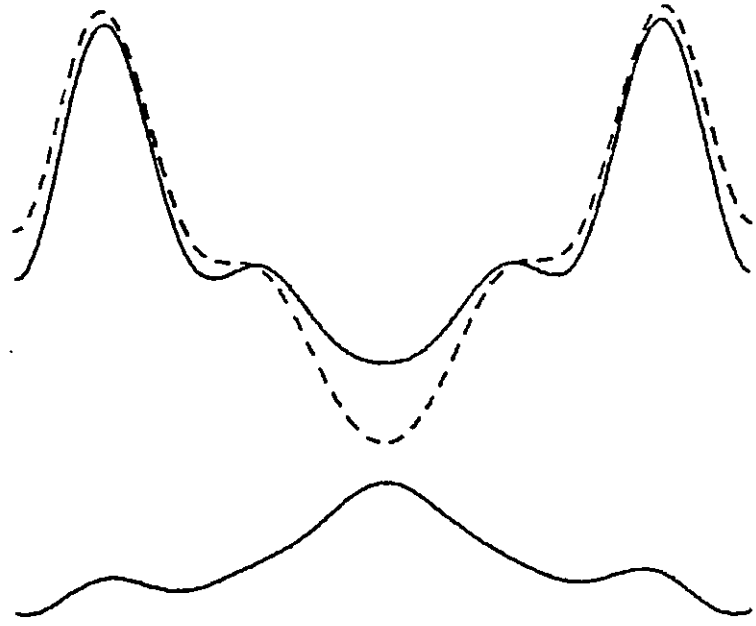

Figure 7.7 Comparison of the two lipid dispersion profiles, CES-brominated cholesterol scaled at Ø.8 (full line) and CES-cholesterol (dashed line). The difference between these two profiles is plotted underneath.

The evaporation specimens produced far higher resolution data than the dispersion specimens (about 6Å instead of 14.8Å) and swelling series were collected for these specimens. The structure factor amplitudes are plotted as a function of the reciprocal space vector R=h/D in figure 7.8. Electron density profiles for the CES-brominated cholesterol evaporation specimen at 100% relative humidity based on the two most probable phasings are shown in figures 7.9a and 7.9b

In order to compare these profiles with the lower resolution lipid dispersion and lipid-protein data, the structure factor amplitudes have been multiplied by a Gaussian distribution as shown in the equation below,

$$F_{new}(R) = F_{old}(R) \times \exp(-Bh^2/4D^2) \qquad (7.3)$$

where $F_{old}(R)$ are the evaporation sample structure factors, $F_{new}(R)$ are the new structure factors of the "smoothed" profile, D is the lamellar spacing, h is the Bragg order and B is the Debye-Waller temperature factor (Stout & Jensen 1968). Smoothing the profile using the above equation is equivalent to increasing the disorder in the sample, hence the name temperature factor. Smoothed profiles of 7.9a and 7.9b are shown in 7.9c and 7.9d respectively, where the temperature factor used is 200.

After smoothing the brominated evaporation data, the phasing chosen as giving a profile most consistent with the dispersion profile is phasing 1 (--+-+--+-0+-), mainly on the basis of peak-to-peak separation. This

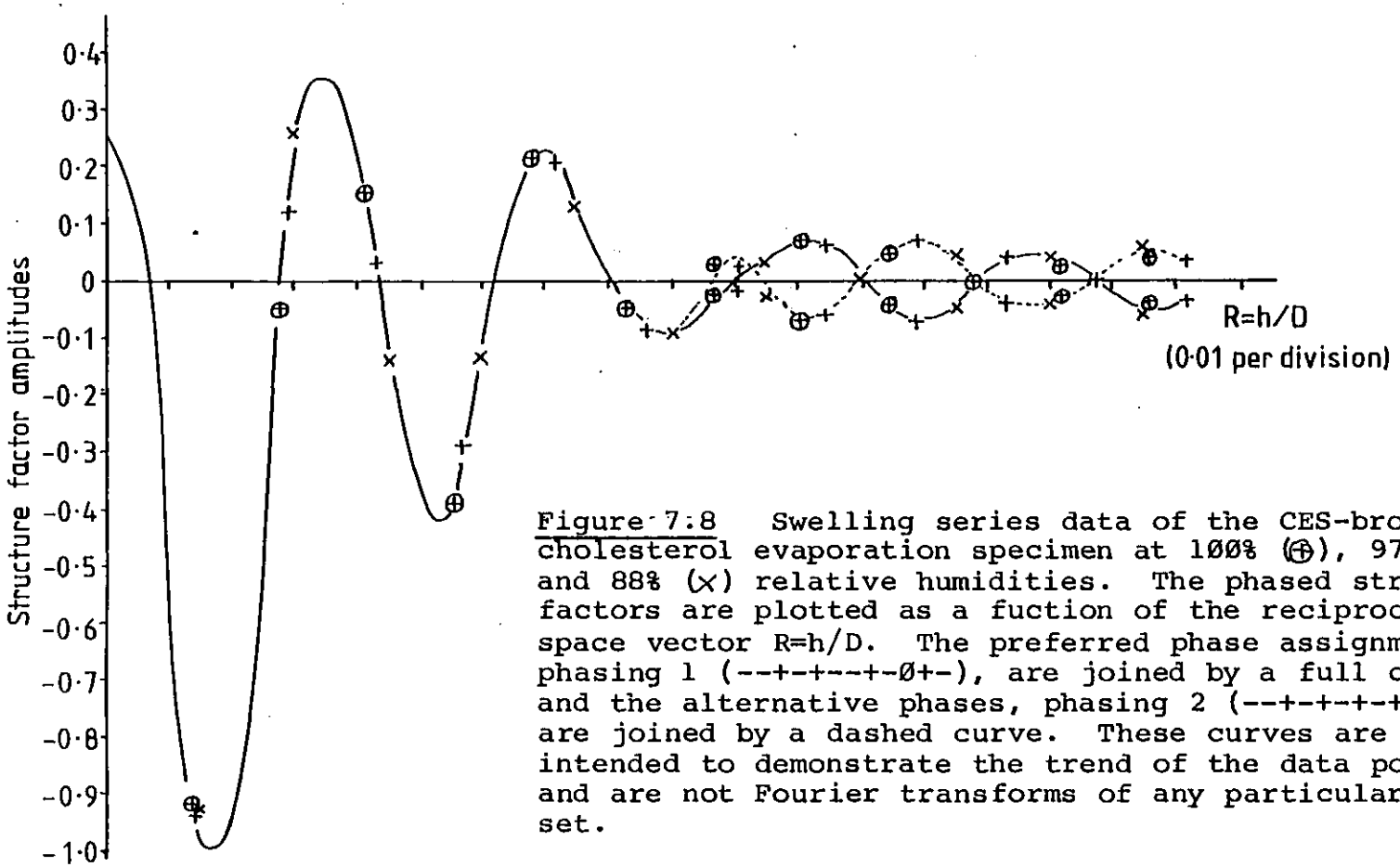

Figure 7:8 Swelling series data of the CES-brominated cholesterol evaporation specimen at 100% (⊕), 97% (+) and 88% (×) relative humidities. The phased structure factors are plotted as a fuction of the reciprocal space vector R=h/D. The preferred phase assignments, phasing 1 (--+-+--+-0+-), are joined by a full curve and the alternative phases, phasing 2 (--+-+-+-+0-+), are joined by a dashed curve. These curves are intended to demonstrate the trend of the data points and are not Fourier transforms of any particular data set.

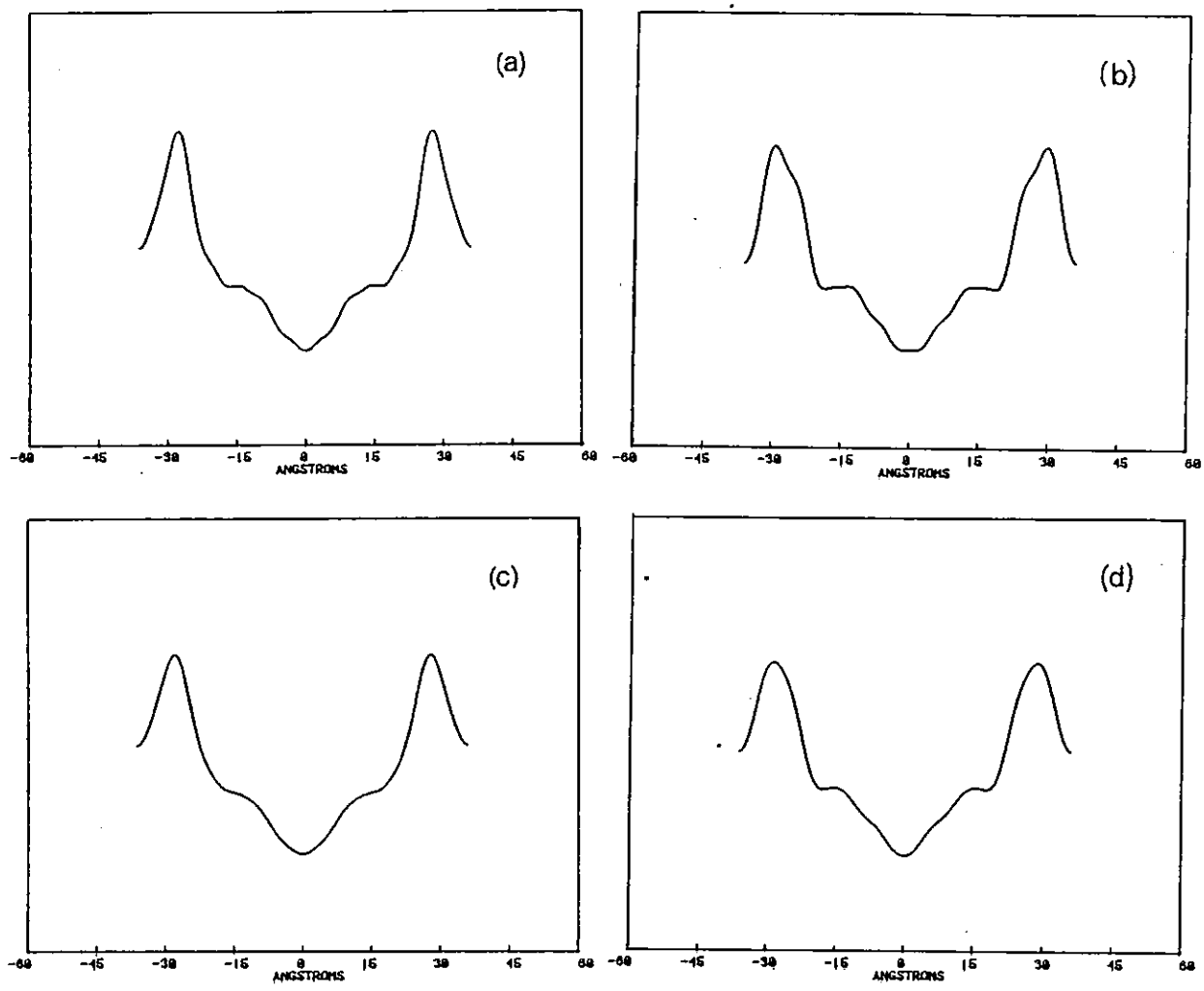

Figure 7.9 Electron density profiles for the CES-brominated cholesterol evaporation specimen obtained using the two most probable phase assignments; phasing 1 (--+-+--+-Ø+-) in (a) and phasing 2 (--+-+-+-+Ø-+) in (b). Smoothed profiles, using temperature factor B=2ØØ, are shown in (c) and (d) for phasings 1 and 2 respectively.

smoothed profile was then compared with the electron density profile for the unbrominated dispersion sample and the resulting difference profile is shown in figure 7.10. This profile gives a more distinct positioning of the bromine atoms and a better defined area of difference than figure 7.7 (the difference profile between unbrominated and brominated dispersion samples) and it is also in better agreement with the difference profiles from the protein-containing samples (figures 7.17 and 7.22).

When compared with the difference profile due to bromine atoms in multilayers of dimyristoyl lecithin-cholesterol multilayers (Franks et al. 1978) the bromine atoms in our CES-cholesterol multilayers seem displaced from the centre of the bilayer. However, considering the differences in width of the bilayer between DML-cholesterol (peak-to-peak distance of 43Å) and CES-cholesterol (56Å), it is not suprising that the bromine atoms reside slightly displaced from the centre of the bilayer in our specimens.

The above analysis of the evaporation samples has concentrated on the brominated sample. Unfortunately the diffraction pattern from the unbrominated evaporation sample shows signs of phase separation. Phase separation in a sample is evidently undesirable, because the compositions of the two phases are then unknown. In this case additional problems were caused because diffraction orders from the two different series appeared at the same or very similar positions on the film, so making intensity measurements of the various orders impossible. Therefore

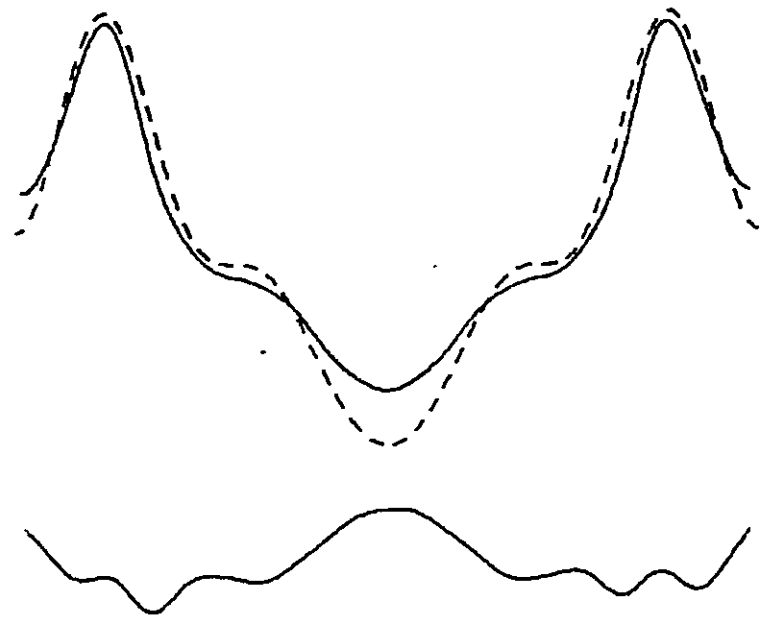

Figure 7:1Ø Comparison of the electron density profiles for the CES-cholesterol dispersion sample (dashed curve) and the smoothed profile of the CES-brominated cholesterol evaporation sample (full line). The difference between these two profiles is shown below.

the lipid dispersion data and not the evaporation data has been used in all further analysis (except when calculating the absolute scale from the bromine difference profile in figure 7.1Ø). Of course, the evaporation specimen containing brominated cholesterol has given excellent data and could still be used in further analysis, but for comparative purposes it seems preferable to use data from equivalent specimens.

Myelin Basic Protein Samples

Diffraction patterns were taken of the cerebroside sulphate-unbrominated cholesterol-myelin basic protein sample (figure 7.11a) at various relative humidities and the resulting structure factors were phased from the swelling series (figure 7.12) and were confirmed by inspection of the possible electron density profiles. The main ambiguity was the phasing of the 3rd order which I determined as positive on the basis of the shape of the hydrocarbon region compared with lower relative humidity profiles. Figure 7.13 shows the electron density profile at 1ØØ% relative humidity resulting from the preferred phasing compared with the electron density at 97% and 88% relative humidities. Comparsion of brominated and unbrominated data confirmed the phasing of the first five orders (figure 7.14). The resulting electron density profiles for the chosen phase assignments are shown in figure 7.15.

Unfortunately, compared with the unbrominated sample, I was never able to achieve equivalent resolution from

Figure 7.11 X-ray diffraction patterns taken of the protein-containing samples at 100% relative humidity using the line-focused camera. Pattern (a) was obtained from the CES-cholesterol-MBP sample, pattern (b) from the CES-brominated cholesterol-MBP sample, pattern (c) from the CES-cholesterol-cytochrome c sample and (d) from the CES-brominated cholesterol-cytochrome c sample.

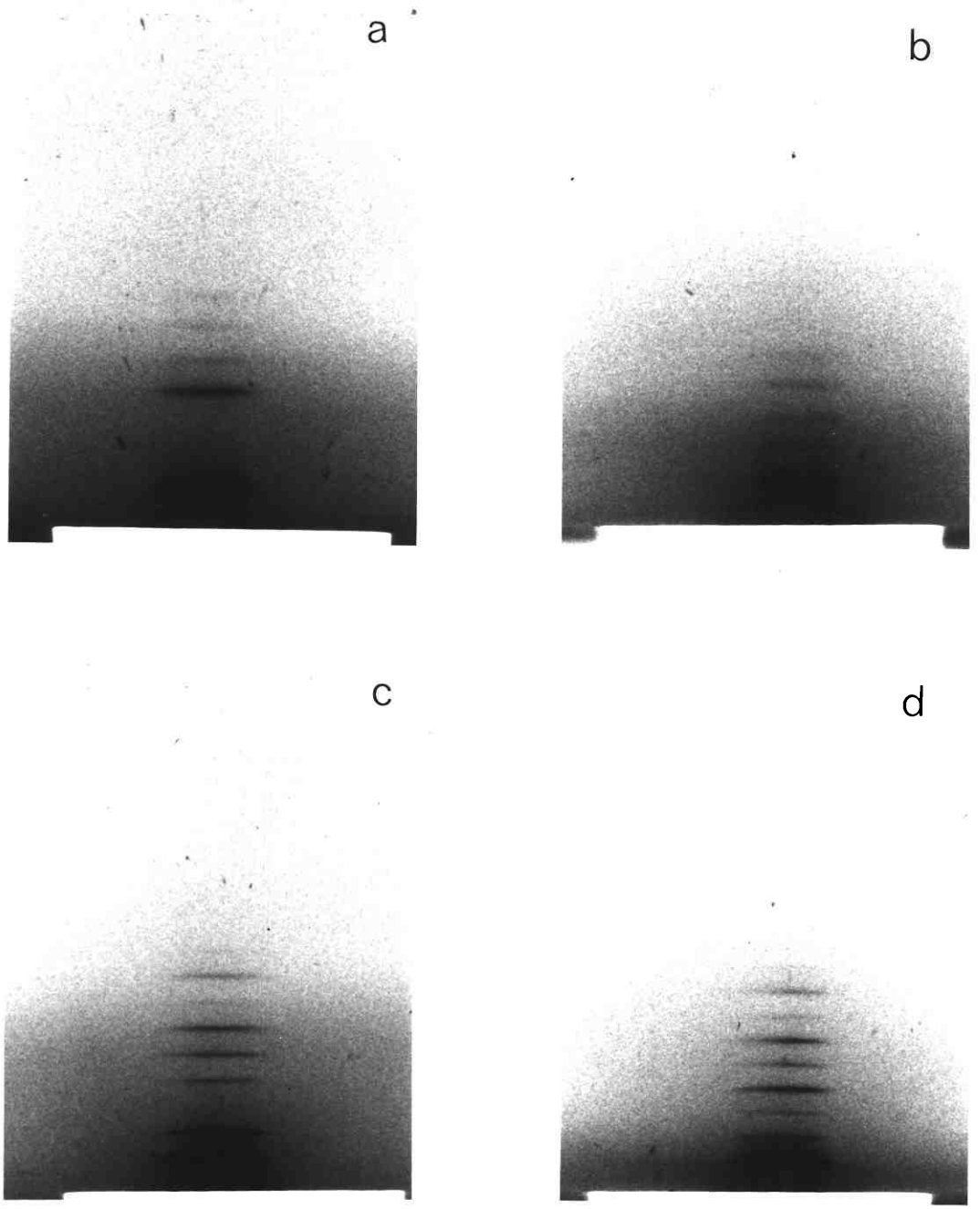
a
b
c
d

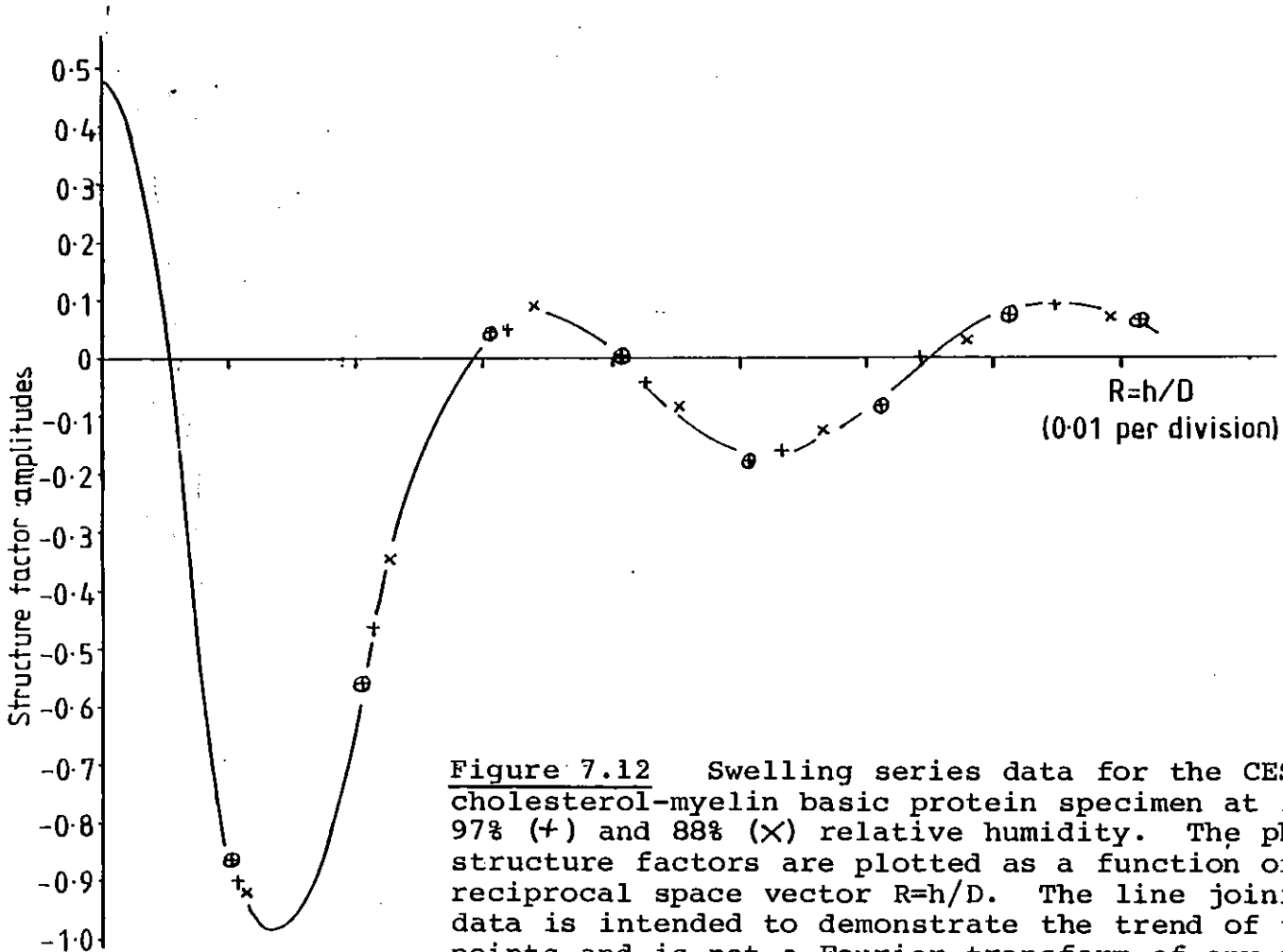

Figure 7.12 Swelling series data for the CES-cholesterol-myelin basic protein specimen at 100% (⊕), 97% (+) and 88% (×) relative humidity. The phased structure factors are plotted as a function of the reciprocal space vector R=h/D. The line joining the data is intended to demonstrate the trend of the data points and is not a Fourier transform of any particular set of data.

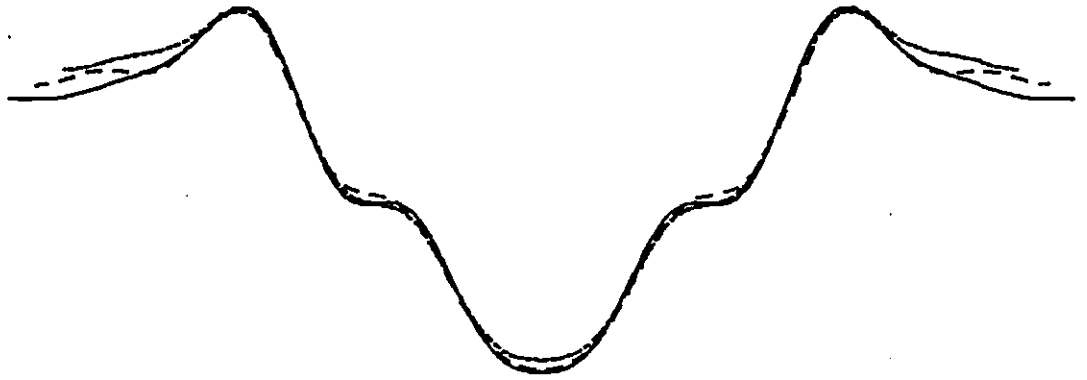

Figure 7.13 Electron density profiles for the CES-cholesterol-myelin basic protein sample at 100% (full line), 97% (dashed line) and 88% (dotted line) relative humidities.

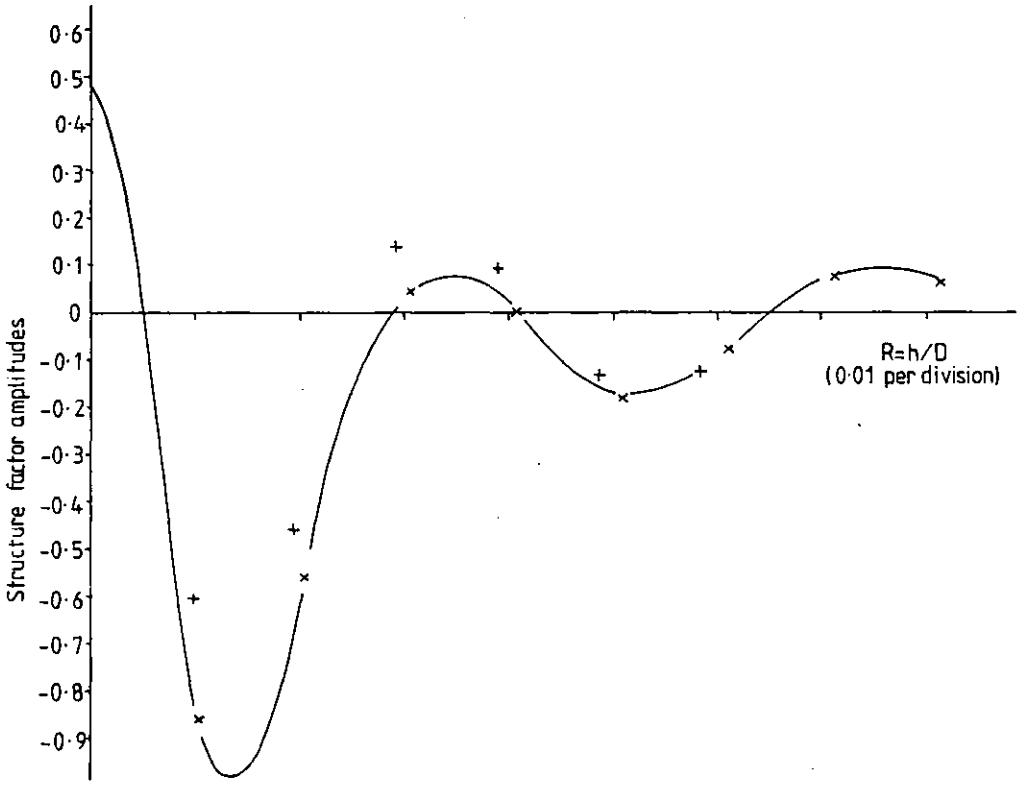

Figure 7.14 Comparison of the CES-brominated cholesterol-MBP structure factors scaled at 0.8 (+) and the CES-cholesterol-MBP structure factors (×) at 100% relative humidity plotted as a function of the reciprocal space vector R=h/D. The line joining the unbrominated data points is intended to demonstrate the trend of the data and is not a Fourier transform of the data.

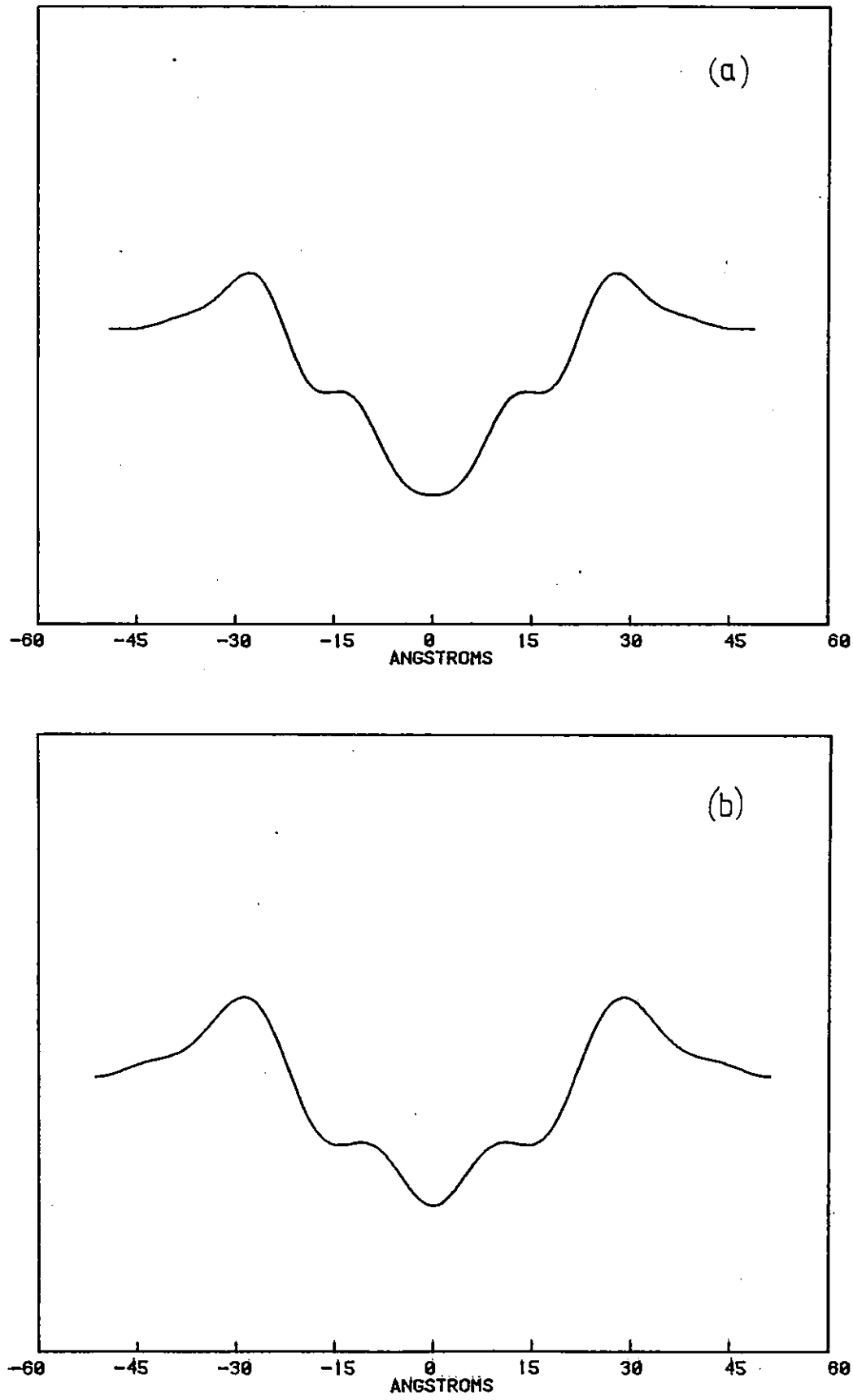

Figure 7:15 Electron density profiles of the CES-cholesterol-myelin basic protein sample (a) and the CES-brominated cholesterol-myelin basic protein sample (b) at 100% relative humidity.

myelin basic protein samples containing brominated cholesterol and found that the observable orders of the diffraction pattern were rather broad (figure 7.11b). This might well be due to variations in the water content during the experiment as I found that different samples, and even different exposures of the same sample, all at 100% relative humidity, varied in lamellar spacing. The structure factors of all the samples are plotted in figure 7.16, although it should be realised that the different samples have different protein contents (see table 7.1). Nevertheless, the assigning of phases seems well confirmed from these data.

In all further analysis in this thesis I have used sample 1 as the CES-brominated cholesterol-MBP sample, as this sample has a similar protein content (33%) to the unbrominated sample (31%). The difference profile between the brominated data scaled at 0.8 and the unbrominated data is shown in figure 7.17.

Cytochrome c Samples

Diffraction patterns collected from the cerebroside sulphate-cholesterol-cytochrome c samples, unbrominated and brominated, are reproduced in figures 7.11c and 7.11d respectively. The signs of the structure factors of this data were initially assigned from study of the swelling series (figures 7.18 and 7.19). The first seven phases were assigned unambiguously, ---0+-- for the unbrominated data and ---++-- for the brominated data. Comparsion of the unbrominated and brominated structure factors, with

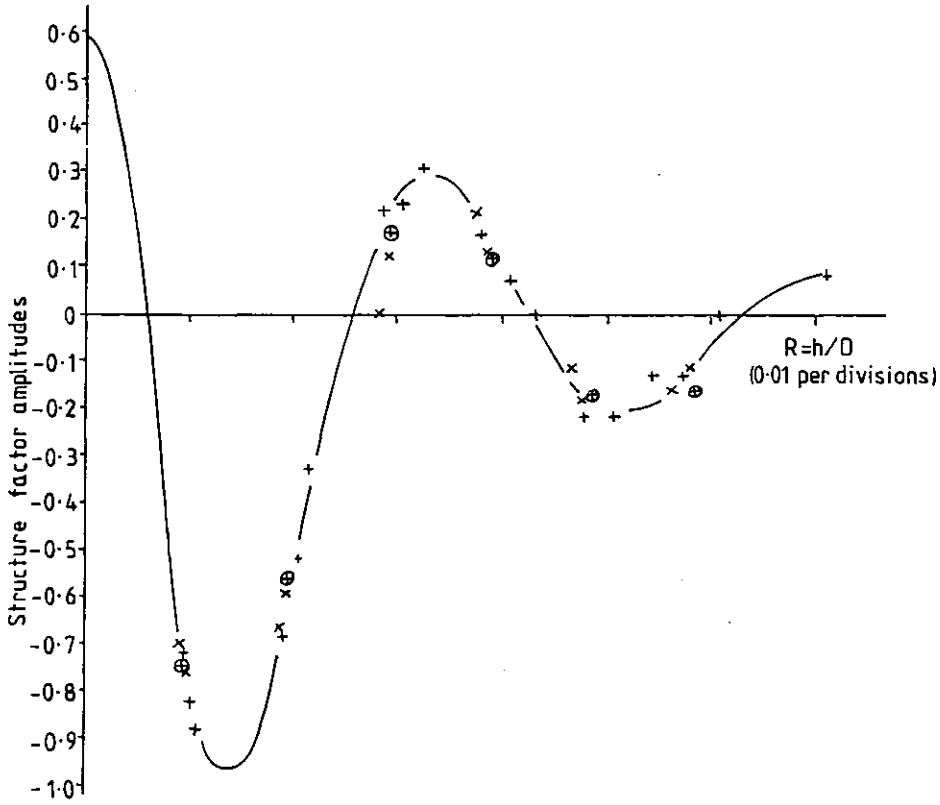

Figure 7:16 CES-brominated cholesterol-MBP structure factors plotted as a function of the reciprocal space vector R=h/D. The data from three different samples with different protein contents at various relative humidities are plotted on the same diagram; sample 1 (⊕), sample 2 (×) and sample 3 (+). The line through the data points is intented to demonstrate the general trend of the data and is not a Fourier transform of any particular data set.

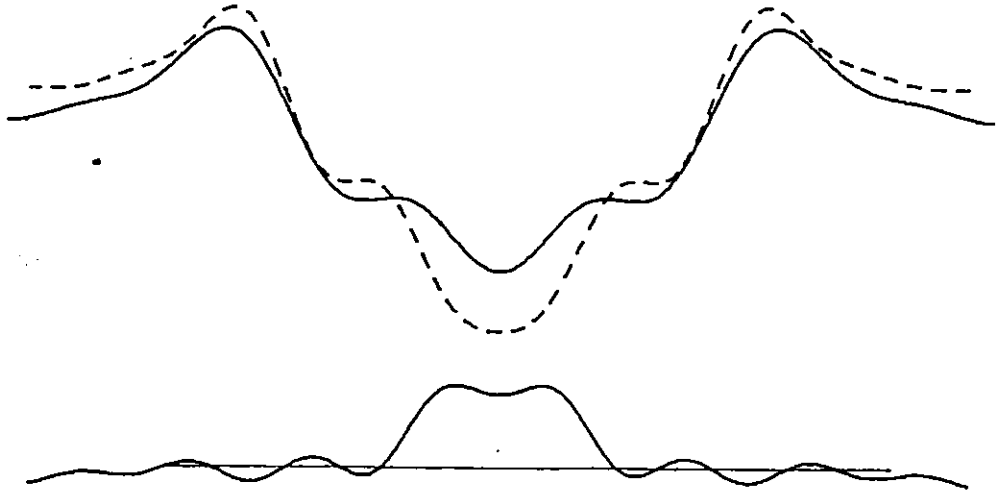

Figure 7:17 Comparison of the electron density profiles of CES-cholesterol-myelin basic protein scaled at Ø.8 (full line) with the profile of CES-cholesterol-myelin basic protein (dashed line). The difference profile is reproduced underneath.

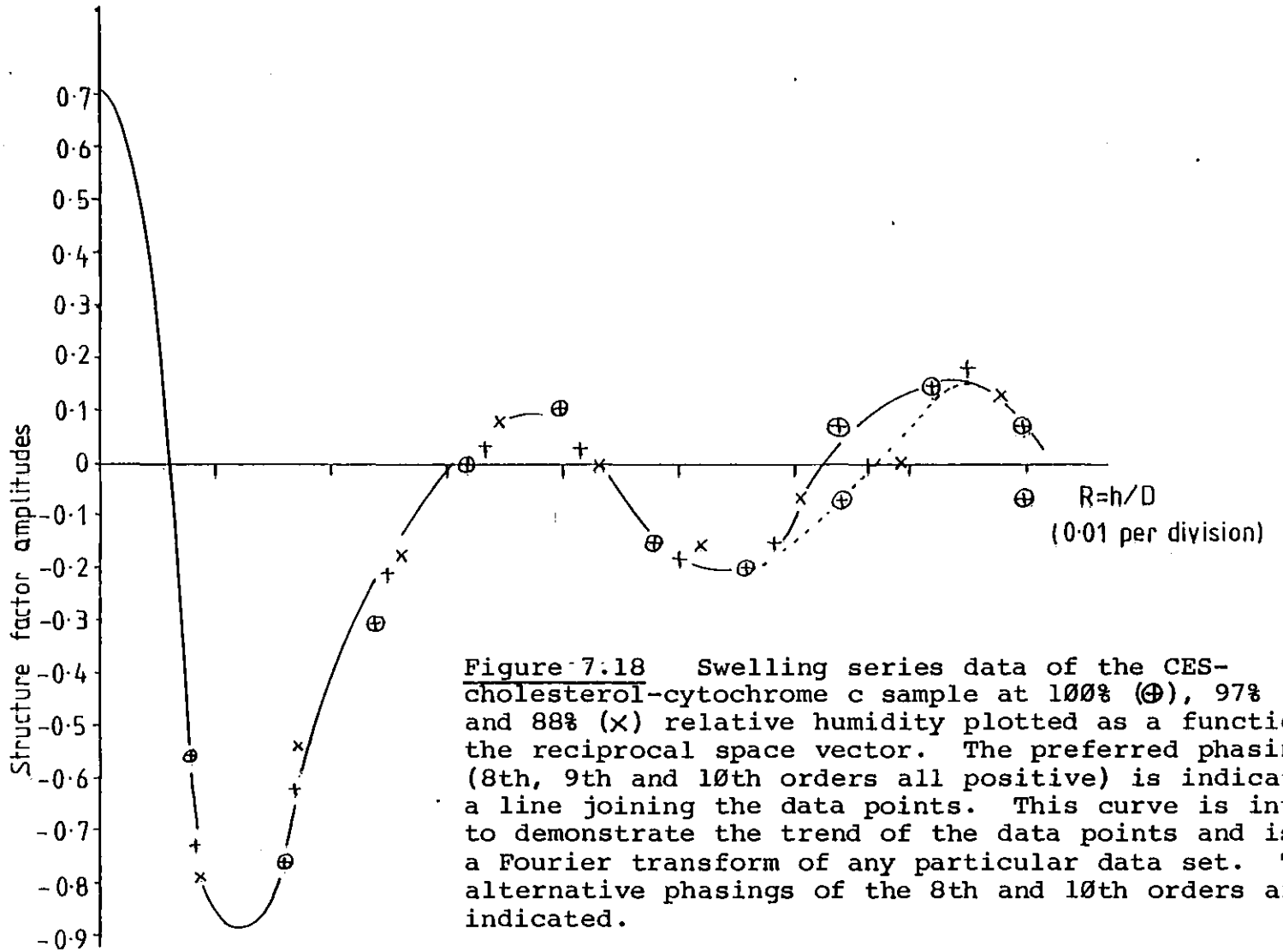

Figure 7.18 Swelling series data of the CES-cholesterol-cytochrome c sample at 100% (⊕), 97% (+) and 88% (×) relative humidity plotted as a function of the reciprocal space vector. The preferred phasing (8th, 9th and 10th orders all positive) is indicated by a line joining the data points. This curve is intended to demonstrate the trend of the data points and is not a Fourier transform of any particular data set. The alternative phasings of the 8th and 10th orders are indicated.

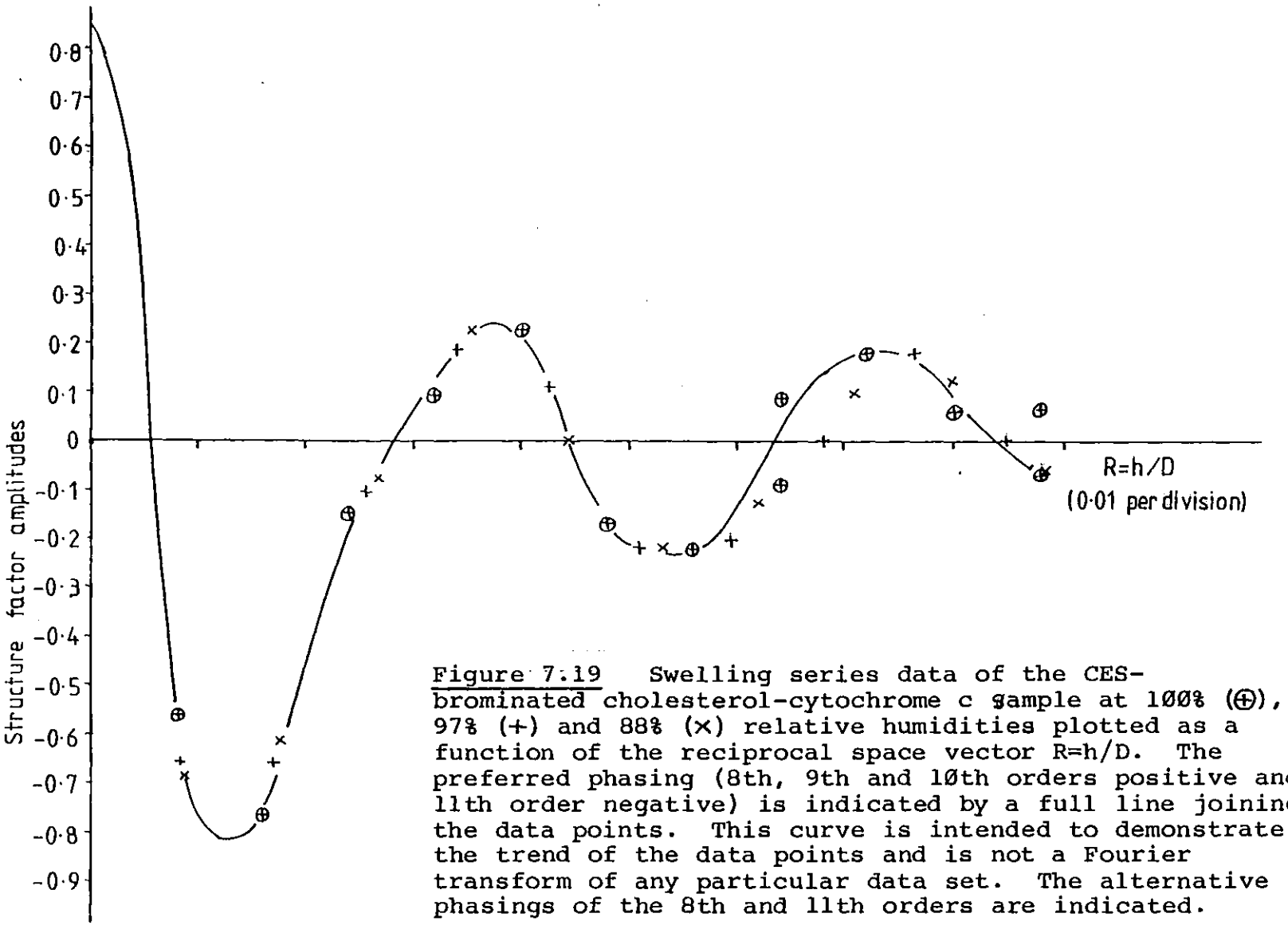

Figure 7.19 Swelling series data of the CES-brominated cholesterol-cytochrome c sample at 100% (⊕), 97% (+) and 88% (×) relative humidities plotted as a function of the reciprocal space vector R=h/D. The preferred phasing (8th, 9th and 10th orders positive and 11th order negative) is indicated by a full line joining the data points. This curve is intended to demonstrate the trend of the data points and is not a Fourier transform of any particular data set. The alternative phasings of the 8th and 11th orders are indicated.

the brominated data scaled by Ø.8, confirmed these phase assignments (figure 7.2Ø) but, unfortunately, the phases of the higher orders were still undetermined.

I decided on a positive 9th order by inspection of the electron density profiles, the hydrocarbon region with the alternative 9th order phasing being very different in shape from the lipid and the lipid-MBP hydrocarbon region. Having assigned a positive phasing to the 9th order, the 1Øth order, as phased using the swelling series, is probably also positive, but this is not conclusive. Inspection of the electron density profiles (figures 7.21a to d) calculated using the four possible phase assignments (8th and 1Øth orders still undefined) confirms that the tenth order is almost certainly positive, as explained below. The phasing with 8th order positive and 1Øth order negative (figure 7.21a) was rejected on the basis of the shape of the hydrocarbon region, the peak-to-peak separation compared with the lipid profile and the the presence of strong ripples in the protein region. The phasing with 8th order negative and 1Øth order negative (figure 7.21b) was rejected on the basis of a very different shape of the hydrocarbon region when compared with the lipid and lipid-MBP hydrocarbon region.

The phasing of the 8th order has never been fully determined. On the basis of the swelling series, I marginally prefer a negative phasing for the 8th order. This phasing results in a profile with a better looking hydrocarbon region, but with a ripple in the protein

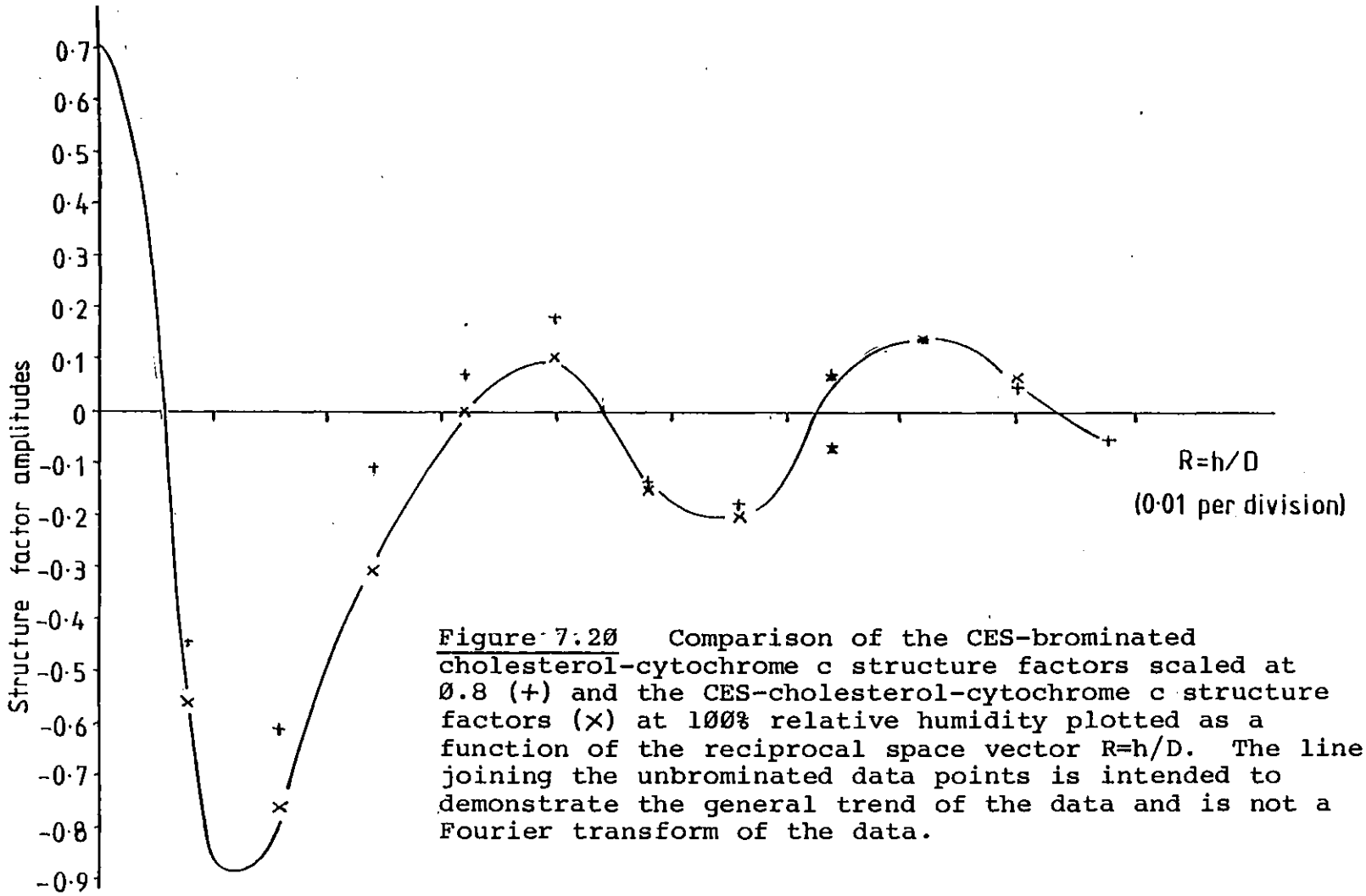

Figure 7.20 Comparison of the CES-brominated cholesterol-cytochrome c structure factors scaled at 0.8 (+) and the CES-cholesterol-cytochrome c structure factors (×) at 100% relative humidity plotted as a function of the reciprocal space vector R=h/D. The line joining the unbrominated data points is intended to demonstrate the general trend of the data and is not a Fourier transform of the data.

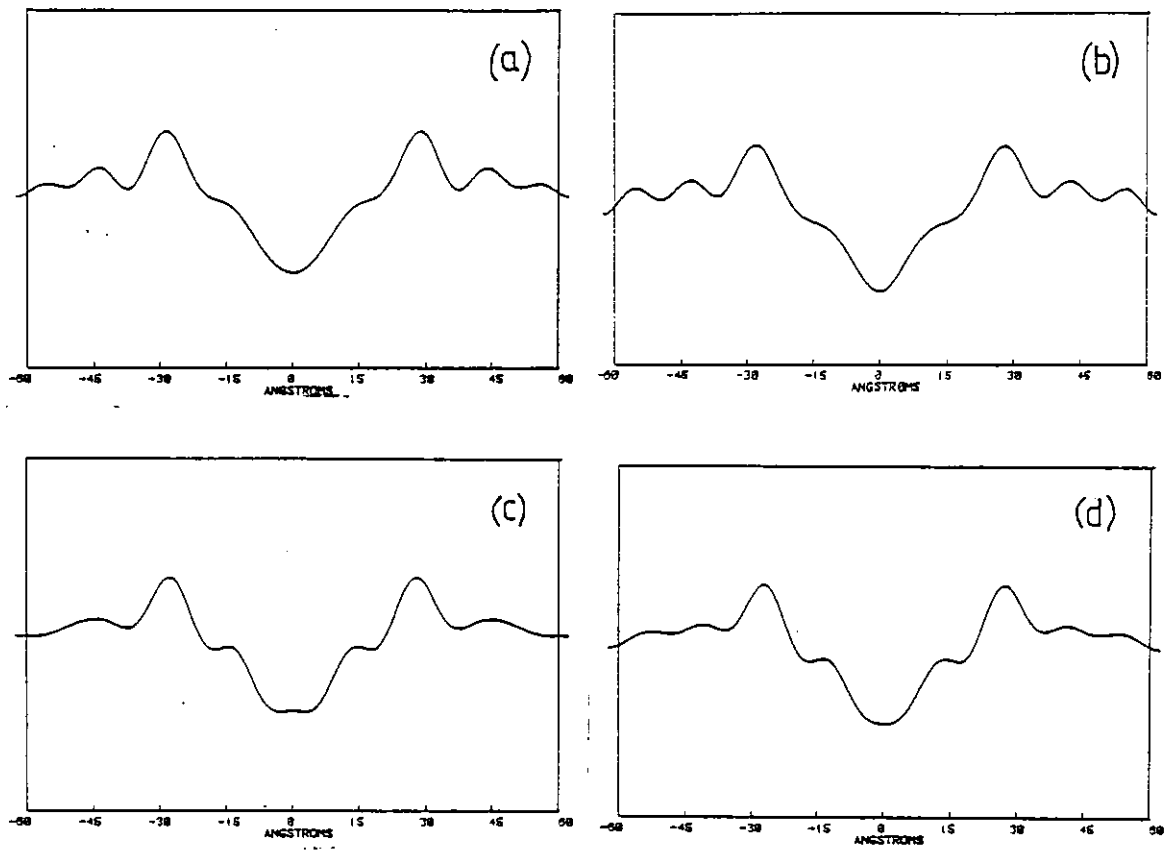

Figure 7.21 Comparison of the various electron density profiles of CES-cholesterol-cytochrome c resulting from the various possible phasings of the 8th and 10th orders. (a) is for the phasing with 8th order positive and 10th order negative and (b) is for the phasing with both 8th and 10th orders negative. These phasings were both rejected. (c) is for the phasing with 8th and 10th order positive and (d) is for the phasing with 8th order negative and 10th order positive.

region (figure 7.21c). In comparision, a positive 8th order produces a profile with a ripple in the centre of the hydrocarbon region, but with a more acceptable protein region, there being no evidence from crystallographic studies to assume anything other than evenly distributed electron density at this resolution (figure 7.21d). This thesis is mainly concerned with the conformation and disposition of the protein and so in all further analysis I have used the phase assignment with the 8th order positive as my preferred phasing, on the basis of the protein shape. However, in most cases I have also shown the results of using the alternative phasing (8th order negative) and it will be seen that this ambiguity of phase does not affect the absolute scaling or our conclusions on the siting of the protein within the membrane.

The phase assignments for the cerebroside sulphate-brominated cholesterol-cytochrome c data follow directly from those of the unbrominated sample, except that the former diffraction pattern at 100% relative humidity exhibits an 11th order. Unbrominated and scaled brominated electron density profiles (scale factor 0.8) for the various possible phasings are compared in figure 7.22. From the difference profiles I determined that the 11th order is negative, this phasing resulting in a similar electron density distribution for the bromine in the cytochrome c samples as in the myelin basic protein samples.

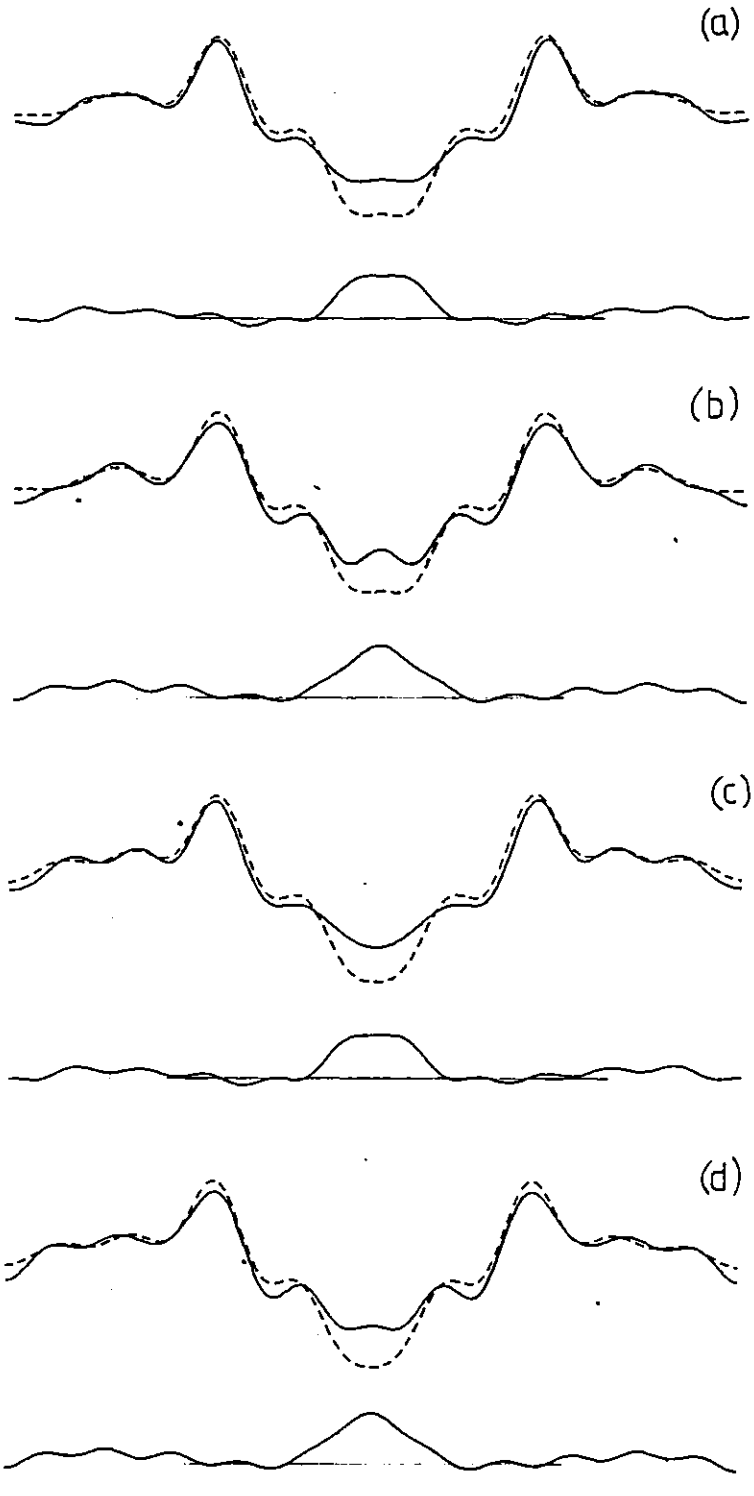

Figure 7.22 Comparison of the electron density difference profiles between CES-brominated cholesterol-cytochrome c scaled at Ø.8 (full line) and CES-cholesterol-cytochrome c (dotted line) for various phasings. (a) and (b) are obtained using the preferred phasing for the unbrominated data (8th order positive) and phasing the 11th order of the brominated data negative and positive in (a) and (b) respectively. (c) and (d) have the alternative phasing of the 8th order (negative) and have the phase of the 11th order of the brominated data negative and positive in (c) and (d) respectively. Profile (a) is preferred, but (c) is a possible alternative.

Relative Scaling of Profiles

The difference profiles between brominated and unbrominated samples (lipid-cholesterol, CES-cholesterol-MBP and CES-cholesterol-cytochrome c samples) have all been presented in the relevent sections. A table of the relevent figures and the chosen relative scalings is given below.

Type of Specimen	Figure	Relative scaling
cerebroside sulphate-cholesterol (dispersion specimens)	7.7	Ø.8
cerebroside sulphate-cholesterol (using evaporation data for brominated sample)	7.1Ø	Ø.85
CES-cholesterol-myelin basic protein	7.17	Ø.8
CES-cholesterol-cytochrome c	7.22	Ø.8

Table 7.2 The figure numbers of the difference profiles which have been presented already in this chapter.

Differences were also calculated between protein-containing and lipid-cholesterol structures, the difference in electron density now being due to the protein. Figure 7.23a shows the difference between CES-cholesterol-myelin basic protein and CES-cholesterol profiles, the lipid data being scaled by Ø.8. Figure 7.23b shows the difference between the equivalent brominated profiles, scale factor Ø.75. Electron density profiles for CES-cholesterol-cytochrome c (8th order positive) and CES-cholesterol (scaled at Ø.75) are compared in figure 7.24a and the equivalent brominated

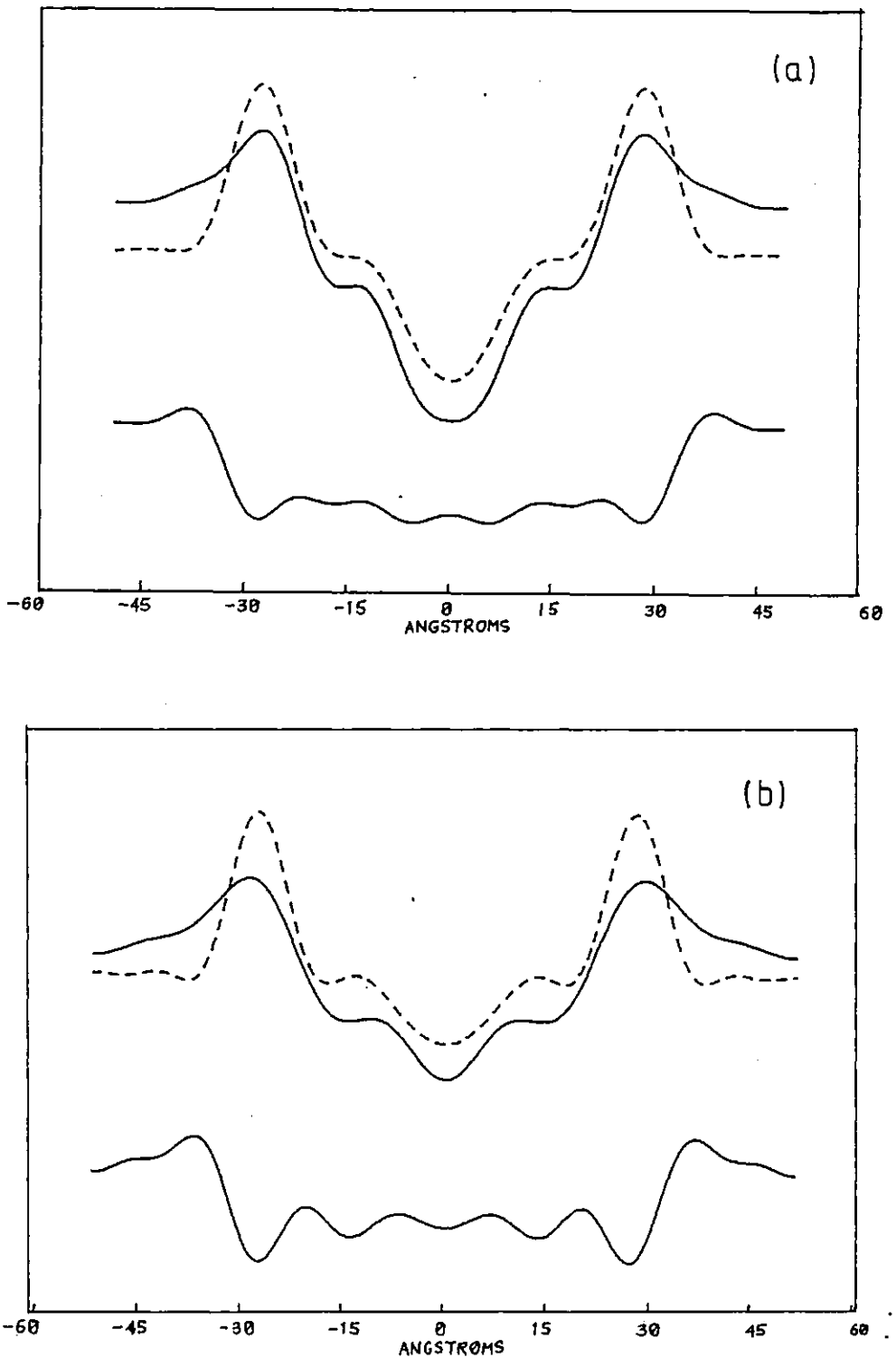

Figure 7.23 The difference profiles between myelin basic protein samples and lipid samples, the difference in electron density being due to the protein. (a) shows the difference between the CES-cholesterol profile (water layer extended) scaled at Ø.8 (full curve) and the CES-cholesterol-myelin basic protein profile at 1ØØ% relative humidity (dashed curve). (b) compares the equivalent brominated profiles, the CES-brominated cholesterol data being scaled by Ø.75.

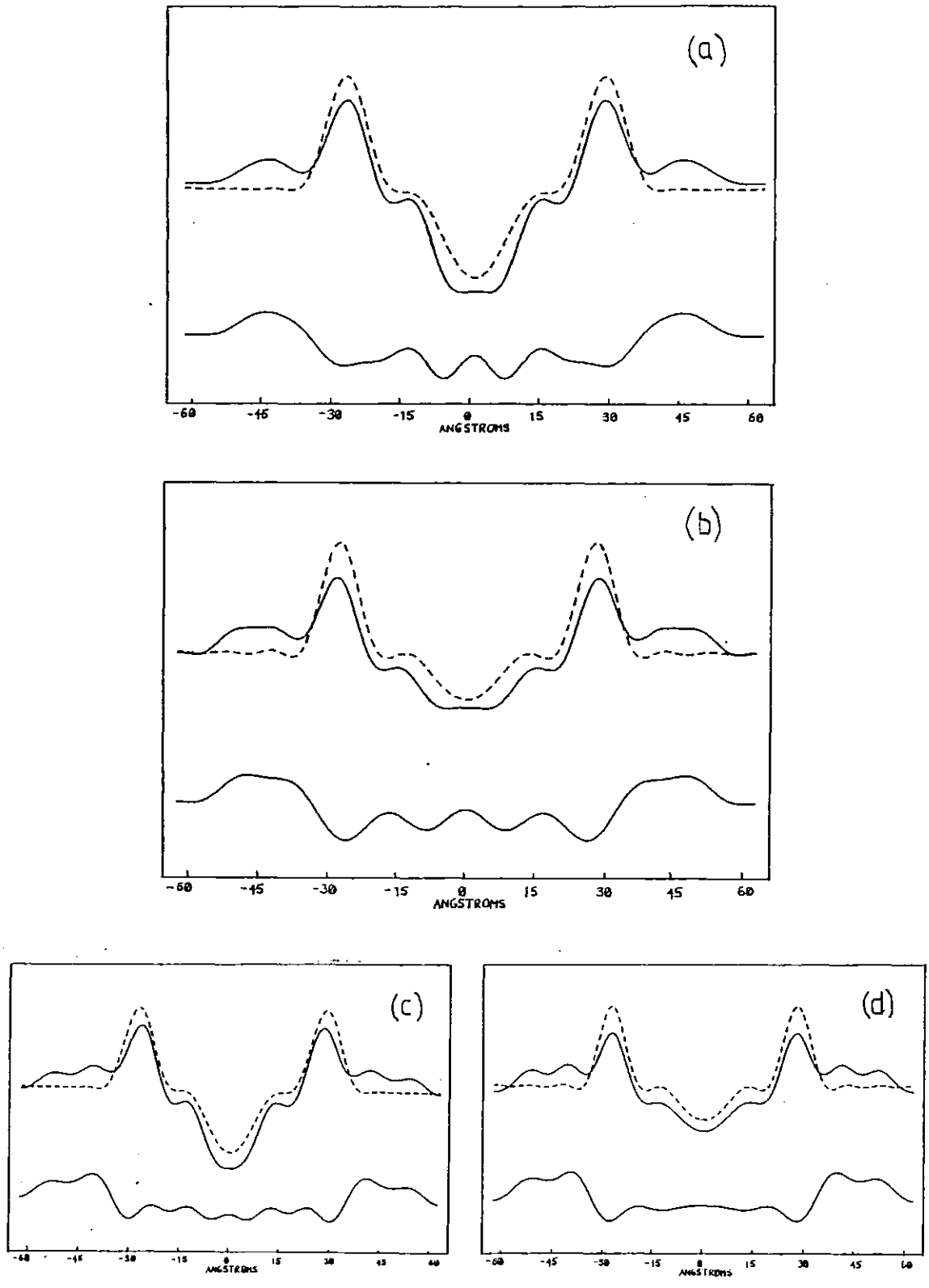

Figure 7.24 The difference profiles between cytochrome c samples and lipid profiles, the difference in electron density being due to the protein. (a) shows the difference between the CES-cholesterol profile (water layer extended) scaled at Ø.8 (dashed curve) and the CES-cholesterol-cytochrome c profile (full curve). (b) compares the equivalent brominated profiles, scale factor Ø.75. (c) and (d) show equivalent profiles to (a) and (b) respectively, except the alternative phasing (8th order negative) has been used for the cytochrome c data.

profiles in figure 7.24b (scale factor Ø.75). The electron density difference profiles using the alternative phasing (8th order negative) are shown in figures 7.24c and 7.24d.

The most important point to notice concerning the protein difference profiles is that in all cases the protein does not penetrate past the lipid head-group peak. In the course of the analysis, a range of relative scalings besides those reproduced in figures 7.23 and 7.24 were investigated, but difference profiles showing protein penetration were never produced. The disposition and conformation of the protein molecules as determined from these difference profiles will be discussed in chapter VIII.

Before considering the absolute scaling of these profiles, it is worth noting the self-consistency of the relative scalings. Figure 7.25 shows the relative scale factors used when comparing the pair of samples joined by the arrow, the sample at the tail of the arrow being the one which is scaled. A scale factor is chosen independently for each pair of samples on the basis of the best looking difference profile, and, at this resolution, it is extremely difficult to assign scale factors to the nearest Ø.Ø5 with any certainty. However, as shown in figure 7.25, the various relative scalings are all consistent with each other within experimental error.

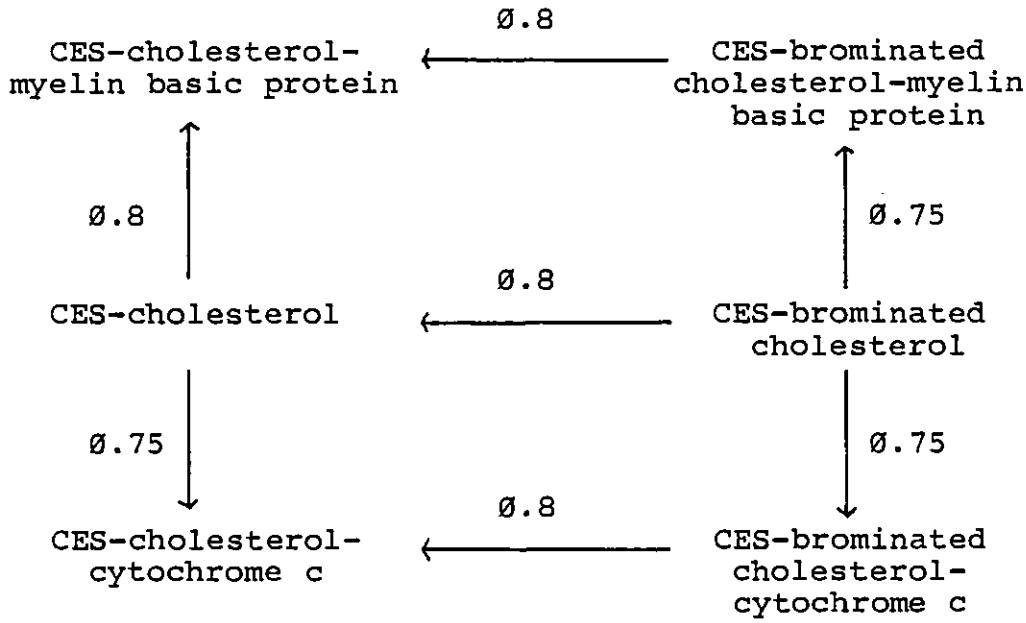

Figure 7:25 Diagram showing the relative scale factors used when comparing the pair of samples joined by the arrow, the sample at the tail of the arrow being the one which is scaled. The relative scale factor is determined empirically for each pair of samples.

Absolute Scaling of Profiles

Calculation of an absolute scale for the electron density profiles requires knowledge of the chemical composition of the membranes. Unfortunately, at the time of writing this thesis, the technique for determining the water content of the samples was not yet operative. Therefore, in order to calculate an electron density scale, an an assumption was required. The assumption made was that the lipid partial thickness remained constant at 51Å (5Ø.7Å for brominated samples) throughout the various experiments. This is reasonable because the peak-to-peak separation is constant within experimental error in all the samples. The value of 51Å for the partial thickness was calculated by assuming an area per unit cell (1 CES molecule + 2/3 cholesterol per monolayer) of $75Å^2$ and a lipid density of $1g/cm^3$. (Franks et al. 1982) measured the area/molecule of polar myelin lipids and 4Ø moles% cholesterol as 72.7Å). The value of 5Ø.7Å for the brominated lipid partial thickness was calculated by assuming changes in area/molecule and density of the same proportion as those observed by Franks et al. 1978.

In order to calculate an absolute electron density scale, the mass density and electron density of the various sample constituents are required. Experiments to measure the mass densities of the various chemical components are at present being carried out in this laboratory by Dr W. Macnaughtan, but as the experimints have not yet been completed, I have had to rely on values in the literature. Table 7.3, shown overleaf, gives the

	Density at 20°C /g cm^{-3}	Electron density /e- $Å^{-3}$	Reference
Water	Ø.998	.334	CRC Handbook 1974 Own calculation
CES + 4Ømol % cholesterol	1.ØØ	.346	Estimate (cf. Mateu et al. 1973) Franks et al. 1982
CES + 4Ømol % brominated cholesterol	1.Ø3	.355	(1) (1)
Myelin basic protein	1/Ø.721	.441	Eylar & Thompson 1969 Kirschner 1971
Cytochrome c	1/Ø.728	.438	Margoliash & Schejter 1966 Own calculation.

(1) Calculated by assuming similar changes in lipid density when using brominated cholesterol to those observed by Franks et al. 1978.

Table 7.3 The values used in this thesis for the density and electron density of the various sample components.

values of mass density and electron density used and the sources of these values.

From the assumption of a constant lipid partial thickness of 51Å (50.7Å for a brominated sample) and knowing the lamellar spacing D and the protein to lipid ratio, the water content of a sample can be calculated. The calculated water contents (in weight %) of the samples of this study are given in table 7.4. It can be seen that these values are very consistent.

The partial thickness of all the components can now be calculated from the weight fraction of the various components and their mass densities (see Franks and Levine 1981). Table 7.5 (overleaf) lists the calculated partial thicknesses of protein, lipid and water in the various samples at 100% relative humidity.

Calculation of the absolute electron density scale requires measurement of the area under the difference profiles (Franks et al. 1978). This area is simply related either to the number of electrons in the unit cell due to the bromine atoms or to the number of extra electrons in the unit cell (relative to water) due to the protein content. The absolute electron density scale in $e^-/Å^3$ per cm is calculated from the measured area under the difference profile (in cm^2), the cross-sectional area of the unit cell in $Å^2$, the number of extra electrons per unit cell and the scaling of the profile across the bilayer in Å per cm. An electron density scale can be calculated independently from each difference profile. In this study, an average value of the absolute electron

Sample	Water content (weight %)
CES-cholesterol (dispersion sample)	30.9
CES-brominated cholesterol (dispersion sample)	30.1
CES-brominated cholesterol (evaporation sample)	29.2
CES-cholesterol-MBP	29.3
CES-brominated cholesterol-MBP (sample 1)	29.8
CES-cholesterol-cytochrome c	31.9
CES-brominated cholesterol-cytochrome c	29.9

Table 7.4 Calculated water contents (in weight %) of the various samples used in this thesis.

Sample	Lamellar spacing (in Å) D	Partial thicknesses (in Å) t_p	t_w	t_l
CES-cholesterol(dispersion)	73.8	-	22.8	51
CES-brominated cholesterol (dispersion)	73.3	-	22.6	50.7
CES-brominated cholesterol (evaporation)	72.4	-	21.7	50.7
CES-cholesterol-MBP	98.2	16.5	30.7	51
CES-brominated cholesterol-MBP	102.7	18.7	33.3	50.7
CES-cholesterol-cytochrome c	124.9	30.4	43.5	51
CES-brominated cholesterol-cytochrome c	124.8	32.6	41.5	50.7

Table 7.5 Partial thicknesses of protein (t_p), water (t_w) and lipid (t_l) in the various samples at 100% relative humidity[1] (note that the lipid partial thickness is fixed).

density scale has been calculated, taking into account the relative scalings of one profile with respect to another, and this averaged value has been used to scale the profiles shown in figures 7.26 to 7.29.

Although the scale of the profile has now been determined, the profile can still be translated with respect to this scale. Its position on the scale is fixed by knowing the absolute electron density of any point on the profile (such as the water layer) or the mean electron density. In this study, the profiles have been fixed relative to the absolute scale using the mean level. The absolute electron density of the mean level is calculated from the partial thickness and the electron density of the various components (tables 7.3 and 7.5). The final scaled profiles are shown in figures 7.26, 7.27, 7.28 and 7.29 for the lipid dispersion samples, the brominated lipid evaporation specimen (original and smoothed profiles), the myelin basic protein samples and the cytochrome c samples respectively.

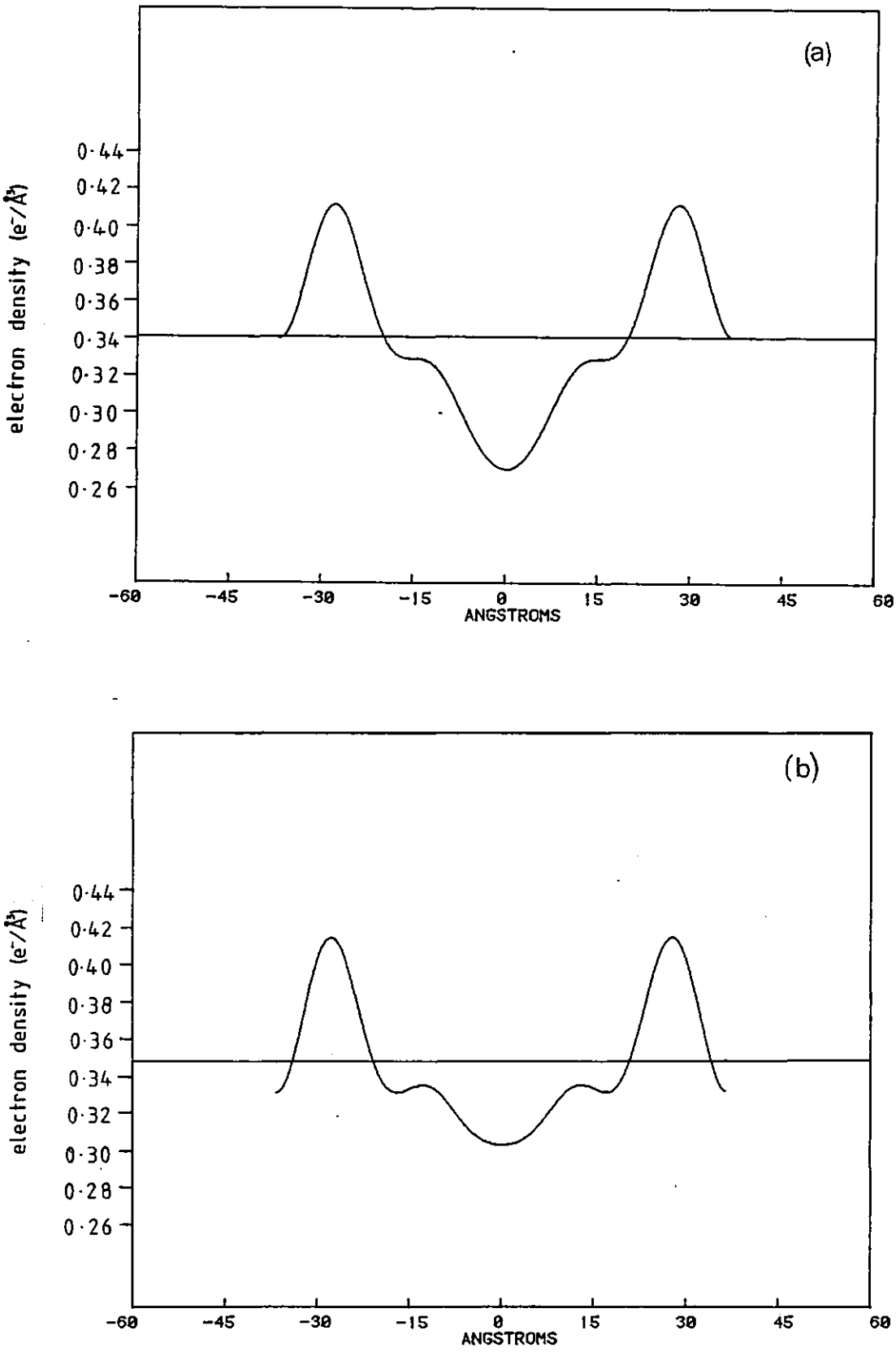

Figure 7.26 Scaled electron density profiles for (a) the CES-cholesterol dispersion sample and (b) the CES-brominated cholesterol dispersion sample. The mean electron density levels are shown in both cases.

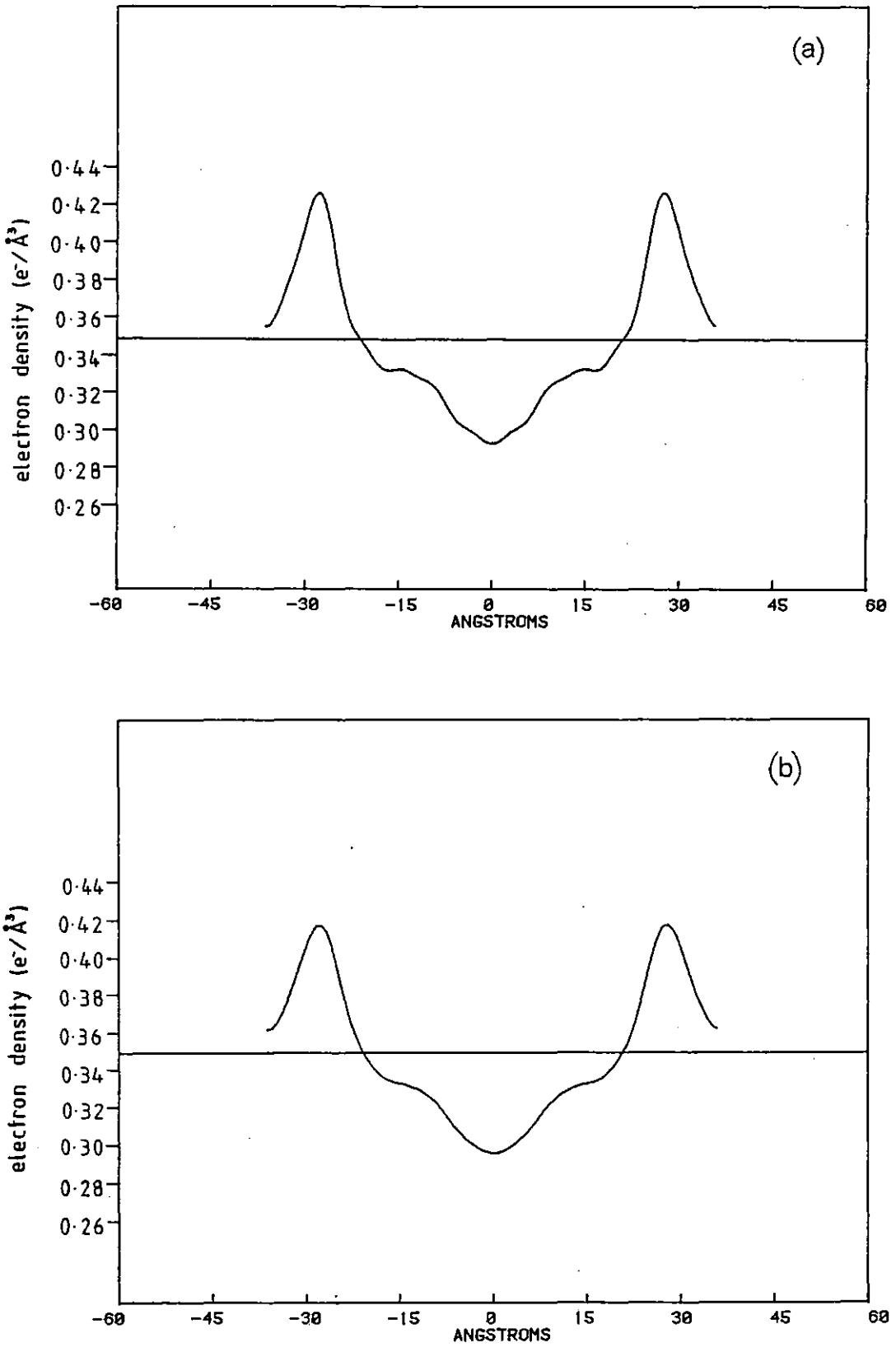

Figure 7.27 Scaled electron density profiles for the CES-brominated cholesterol evaporation sample. (a) is the profile obtained using the original high resolution data and (b) is the lower resolution smoothed profile (temperature factor B=200). The mean electron density levels are shown in both cases

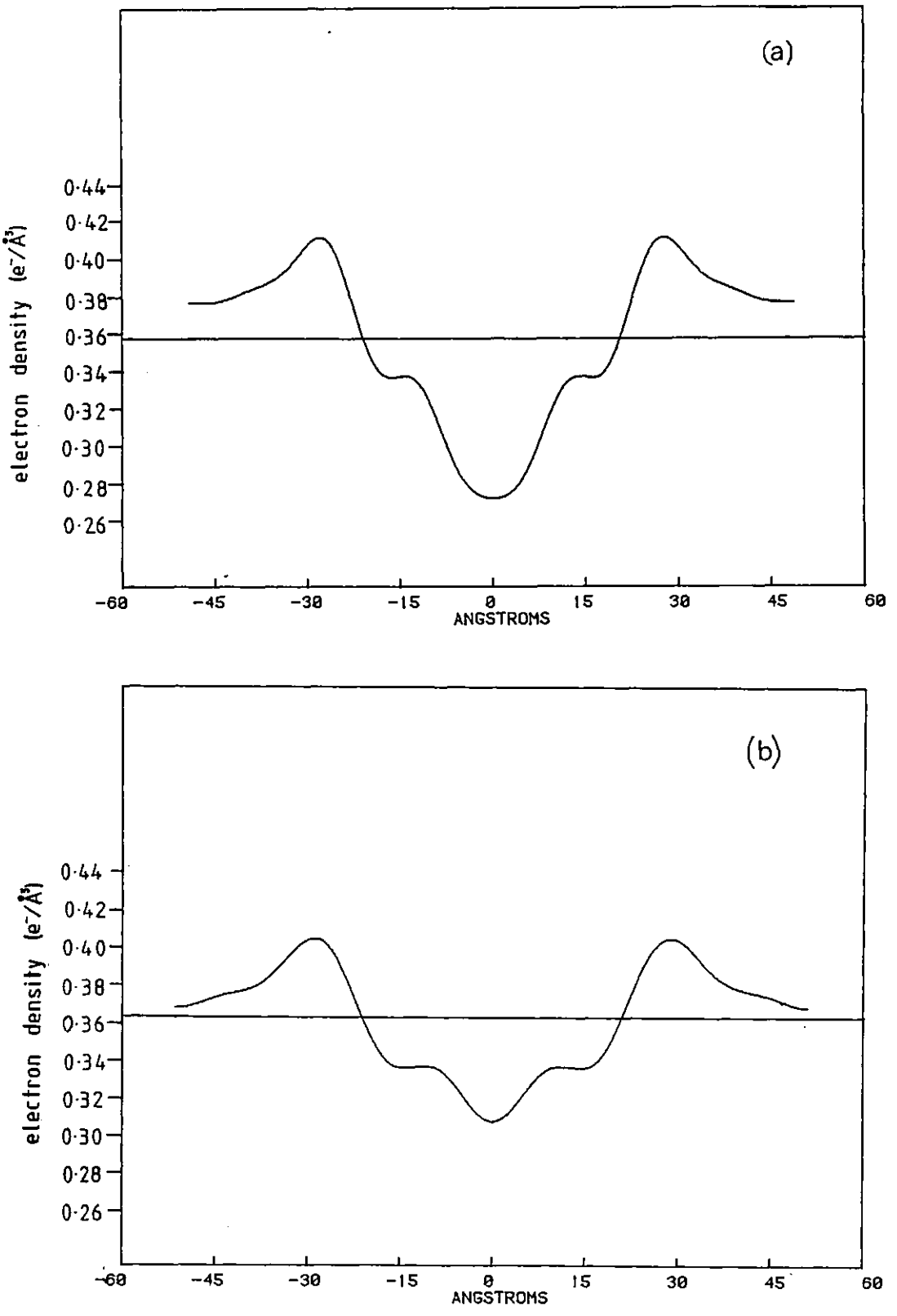

Figure 7:28 Scaled electron density profiles for (a) the CES-cholesterol-myelin basic protein sample and (b) the CES- brominated cholesterol-myelin basic protein sample (sample 1). The mean electron density levels are shown in both cases.

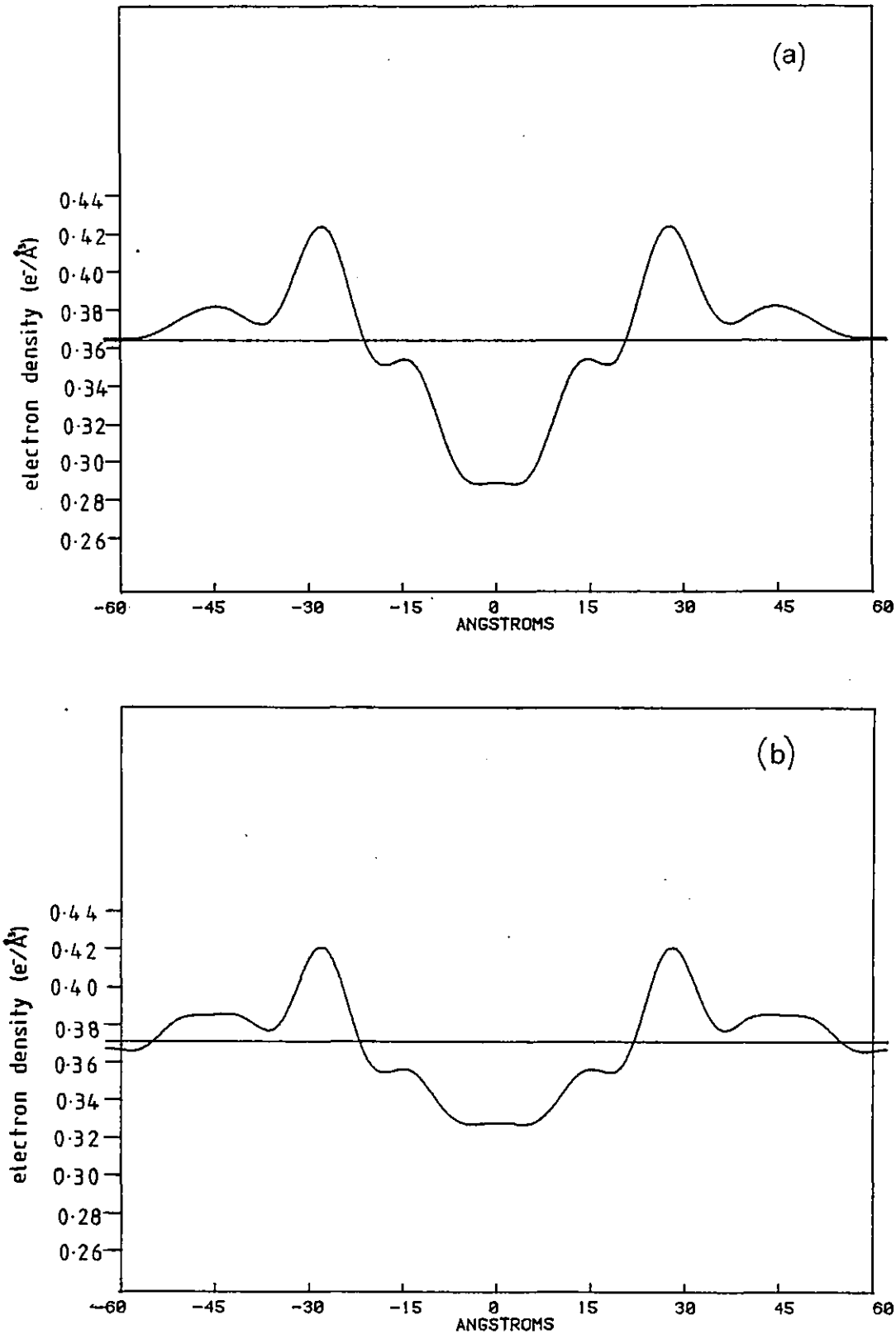

Figure 7:29 Scaled electron density profiles for (a) the CES-cholesterol-cytochrome c sample and (b) the CES-brominated cholesterol-cytochrome c sample (phasing 8th order positive). The mean electron density levels are shown in both cases.

CHAPTER VIII

DISCUSSION AND CONCLUSIONS

The position of the protein in the membrane as determined from these experiments is shown overleaf in figures 8.1 and 8.2 for myelin basic protein and cytochrome c respectively. In these diagrams the difference profile has been set to zero in the protein-free region for clarity (see also figures 7.23 and 7.24). Figures 8.1 and 8.2 result from using lipid and lipid-protein samples containing 40 moles% cholesterol, but similar profiles result if lipid and lipid-protein samples containing brominated cholesterol are compared (see figures 7.23b and 7.24d).

The most important point to note is that neither protein penetrates into the lipid bilayer past the lipid head-group peak. This will be discussed in detail later in this chapter.

Table 8.1 gives details of the width of the two proteins and the distance of the protein molecules from the lipid head-group as determined in this thesis. An initial glance at the profiles and at the table would suggest a closer apposition and hence, prehaps, a different interaction between the myelin basic protein and the lipid head-groups than between the cytochrome c and the lipid head-groups. However, considering the cytochrome c as a sphere of roughly 30Å diameter and considering the myelin basic protein as an cigar-shaped

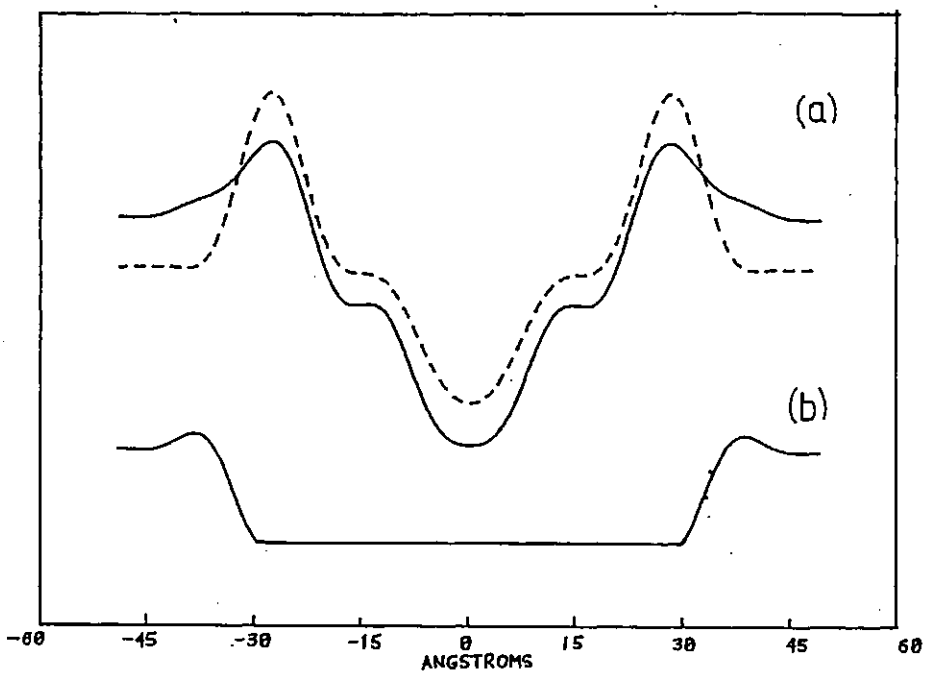

Figure 8.1 Difference profile (set to zero in the protein free region) showing the position of the myelin basic protein in a cerebroside sulphate-cholesterol-MBP membrane. The two profiles which are compared, the CES-cholesterol profile (dashed line) and the CES-cholesterol-MBP profile (full line), are shown in (a) and the electron density due to the myelin basic protein is shown in (b).

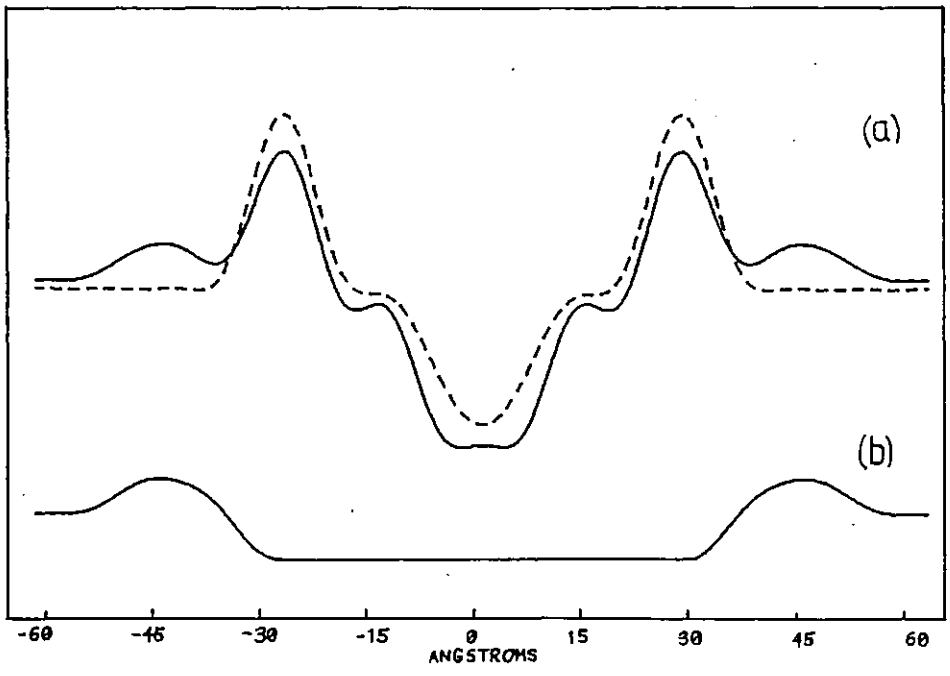

Figure 8.2 Difference profile (set to zero in the protein free region) showing the position of the cytochrome c in a cerebroside sulphate-cholesterol-cytochrome c membrane. The two profiles which are compared, the CES-cholesterol profile (dashed line) and the CES-cholesterol-cytochrome c profile (full line), are shown in (a) and the electron density due to the cytochrome c is shown in (b).

	MBP	cytochrome c
Total width of protein	22Å	32Å
Width of protein (at half height)	19Å	27Å
Distance of protein peak from lipid head-group peak	8Å	16Å
Distance of protein (at half height) from lipid head-group	4Å	7Å

Table 8.1 Comparsion of the dimensions and disposition of the cytochrome c and myelin basic protein in reconstituted membranes as determined from electron density difference profiles.

molecule 150Å × 15Å × 15Å, packing restrictions of these molecules on the surface of the bilayer would seem to result in similar electron density profiles to those shown, even if the type of interaction was the same in both cases.

It can be seen from the cytochrome c profile in figure 8.2 that the electron density level at the mid-point between the two bilayers (i.e. at the edge of the profile) does not fall to the electron density level of water. Considering the cytochrome c molecules as symmetric spheres of constant electron density, this mid-point electron density level can be explained in terms of interlocking of the planes of cytochrome c molecules. The cytochrome c molecules may all be orientated such that one particular area on the surface of the protein molecule interacts specifically with the lipid head-groups. Alternatively the cytochrome c molecules might be randomly orientated on the bilayer surface and could be considered as positively charged spheres interacting electrostatically and non-specifically with a negatively charged plane of lipid head-groups. Due to the roughly spherical shape of the cytochrome c molecules, the difference between these two structural models cannot be determined by low-angle X-ray diffraction. In comparison, the electron density due to one myelin basic protein molecule is asymmetric indicating that the myelin basic protein molecule is asymmetric and is orientated with respect to the lipid bilayer with a specific area of the protein molecule interacting with the lipid bilayer.

Hydrophobic Interaction of MBP with Lipid?

As already discussed, the results of our experiments show no penetration of the protein molecules past the peak of electron density corresponding to the position of the lipid head-groups. This is, in the case of the myelin basic protein, in contradiction with the widely held belief that myelin basic protein interacts with the lipids, at least in part, hydrophobically. The amino acid sequence of myelin basic protein contains segments, five to nine amino acids long, containing only apolar and hydrophobic amino acids (Eylar et al. 1971). According to Boggs et al. (1982) "there is abundant evidence that these hydrophobic segments can interact with the lipid fatty acid chains either by partially penetrating into the bilayer ... or by deforming and expanding the bilayer such that the fatty acid chains are exposed to the hydrophobic regions of the protein". The schematic diagrams demonstrating these two types of lipid-protein interaction are reproduced from Boggs et al. (1982) in figure 8.3.

The evidence for hydrophobic interaction of the myelin basic protein with lipid is summarised below and it is compared with similar evidence for cytochrome c where available. There have been four main areas of experiments in this field, monolayer studies, vescicle permeability, differential scanning calorimetry and various spectroscopic studies, and these will be discussed in turn. The only studies which will be discussed in detail are the monolayer studies, as this is the only area of which I have direct experience.

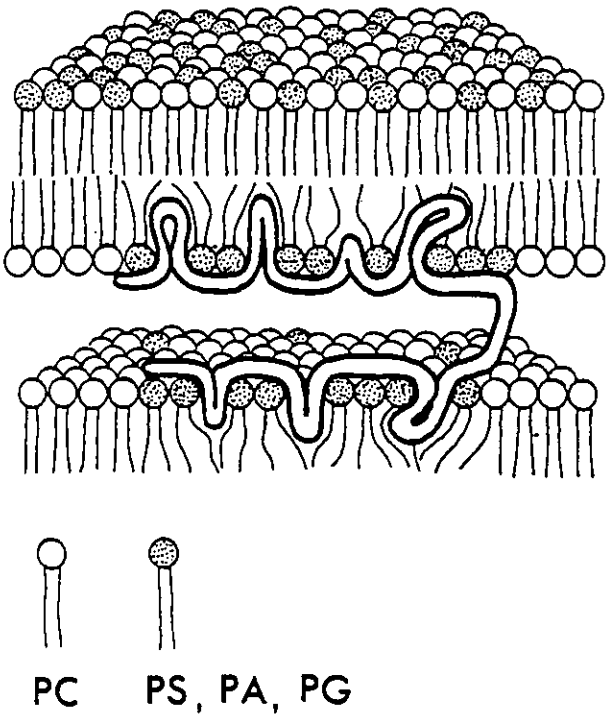

Figure 8. Schematic representation of myelin basic protein bound to lipid bilayer. Protein is shown bent at Pro-Pro-Pro region in center of sequence, with each half interacting with adjacent bilayers. However, it is probably just as likely that both halves of the protein interact with the same bilayer. Hydrophobic segments are shown penetrating into the lipid bilayers. In a mixture of lipids, acidic lipids such as PS, PA, and PG are separated out and bound to the protein as indicated.

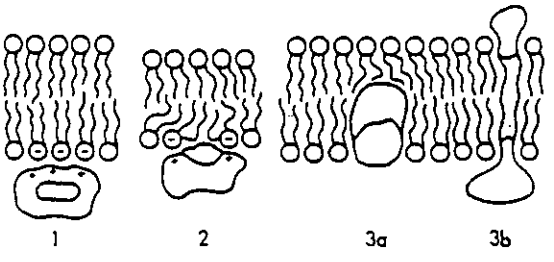

Figure 9. Schematic representation of different types of lipid-protein interaction: (1) electrostatic only, (2) electrostatic plus hydrophobic (shaded) resulting in deformation of the bilayer, (3a,b) hydrophobic interaction. The interaction of basic protein with lipid may be of type 2 while lipophilin may be of type 3. From Papahadjopoulos et al. (1975).

Figure 8.3 Schematic diagrams and figure legends reproduced from Boggs et al. (1982) demonstrating two possible methods of hydrophobic interaction between lipid and protein. Figure (a) demonstrates protein penetration and figure (b2) demonstrates bilayer deformation.

Monolayer Studies

The interaction of cytochrome c and myelin basic protein with various lipid monolayers has been studied by Quinn and Dawson (1969a, 1969b) and by Demel et al. (1973) respectively. Both groups have observed an increase in the surface pressure of a lipid monolayer held at constant area when protein is injected underneath. The degree of pressure increase depends on the monolayer constituents and on the initial surface pressure, the lower initial pressures showing the greatest pressure increase. For both proteins, the effect was more marked with acidic lipid monolayers than with neutral; for example, lecithin monolayers. Cytochrome c injected beneath a cardiolipin monolayer at 25 dynes/cm produced an increase in pressure of 8 dynes/cm and myelin basic protein injected beneath a cerebroside sulphate monolayer at 27 dynes/cm resulted in a pressure increase of 10 dynes/cm. By comparing the results for both proteins interacting with a variety of monolayers it can be seen that the extent of the effect is similar for the two proteins.

Unfortunately both groups concentrated their experiments at low initial pressures, 2-10 dynes/cm, where larger effects are seen, instead of the higher surface pressures where the packing of the lipid molecules is more akin to that found in natural membranes. Also, with one exception which will be discussed later, there was no measurement of the change in area per molecule if the monolayer was held at constant pressure. At high surface pressures (30-40 dynes/cm) the π-A isotherm is very steep

and large pressure changes correspond to only small changes in area per molecule.

The work of Demel et al. (1973) has frequently been quoted as evidence of insertion of hydrophobic parts of the basic protein molecule into the membrane. Two particular observations are reported as demonstrating hydrophobic interactions between the myelin basic protein and cerebroside sulphate. Firstly, the increase in area at constant pressure was measured for a cerebroside sulphate monolayer at a surface pressure of 10 dynes/cm. An area increase of 200% was found after interaction with the myelin basic protein. Using the quoted lipid to protein ratio of 30:1, one can calculate that each protein molecule covers an area of about 3600$Å^2$ and so is only about 10Å thick. Therefore, at these low surface pressures instead of the protein molecule lying beneath the lipid surface with some hydrophobic penetration, the whole protein molecule has probably entered the monolayer and may have denatured at the air-water interface.

A more convincing experiment was undertaken by Papahadjopoulos et al. (1975) in which the increase in monolayer area was measured at a constant surface pressure of 25 dynes/cm when protein was injected beneath a phosphatidyl serine monolayer. Results showed that injection of myelin basic protein up to a subphase concentration of 1.6 µg/ml caused a 68% increase in the surface area of the monolayer after one hour and injection of cytochrome c up to a subphase concentration of

2.Ø µg/ml caused a 38% increase in the monolayer area. The constant surface pressure of 25 dynes/cm is evidently more relevant to the state of the lipids in natural membranes than the 1Ø dynes/cm used by Demel et al. but the monolayer may still be in a relatively expanded state and insertion of the whole protein molecule into the monolayer may still be occuring. However, even if hydrophobic penetration is occuring in the monolayer, as suggested by Demel et al., this is not necessarily indicative that penetration will similarly occur in the bilayer, as the forces acting in a monolayer and in a bilayer are different (Rand 1981).

The second observation of Demel et al. which is quoted as indicating hydrophobic penetration of the protein into the bilayer, was that the surface pressure increase is affected by the lipid chain length. Figure 8.4, which demonstrates this, is reproduced below from Demel et al. (1973). Although not stated, these results

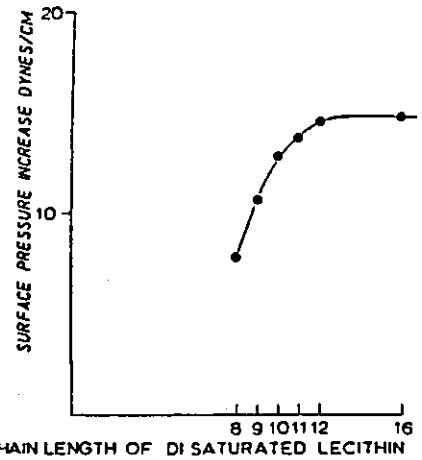

Figure 8.4 The effect of lecithin fatty acid chain length on the surface pressure increase after injection of myelin basic protein beneath the lecithin monolayer. (Reproduced from Demel et al. 1973)

were evidently collected for a low initial surface pressure, probably 10 dynes/cm, and therefore of doubtful relevance, as discussed above. Also the lipid used was lecithin, which shows no interaction above 30 dynes/cm. No reasoning is given as to why these results demonstrate hydrophobic interactions. An alternative explanation is that a conformational change or insertion into the head group region takes place which requires a certain increase in the area per molecule. The pressure-area curves of the longer chain length lecithins are steeper, at 10 dynes/cm, than those for the shorter chain length (see van Deenen et al. 1962) and so, for a given change in area, the pressure difference for the longer chain lengths must necessarily be greater.

A companion paper to that by Demel et al. (1973) concerns the protection of the myelin basic protein against the action of proteolytic enzymes after interaction of the protein with a lipid monolayer (London et al. 1973). Specific regions of the protein molecule were shown to be protected after interaction with cerebroside sulphate. However, this only points to a strong interaction between protein and lipid and not necessarily to a hydrophobic interaction. Also it should be noted that at an initial surface pressure of 30 dynes/cm, the protein is no longer protected from trypsin degradation.

Permeability Studies

Papahadjopoulos et al. (1975) measured the change in

sodium ion permeability of sonicated phosphatidyl serine vesicles when protein was added outside the vesicles. Addition of myelin basic protein up to a concentration of about 1 mg/ml induces a large increase (about 1ØØØ fold) in the $^{22}Na^{+}$ efflux from inside the vesicles. A similar increase in vesicle permeability was observed with cytochrome c but only at the much higher concentration of 1Ø-4Ø mg/ml. In a similar study Gould and London (1972) have studied the leakage of glucose from preloaded liposomes. Addition of myelin basic protein to the liposomes caused a 3-4 fold increase in the leakage rate, whereas addition of cytochrome c has no effect. However, in neither case was the control experiment carried out to measure the effect of adding Ca^{2+} ions to the liposome solution.

Differential Scaning Calorimetry

Addition of myelin basic protein decreases the phase transition temperature and enthalpy of melting of various lipids (Papahadjopoulos et al. 1975, Boggs & Moscarello 1978, Epand & Moscarello 1982). These decreases in the transition temperature and enthalpy of melting have also been observed on the addition of cytochrome c to lipid (Chapman et al 1974, Papahadjopoulos et al. 1975). Papahjopoulos et al. have explained their results for both myelin basic protein and cytochrome c in terms of surface binding of the protein followed by either partial penetration of the protein into the bilayer or deformation of the bilayer. However, Chapman et al.(1974) have interpreted their results for cytochrome c as being due to

the electrostatic interactions between the lipid and protein, the interaction of the charged lipid head-groups with the charged groups in fixed positions on the globular protein causing reorganisation of the lipid and, therefore, less efficient packing of the lipid chains.

Various Spectroscopic Techniques

Jones and Rumsby (1975) have studied the tryptophan fluorescence of myelin basic protein and their results suggest that the tryptophan residue is largely exposed to the solvent when the myelin basic protein is in aqueous solution. However, when sodium dodecyl sulphate, an ionic detergent, is added to the myelin basic protein solution, the change in the intrinsic fluorescence of the tryptophan indicates that the tryptophan residue interacts with the hydrocarbon chain region of the detergent. Similar results have been observed when the protein interacts with lipid vesicles (Boggs et al. 1982).

The results of the tryptophan fluorescence studies are in agreement with the N.M.R. studied of Liebes et al. (1976). They have observed broadening of the ^{1}H-NMR resonance lines of the aliphatic and aromatic residues of the myelin basic protein on interaction with sodium dodecyl sulphate (SDS), suggesting hydrophobic interaction of these residues with the detergent micelle. However, in both the above cases the results could be due to conformation changes of the protein on binding which moves the tryptophan and other aromatic residues into a more hydrophobic environment within the protein.

The effect of the protein on fatty acid spin labels has been studied by Boggs and Moscarello (1978b). A series of fatty acid spin labels with the nitroxide group located at different points along the chain were incorporated into lipid vesicles. Interaction of the myelin basic protein with the lipid vesicles above their phase transition greatly decreased the motion of the lipid fatty acid chain near the polar headgroup region, but had little or no effect near centre of the bilayer. This was reported "as being consistent with the concept of partial penetration of some regions of the sequence into the bilayer" (Boggs et al. 1982). However similar electron spin resonance studies by Chapman et al. (1974) have been interpreted in terms of electrostatic interaction between lipid and protein. Spin label studies were also carried out below the phase transition temperature of the lipids, and the results correlated with differential scanning calorimetry results (Boggs & Moscarello 1978b).

Conclusion

From the above brief review it can be seen that for almost every experiment reported as showing evidence of hydrophobic interaction between myelin basic protein and lipid, equivalent effects are observed when studying the interaction between cytochrome c and lipid. Various authors have postulated, on the basis of their results, that cytochrome c is another protein which interacts hydrophobically with the lipid (Papahadjopoulos et al. 1975, Quinn and Dawson 1969). However, cytochrome c is an

extremely stable molecule (Margoliash & Schejter 1966) and X-ray diffraction and circular dichroism studies (Gulik-Kryzwicki et al. 1969, Gulik-Kryzwicki 1975) on cytochrome c-phosphatidyl inositol complexes have shown that the interaction is purely electrostatic. It is important to realise that Gulik-Kryzwicki et al. determined the composition of their samples and found that the lipid partial thickness was the same in the presence and absence of protein. This would not be the case if the interaction of cytochrome c with the lipid bilayer occurred either by hydrophobic penetration of the protein into the hydrocarbon region ,or by deformation or expansion of the bilayer so exposing the fatty acid chains to hydrophobic regions of the protein (see figure 8.3).

It appears that the strongest evidence from the literature is that both myelin basic protein and cytochrome c interact with acidic lipid in the same way, although the interaction between myelin basic protein and lipid is stronger, possibly due to the larger contact area with the lipid bilayer. The evidence for hydrophobic interaction of these two proteins with the lipid bilayer is indirect and inconclusive and , in my view, the results can probably be interpreted in terms of strong electrostatic binding of the lipid polar headgroups with particular sites on the protein.

In this study, the conformation and disposition of myelin basic protein and cytochrome c in bilayers of cerebroside sulphate and 40mol % cholesterol has been directly investigated using low angle X-ray diffraction.

The results clearly demonstrate that both proteins reside on the bilayer, with little or no penetration beyond the position of the lipid headgroup peak in the membrane electron density profile. Thus there is no direct evidence for any hydrophobic interactions between these proteins and the lipid hydrocarbon chains.

REFERENCES

Bangham, A.D. (1982) Techniques in Lipid & Membrane Biochemistry B42Ø, 1-25
in Techniques in the Life Sciences B4/11, Elsevier Science Publishers, Ireland Ltd.

Bernstein, S. (1938) J. Amer. Chem. Soc. 6Ø, 1511

Bikerman, J.J. (1939) Proc. Roy. Soc. (London) A17Ø, 13Ø-144

Blaurock, A.E. (1973) Biophys. J. 13, 29Ø-298

Blodgett, K.B. (1935) J. Amer. Chem. Soc. 57, 1ØØ7-1Ø22

Blodgett, K.B. & Langmuir, I. (1937) Phys. Rev. 51, 964-982

Boggs, J.M. & Moscarello, M.A. (1978a) Biochim. Biophys. Acta 515, 1-21

Boggs, J.M. & Moscarello, M.A. (1978b) J. Membrane Biol. 39, 75-96

Boggs, J.M., Moscarello, M.A. & Papahadjopoulos, D. (1982) Chapter 1 in "Lipid-Protein Interactions", Volume 2, pp 1-51, Editors: Jost, P.C. & Griffith, O.H. John Wiley & Sons

Brady, G.W., Murthy, N.S., Fein, D.B., Wood, D.D. & Moscarello, M.A. (1981) Biophys J. 34, 345-35Ø

Caspar, D.L.D. & Kirschner, D.A. (1971) Nature New Biol. 231, 46-52

Chapman, B.E. & Moore, W.J. (1976) Biochem. Biophys. Res. Comm. 73, 758-766

Chapman, B.E. & Moore, W.J. (1978) Aust. J. Chem. 31, 2367-2385

Chapman, D., Urbina, J. & Keough, K. M. (1974) J. Biol. Chem. 249, 2512-2521

CRC Handbook of Physics and Chemistry (1974) 1974-1975, 55th edition, Editor: Weast, R.C., CRC Press

Demel, R.A., London, Y., Geurts van Kessel, W.S.M., Vossenberg, F.G.A. & van Deenen L.L.M. (1973) Biochim. Biophys. Acta 311, 507-519

Dickerson, R.E., Takano, T., Eisenberg, D., Kallai, O.B., Samson, L., Cooper, A. & Margoliash, E. (1971) J. Biol. Chem. 256, 1511-1535

Dickerson, R.E. (1972) Scientific American 226, No. 4, 58-72

Epand, R.M., Moscarello, M.A., Zierenberg, B. & Vail, W.J. (1974) Biochemistry 13, 1264-1267

Epand, R. & Moscarello, M. (1982) Biochim. Biophys. Acta 685, 230-232

Esen, A. (1978) Anal. Biochem. 89, 264-273

Eylar, E.H. & Thompson, M. (1969) Arch. Biochem. Biophys. 129, 468-479

Eylar, E.H., Brostoff, S., Hashim, G., Caccam, J. & Burnett, P. (1971) J. Biol. Chem. 246, 5770-5784

Fazekas de St. Groth, S., Webster, R.G. & Datyner, A. (1963) Biochim. Biophys. Acta 71, 377-391

Franklin, B. (1774) Philosophical Transactions 64, part 1, 445-460

Franks, N.P., Arunachalam, T. & Caspi, E. (1978) Nature 276, 530-532

Franks, N.P. & Lieb, W.R. (1979) J. Mol. Biol. 133, 469-500

Franks, N.P. & Levine, Y.K. (1981) pp 437-487, in Membrane Spectroscopy, Editor: Grell, E., Springer-Verlag Berlin Heidelberg

Franks, N.P. & Lieb, W.R. (1981) Chapter 8 in Liposomes: From physical structure to therapeutic applications, Editor: Knight, C.G., Elsevier/North-Holland Biomedical Press

Franks, N.P., Melchior, V., Kirschner, D.A. & Caspar, D.L.D. (1982) J. Mol. Biol. 155, 133-153

Frankuchen, I. (1938) Phys. Rev. 53, 909

Gaines, G.L. (1966) Insoluble monolayers at liquid-gas interfaces, Interscience Publishers

Gaines, G.L. (1977) J. Colloid Interface Sci. 62, 191-192

Gould, R.M. & London, Y. (1972) Biochim. Biophys. Acta 290, 200-218

Green, J.P., Phillips, M.C. & Shipley, G.G. (1973) Biochim. Biophys. Acta 330, 243-253

Gulik-Krzywicki, T. (1975) Biochim. Biophys. Acta 415, 1-28

Gulik-Krzywicki, T., Shechter, E., Luzzati, V. & Faure, M. (1969) Nature 223, 1116-1121

Hardy, W.B. (1912) Proc. Roy. Soc. (London) A86, 610-635

Hasmonay, H., Caillaud, M. & Dupeyrat,M. (1979) Biochem. Biophys. Res. Comm. 89, 338-344

Huang, C., Wheeldon, L. & Thompson, T. E. (1964) J. Mol. Biol. 8, 148-160

Hwang, J., Korenbrot, J.I. & Stoeckenius, W. (1977) J. Membrane Biol. 36, 115-137

Jaenicke, L. (1974) Anal. Biochem. 61, 623-627

Jones, A.J.S. & Rumsby, M.G. (1975) J. Neurochemistry 25, 565-572

Johnston, D.S., Sanghera, S., Manjon-Rubio, A. & Chapman, D. (1980) Biochim. Biophys. Acta. 602, 213-216

Kirschner, D.A. (1971) PhD. Thesis, Harvard University

Ladbrooke, B.D., Williams, R.M. & Chapman, D. (1968) Biochim. Biophys. Acta 150, 333-340

Langmuir, I. (1917) J. Proc. Amer. Chem. Soc. 39, 1848-1906

Langmuir, I., Schaefer, J. & Sobotka, H. (1937) J. Proc. Amer. Chem. Soc. 59, 1751-1759

Levine, Y.K., Bailey, A.I. & Wilkins, M.H.F. (1968) Nature 220, 577-578

Liebes, L.F., Zand, R. & Phillips, W.D. (1976) Biochim. Biophys. Acta 427, 392-409

London, Y., Demel, R.A., Geurts van Kessel, W.S.M., Vossenberg, F.G.A. & van Deenen, L.L.M. (1973) Biochim. Biophys. Acta 311, 520-530

M^{c}Intosh, T.J., Waldbillig, R.C. & Robertson, J.D. (1977) Biochim. Biophys. Acta 466, 209-230

M^{c}Knight, G.S. (1977) Anal. Biochem. 78, 86-92

Margoliash, E. & Schejter, A. (1966) Advances in Protein Chemistry 21, 113-286

Martenson, R.E. (1980) pp49-79, in "Biochemistry of Brain", Editor: Zumar, S., Pergamon Press

Mateu, L., Luzzati, V., London, Y., Gould, R.M., Vossenberg, F.G.A. & Olive, J. (1973) J. Mol. Biol. 75, 697-709

Montal, M. & Mueller, P. (1972) Proc. Nat. Acad. Sci. 69, 3561-3566

Morell, P. & Norton, W.T. (1980) Scientific American 242, No. 5, 74-89

Mueller, P., O'Rudin, D., Tien, H.T. & Wescott, W.C. (1963) J. Phys. Chem. 67, 534-535

Nakaghara, H., Fukuda, K., Akutsu, H. & Kyogoku, Y. (1978) J. Colloid Interface Sci. 65, 517-526

O'Brien, F.E.M. (1948) J. Sci. Instr. 25, 73-76

O'Brien, J.S. (1965) J. Lipid Res. 6, 537-544

Papahadjopoulos, D., Moscarello, M., Eylar, E.H. & Isac, T. (1975) Biochim. Biophys. Acta 401, 317-335

Perutz, M.F. (1954) Proc. Roy. Soc. (London) A225, 264-286

Pockels, A. (1891) Nature 43, 437-439

Pockels, A. (1893) Nature 48, 152-154

Quinn, P.J. & Dawson, R.M.C. (1969) Biochem. J. 113, 791-803

Quinn, P.J. & Dawson, R.M.C. (1969) Biochem. J. 115, 65-75

Rand, R.P. (1981) Ann. Rev. Biophys. Bioeng. 10, 277-314

Rothman, J.E. & Lenard, J. (1977) Science 195, 743-753

Rumsby, M.G. (1978) Biochem. Soc. Trans. 6, 448-462

Shannon, C.E. (1949) Proc. Inst. Radio Engrs. N.Y. 37, 10-21

Shipley, G.G., Leslie, R.B. & Chapman, D. (1969) Nature 22, 561-562

Stout, G.H. & Jensen, L.H. (1968) X-ray structure diffraction, The Macmillan Co.

Thorne, C.J.R. (1978) Tech. in Protein & Enzyme Biochem. B1Ø4, 1-18

Van Deenen, L.L.M., Houtsmuller, U.M.T., de Haas, G.H. & Mulder, E. (1962) J. Pharmacy & Pharmacology 14, 429-444